2018-06-07

Interference Modelling and Broadcast Protocols for Cognitive Radio Mesh Networks

Gaafar, Mohamed

UNIVERSITY OF CALGARY

Interference Modelling and Broadcast Protocols for Cognitive Radio Mesh Networks

by

Mohamed Gaafar

A THESIS

SUBMITTED TO THE FACULTY OF GRADUATE STUDIES

IN PARTIAL FULFILLMENT OF THE REQUIREMENTS FOR THE

DEGREE OF DOCTOR OF PHILOSOPHY

GRADUATE PROGRAM IN ELECTRICAL AND COMPUTER ENGINEERING

CALGARY, ALBERTA

JUNE, 2018

Abstract

The main aim of this thesis will be the modeling and characterization of wireless interference experienced by Wireless Sensor Networks (WSNs) especially in industrial applications. A comparative study between two broadcasting techniques, namely flooding and Network Coding (NC) was performed, in order find which has better performance in the presence of interference. The study aimed at finding which protocol had better timing and energy efficiency for different interfering network parameters. An interference model was proposed that simultaneously models the probability density function of the interference envelope, the temporal and spatial correlation. The model also allows for the synthesis of interference signals that relate to the interfering network parameters. When simulating a network, the performance metrics of the network were shown to be similar when using synthesized interference from the model or using interference that is simulated from an interfering network. Two measurement campaigns were performed in this thesis. The first campaign was a multi-antenna measurement characterize the small-scale and large-scale channel effects in a gas refinery. The second measurement campaign measured interference statistics such as the probability density function, temporal correlation, and the spatial correlation of the interference.

Acknowledgements

I would to thank God, the most knowledgeable, for all the blessings and knowledge that he has bestowed on me. Next, I would like to thank my parents for all their patience and the guidance they have given me to help me reach where I have reached in life. To my wife and son, I would like to thank them for the extreme patience they had and for always being by my side.

To my supervisor, Prof. Geoffrey Messier, I would like to say that I would not have been able to have reached the point I have without his efforts. I have learnt so much from him that has helped me grow both as a researcher and as a person. I would also like to thank my colleagues at the F.I.S.H lab, Mike Wasson and Devin Smith, for the work they had done on the software defined radios and for helping me with my measurements. I would also like to thank Prof. Hassan Aboushady, Dr. Ahmed Ashry, Dr. Alp Kilic, and Dr. Delaram Haghighi from LIP6 France, for all the help during my masters degree and for technical knowledge they passed on to me in FPGA and ASIC design.

I would also like to give a special thanks to all my teachers. Those in school, bachelors, masters, and my PhD. I have had some great teachers who have taught me how to learn, how to love what I learn, and how to do my best to pass along what I have learnt to others. It is because I have always been blessed with great teachers and role models that I have become the person I am today.

Table of Contents

List of Tables

List of Figures

Chapter 1

Introduction and State of the Art

Recently there has been an increased necessity to move from wired network topologies towards wireless networks for industrial applications. This migration needs a further understanding of the industrial wireless channel and the issues of co-existence with other wireless networks. The wireless spectrum has become very congested in recent years and is expected to only get worse. New techniques are necessary to resolve the issue of spectrum congestion and the co-existence of multiple standards on a single band. This does create the necessity for the modeling and characterization of other interferers on the same band as well as the modeling the wireless propagation environment being used.

This chapter is divided into 6 sections. Section 1.1 will give a brief history of Wireless Sensor Networks (WSNs) and discuss the state of the art systems used in wireless communications especially those relating to industrial applications. Section 1.2 will discuss the problem of spectrum congestion and Cognitive Radio (CR) will be discussed as a solution to this. Section 1.3 will give a brief introduction to the use of broadcasting. Section 1.4 will discuss the importance of interference modeling. Section 1.5 will discuss recent work on measurements of the wireless channel propagation effects for industrial environments as well as interference measurements. Finally, Section 1.6 will summarize the main contributions of the thesis.

1.1 Industrial Applications of Wireless Sensor Networks (WSNs)

This section will introduce WSNs, first giving a brief history and then it will discuss the current trends in wireless communication systems, especially in the field of Machine-to-Machine (M2M) communications. Current trends in wired and wireless industrial networks will then be discussed.

1.1.1 WSN History

A WSN is a collection of spatially distributed sensors that measure or monitor physical parameters such as temperature, pressure etc. WSNs first started being used in the 1950s by the American Military to detect and track Soviet submarines. The system was called the Sound Surveillance System (SOSUS) and it consisted of acoustic sensors that were distributed around the Pacific and Atlantic oceans [1]. This system is still used actively until this day, but less for military purposes and more for monitoring sea wildlife and volcanic activity [2]. In 1980, the United States Defense Advanced Research Projects Agency (DARPA) started work on the Distributed Sensor Network (DSN) project. The predecessor to the Internet, Advanced Research Projects Agency Network (ARPANET), had been online for a few years and it began to be questioned if ARPANET's approach of communication could be extended to DSNs [3]. DARPA was again the front runner in WSN research by launching a research program called SensIT [4], which was the first self-contained distributed WSN introducing new capabilities such as ad-hoc communications. IEEE also saw the importance of WSNs and initiated the first Wireless Personal Area Networks (WPANs) in 2003 which then led to the 802.15.4 standard which is one of the most famous WSNs used today [5].

Recent advancements in Integrated Circuit (IC) fabrication, digital modulation and networking techniques have all aided the development of WSNs. New wireless Micro Controller Units (MCUs)-System-On-Chip (SoC) are devices that have MCUs with RF transceivers on single chips which offer high performance low-cost units that need as little as a battery to be ready for deployment. The use of Micro Electro Mechanical Systems (MEMS) in sensor design have also aided in producing small, low-cost sensors [6]. Further advancements may very well see WSNs connect us to the physical world just as the Internet helps us share information anywhere around the world.

The main aim of using sensors for monitoring in industrial applications is to be able to collect large amounts of data, from hundreds or thousands of sensors, for real-time sensing and control of industrial processes. Sensing has been used for decades and is now a necessity for industrial

applications [7]. Factories and industrial processes have become more automated and sensing has become important to monitor machine health and status. Using sensors to monitor has become vital for increased maintainability, performance and for safety reasons for industrial processes. In 2007, the IEEE, in cooperation with National Institute for Standards and Technology (NIST), launched the IEEE 1451 smart transducer interface standard [8] to facilitate plug and play of sensors to industrial networks. However, WSNs are not so prevalent in many consumer and industrial applications. They should, however, quickly find their way into many applications should they prove their reliability to increase the confidence of their use in more sensitive industrial applications.

1.1.2 State of the Art Wireless Machine to Machine (M2M) Communications

With the increased use of networks and automated systems, the term M2M communications began to emerge. This is a broad term that refers to any information exchange between machines with no or little manual or human intervention. According to M2M magazine (now Connected World), there are ”six pillars” of M2M technology namely remote monitoring, RFID, sensor networking, smart services, telematics, and telemetry [9]. The field of M2M emerged in 1995 when Siemens introduced a GSM data module called M1, which would allow messaging between devices over wireless networks for industrial purposes where faxes would be sent via PC or SMS messages [10]. In recent years, M2M technology has found many applications in everyday life. In industrial field applications, such as oil drill sites, many parameters such as temperature, pressure and flow rate can be monitored with remote sensors and the data sent back to a central control location. This data can then be used by computers to automatically adjust the necessary equipment to improve performance and reduce the cost and hazard of having humans do it on site. M2M has also found many uses some of which include medical applications, security, and traffic control.

With the emergence of M2M, the term Cyber Physical Systems (CPSs) began to appear, which refers to integrated systems with computers, communication networks and control technologies. The term Cyber Physical Systems was first used by Gill Helen in 2006 [11]. CPSs are the evolution of M2M systems [12], in that not only do they improve machine-to-machine communications, but

the general interaction between the physical world and the cyber-computer-based world with the emphasis on real-time sensing and control. The emphasis of CPSs is on the closed-loop real-time control of physical systems. CPSs, like M2M, have paved the way for applications such as smart grids and smart cities, which could mean the emergence of energy aware buildings and cities. In general, the term ”smart” is used to sell a concept that involves the intelligent automatic control of day to day systems. Autonomous driving and smart factories are other examples of applications CPSs can be used for.

A more general term, Internet of Things (IoT), has recently emerged and it defines systems that fall under the same umbrella as M2M and CPS. IoT considers a system with three key features: ubiquitous sensing, network of networks and intelligent processing. When it comes to the terms WSN, M2M, CPS and IoT, there are varying definitions over time and by different academic communities which has caused a lot of confusion on the exact definitions of each term, however, common definitions can be found for each. WSN refers to a wireless network with sensors exchanging information with the end goal of sending this information to specific nodes in the network to be stored or processed. M2M defines networks (wired or wireless) that connect different machines and remote devices with the end goal of reducing human interaction. CPSs are systems that combine computing, networks, and the physical world with the emphasis on real-time sensing and control. Finally, IoT involves networks that connect ”things”, be they devices, machines, or humans, to improve the cyber-physical-social interaction. If CPSs were defined to include the social/human interaction (which they recently were) then CPSs and the IoT are basically very similar or can be considered as the exact same thing [13].

In general, the simplest form of these intelligent networks would be a WSN. However, with the advancements in communications, networking, and computing, we will find ourselves converging towards more intelligent and globally connected networks between humans, devices, machines, or ”things” in general. Some real-life examples have already been implemented but for more complicated systems to emerge there still needs to be further technological advancements. An example

is the emergence of cloud computing that makes it possible for the processing of huge amounts of data that may not be processed locally. Also, recent advancements in control techniques coupled with newer more efficient fabrication methods will allow for simpler and more cost-effective implementation of such complicated systems. With many upcoming wireless standards and wireless spectrum becoming more congested, advancements are needed in the fields of interference awareness and collaborative communications.

I believe that the first applications that will benefit from such complicated intelligent systems will be industrial networks. The industrial environment has plenty of machines, sensors monitoring the state of these machines, and humans directly or indirectly dealing with these machines. Factories are moving increasingly towards intelligent networks that combine all these components allowing seamless, safe, and efficient interaction between them. Applications such as smart factories will soon become a reality. The advantages of such systems are very attractive; however, their implementation will need a deeper understanding of the requirements of industrial applications, the industrial networking environment, and improvements in communication techniques. Some of these issues will be tackled in this thesis with the main aim of aiding in the design of such systems for the industrial factories of the future.

1.1.3 Industrial Wired Control Networks (NWs)

An industrial control network is a system of sensors, machines and equipment interconnected with each other to control certain processes. A need for this began with the automation and increased complexity of industrial processes. Industrial networks differ from commercial networks in that there are greater constraints and Quality of Service (QoS) requirements. They also require great determinism and reliability due to the sensitive nature of certain processes. There are shorter latency requirements (as small as 250 μs) and shorter packets are used that may have periodic and aperiodic traffic [14]. The strict networking requirements, coupled with the fact that the information will be used in closed-loop control of highly sensitive processes, makes network design for industrial networks different from that of commercial networks.

Figure 1.1 shows a hierarchal representation of how a traditional industrial network would be set up. Industrial networks are usually more complex than regular networks. While regular networks may consist of a group of Local Area Networks (LANs) connected to a backbone of a Wide Area Network (WAN), industrial networks may consist of multiple levels of networks in a hierarchical manner [14]. The figure shows plants which are usually buildings with industrial processes taking place in them. The plant has sensors and actuators shown by "S" and "A", respectively. The first level in the hierarchy is for instrument-controller connections, connecting sensors and actuators to Programmable Logic Controllers (PLCs). PLCs are programmable controllers that are used to obtain data from sensors and instruments, process it and give commands back to control certain processes. There may also be a level for controller-controller connections. PLCs are then connected to a Supervisory Control and Data Acquisition (SCADA) system which is a software layer that is usually above the control layer in the hierarchy. The main aim of this layer is usually data acquisition and the presentation of the Human Machine Interface (HMI). Finally, there is a layer for the external communications with the outside World. This network infrastructure is usually unicast and with growing traction for smart industrial networks, there is a general trend for the migration towards wireless mesh networks.

Due to the sensitivity of industrial processes and their strict requirements, wired sensor networks have been used for decades since the wired channel is found to be stable and often more reliable than wireless channels. However, in an industry like the petroleum industry, oil refineries can have up to $100,000$ sensors and $10,000$ equipment controllers (actuators) [15]. The cost of wired cables that meet the required shielding standards may range in cost from $\$200$ to $\$2,000$ per foot [16]. The cost of using wired networks is very costly and this may be the main reason that would cause migration towards WSNs. The other problem that wired sensor networks have is that the network is not flexible since the installation and movement of sensors and cables is difficult. Should WSNs prove their reliability and effectiveness in industrial environments, they will be a strong competitor to current wired networks.

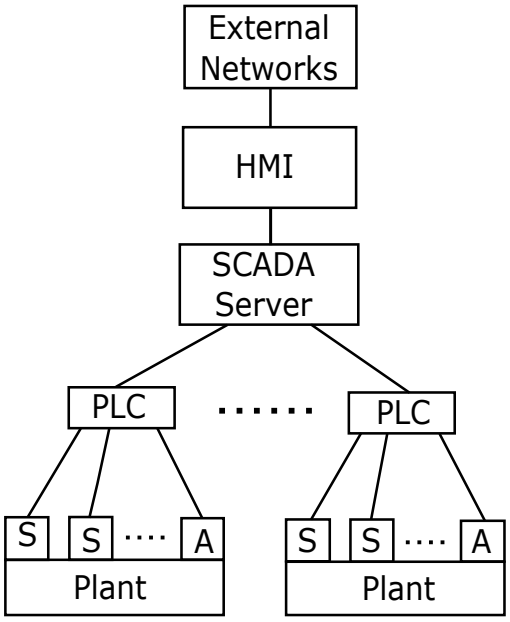

Figure 1.1: Hierarchical representation of industrial network

In industrial applications, the latency of the signal is very critical. Data sent from sensors must reach controllers quickly for controllers to send back control information that may be used for very sensitive processes and a high latency may affect the stability of these control loops. Another critical factor is the energy efficiency of these networks. Having energy efficient networks would increase the lifetime of batteries in sensors, and this is very important since it is impractical to have to change sensor batteries regularly, especially if they are in remote or dangerous locations. The idea of using batteries for WSNs is to have remote sensors and to remove the need for wiring.

1.1.4 Wireless Networks in an Industrial Setting

WSNs in the industry use one of the most prominent wireless technologies, the IEEE 802.15.4 standard [5] which operates at two bands but is mostly used at the 2.4 GHz Industrial, Scientific and Medical Radio (ISM) band. It defines the physical (PYH) and Medium Access Control (MAC) layers of the OSI network stack. It is compatible with two main higher-level standards, namely ISA100.11A [17] and the WirelessHART [18] standards which are used for instrumenta-

tion and control in industrial applications. There have been many comparisons between the two standards. Some comparisons support the idea that the ISA100.11A standard is better for features such as backbone routing and flexible time-slots [19]. Other comparisons showed that industry was more inclined towards WirelessHART with 39% of end users using it [20]. Some differences include configurable time-slots for ISA100.11A versus fixed 10 ms time-slots for WirelessHART. ISA100.11A supports backbone routing while WirelessHART does not. The decision to choose a standard would depend on the application requirements and the environment the WSN is setup in.

The use of smart WSNs for industrial applications is attractive especially with the emergence of the field of IoT. This new direction requires that new and innovative techniques become readily available. However, due to the sensitive nature of industrial application, the use of WSNs is met with a few concerns. One concern is the reliability of sensitive transmissions in a WSN. This concern arises, in part, due to increased congestion in the wireless spectrum especially in the ISM band. Factories in an urban environment will find that they may be competing with many wireless standards in the ISM band and CRs are a promising solution to this problem. A WSN based on nodes using CR technology would mean the nodes need to scan multiple bands and take a decision on which band they will use. Cooperative spectrum sensing is a promising field that is emerging where multiple nodes in a CR may share their information from their spectrum sensing which would improve decisions taken by individual nodes.

WSN design requires knowledge about the wireless propagation channel in the factory environment. A more realistic channel model would help simulate real network scenarios that could be used to calculate the network capacity, latency, and reliability. This knowledge would affect decisions such as the required transmit power of nodes, node separation and the practicality of techniques such as spatial and frequency diversity for increased reliability. This in turn would help us understand how close the application of WSNs would be to the requirements of industrial applications.

1.2 CRs for Industrial WSNs

This section will introduce the concept of CRs and their importance in WSNs and is divided into 2 subsections. The first section will describe CRs, give a brief history and discuss the importance of CRs in WSNs. The second section will discuss spectral sensing in more detail.

1.2.1 History and Main Applications

A CR is an intelligent transceiver that can be programmed to have the capability of detecting wireless channels and operating while causing little interference on the channel. Once an available channel is detected, it may decide to occupy this channel with the requirement to maximize its channel utilization while minimizing its interference on other users of the channel. In general, a CR may reconfigure multiple parameters such as waveform, protocol, and operating frequency.

CRs were first proposed by Joseph Mitola III in 1998 [21]. A CR was considered to be an evolution of reconfigurable transceivers known as Software Defined Radios (SDRs). The fixed allocation of spectrum has been shown to be very inefficient [22], with great congestion in cellular networks and ISM bands and insufficient use of other bands such as radio and military. Some licensed bands with primary users (PUs) that pay for use of the band, may still be used inefficiently and CRs would allow unlicensed users, or secondary users (SUs), to make use of the band during idle periods. The first CR standard was published in 2011, IEEE 802.22, which allows the use of spectral sensing for finding idle bands. Channel hand-off and channel switching is also necessary to ensure that a SU does not occupy an idle channel for too long to reduce interference on PUs.

Industrial WSNs operate in harsh conditions and use bands where they may have to contend with other wireless standards and a lot of work has been proposed for the use of CRs in industrial WSNs [23, 24]. CR is a practical solution for industrial WSNs, since it allows the intelligent, efficient, and flexible use of the spectrum. Recent advancements in transceiver design would allow for the use of CRs, however, the strict reliability, timing, and energy constraints that industrial

WSNs need remain a barrier. More research that shows that such systems are applicable, cost effective, and reliable is needed before industrial applications begin to use such systems.

1.2.2 Spectrum Sensing

Spectrum sensing is the ability of a SU to sense a large spectrum and be able to decide which band it will use so that it reduces the amount of interference it causes on PUs of that band. There are multiple considerations that a SU could take when sensing. One is that it is necessary to continuously sense so that it is aware of spectrum usage. It should also do this while using a given band so that if a given PU begins to use a band it is on, it can switch to another band. More information can be obtained from a channel than just whether it is being used or not such as the type of signals or standards using the band. This would allow for the SU to differentiate between PU and SU usage of the band which would allow a SU to decide not to compete for a band with a PU while it may choose to compete with another SU for the same band. Other priori statistics of PU occupants of bands such as the average transmission times, inter-arrival times and transmit powers may provide better decisions of which bands a SU occupies and for how long in order to minimize interference on PUs.

There are many types of spectral sensing and they can be categorized in many ways. They may be divided into coherent or non-coherent methods, wide-band or narrow-band, and blind or priori based. A crucial difference is whether the method is blind or uses priori knowledge in the decision. Examples of blind detection methods are energy detection [25] and eigenvalue-based detection [26]. Examples of sensing techniques that use priori knowledge are the matched filter method [27] and cyclostationary feature detection method [28]. Methods that use priori knowledge are more complicated and need more processing but produce better decisions on which bands to occupy, for how long to occupy them, and what transmit power a SU should use.

Collaborative spectral sensing is a technique by which multiple SUs each share their information acquired from sensing the channel. There are two types of collaborative spectrum sensing, central and distributed [29]. The central method needs a central node that performs the calculations

based on the gathered sensing information from all nodes and then broadcasts all that information back to the nodes. This method has the advantage of reducing calculations at each node and only a single broadcast from this node every fixed period, however, should links to this main node fail, the operation of the WSN may be affected. The distributed method assumes that each node gathers the information from all other nodes and each node independently takes a decision based on the available information. This method may need more broadcasts but allows the WSN to be flexible and robust since each node is able to take decisions on its own. In either case, the advantage of collaborative spectrum sensing is the increased accuracy of decisions taken by SUs, however, the main disadvantage is the increase in required broadcasts of sensing information. Therefore, more efficient broadcasting techniques are necessary. Also, realistic interference models would help develop better sensing techniques and deciding which sensing information would result in better decisions.

1.3 Broadcast Techniques

Broadcasting is the process of a single node sending a packet to all other nodes in the network. Broadcasting is commonly used in the transmission of control information such as alarms, and networking information such as routing tables. Recently, collaborative communications have found a need for efficient broadcasting techniques for them to be usable. There is a clear benefit in CRs making use of collaborative communications in spectral sensing, but how practical this is will depend on how efficient the broadcast protocol is. Another key factor is how resilient the broadcast technique is to interference since these operations would be occurring with other PUs using the band and other SUs also competing for the band. The work in Chapter 2 will compare two broadcasting techniques for WSNs, namely flooding and Network Coding (NC), in the presence of an interfering PU network.

One of the techniques that will be used in the thesis is flooding. Many variations exist, but at its simplest, flooding works by a node sending out a packet and every other node that receives

this packet transmits it only once. This process is repeated until every node that has received the packet has transmitted it once. This method of broadcast consists of many transmissions, many of which are redundant, but is simple and does effectively spread a packet across the network. Other applications for flooding include on-demand routing protocols that use flooding to find the best route for a certain destination. Examples are Dynamic Source Routing (DSR) [30], Ad hoc On demand Distance Vector (AODV) [31] and Zone Routing Protocol (ZRP) [32] where the location of other nodes is assumed to be unknown. Other techniques such as Location-Aided Routing (LAR) [33] and Distance Routing Effect Algorithm for Mobility (DREAM) [34] make use of Global Positioning System (GPS) information to find the best route. The broadcast information is usually vital and therefor it is important to send it to every user even if it is at the cost of increased network congestion. Even with its obvious inefficiency, regular flooding is still widely used because of its simplicity.

The second technique that will be used is NC, which was first suggested in [35] and it can improve network capacity, data rates and network security. NC is a technique used to combine several packets in a single packet, and the receiving node receives many such packets and uses them to decode them to obtain the original packets. There are many types of NC techniques and they differ in the method of mixing the packets and in its desired application. One important use in broadcasting multiple packets which could be used in applications such as cooperative communications.

The work in this thesis will compare these two broadcasting techniques, flooding, and NC, in the presence of interference. A lot of work discusses cooperative communications and it is common to find in CR literature the assumption of availability of information at all participating nodes. No work was found to study the use of broadcasting in CRs for WSNs and how it would affect the time and energy efficiency of the WSN. The study of the resilience of broadcast techniques to interference is important especially since SUs will find that PUs and other SUs will be interfering with them. This thesis performs a comparative study of the time and energy efficiency of the two broadcasting techniques in the presence of interference from a PU network.

1.4 Interference Modeling

An important concern of CRs is to minimize the interference caused on PUs, therefore, a lot of research has been conducted on this point. The work in [36] characterizes the aggregate interference caused by SUs on a PU. In [37], they characterize the aggregate interference of SUs on PUs by modelling its probability density function as well as time-variation statistics such as the auto-correlation function. The work in [38] produced temporal and spatial correlation coefficients for the interference from a PU and used it to help in deciding which SU node to choose in collaborative spectral sensing. There is little research that focuses on the interference that PUs cause from the perspective of a SU. The work in this thesis aims to model this interference and study how this interference would affect CR protocols especially band intensive techniques such as broadcasting in cooperative communication.

One important part of creating models is the ability to reproduce signals with the same characteristics. There has been extensive work that has been done in the modeling of the probability density function of the power of interference signals. A famous distribution is the Middleton model [39] and other models characterize it as stable distribution [40–42], Gaussian [43], K-distribution [44] and log-normal [45]. There has also been work done in modeling the temporal correlation of interference [46, 47]. The work in [38, 47] produced a spatial-temporal correlation coefficient for interference.

However, there has been no work that simultaneously models all these interference characteristics and provides a method to synthesize signals with all these characteristics simultaneously. It is important to be able to create synthesized interference that would allow for testing of protocols that a CR may use while experiencing this interference. The work in thesis includes a proposed interference model that simultaneously accounts for the probability density function, temporal correlation, and spatial correlation. It also allows for the synthesis of these interference signals that was showed to produce network performance similar to that of when simulated interference is used.

1.5 Wireless Channel Measurements for Industrial Applications

This section will discuss the importance of having channel propagation and interference measurements and a brief look at previous work and a discussion of related work and then measurements performed in this thesis will be described. The section is divided into 2 subsections. Section 1.5.1 will discuss the channel propagation measurements and Section 1.5.2 will discuss the interference measurements.

1.5.1 Channel Propagation Measurements

Even though WSNs show great promise, there is still much more evidence required for it to fully replace their wired counterpart. Gas refineries may pay a lot more for wired networks simply because a lot is known about them and they have been used for a long time. There is still a lot to be learnt about the wireless channels in gas refineries and how reliable wireless systems would be in that environment. There have been many propagation measurement campaigns that have been performed at industrial environments. The path loss and shadowing distributions in a factory environment using Received Signal Strength Indicator (RSSI) at 2.4 GHz have been performed in [48, 49]. Vector analyzers were used to calculate the path loss, Root Mean Square (RMS) delay, time dispersion and K-Factors at 2.4 GHz [50–52] and 5 GHz [53]. Large and small-scale channel statistics were also measured at 1.3 GHz in a factory [54]. Statistical measurements of the path gain coefficients, the path inter-arrival times, and the number of paths were made in [55]. Similar measurements were also made in a university hall filled with machinery [56]. However, these measurement campaigns have mostly taken part only in manufacturing and factory environments.

Previous propagation measurements at a gas refinery have been scarce. The difference in environments may be significant since gas refineries contain mostly metallic buildings and structures. Only a single measurement was performed at a gas refinery which had a few average power measurements collected with 802.15.4 modems [57]. However, using average power measurements does not give many vital pieces of information especially the small-scale effects of the channel.

This thesis will present the first multi-antenna propagation measurement campaign performed at an operating gas refinery. The aim of this campaign is to capture the large and small-scale channel statistics of the gas refinery propagation environment. Using these measurements, large-scale channel effects, namely path loss exponents and shadowing, were measured. Also, small-scale channel measurements allowed us to calculate the propagation channel K-factors, coherence bandwidth and antenna correlation at the gas refinery.

1.5.2 Interference Measurements

For a WSN to operate in a gas refinery environment, knowing only the kind of propagation channel to be expected is not enough. It is also important to study the effect that the interference of a PU network would have on an industrial CR WSN. Measurements have been performed to extract statistics of interference at various bands. The work in [58] performed interference measurements at the 868 MHz ISM band and extracted probability density functions for the received power levels. In [59] measurements were performed at the 918 MHz, 2.44 GHz, and 4.0 GHz bands and produced peak amplitude, pulse duration, and inter-arrival time distributions.

Most CR literature is more concerned about the interference that SUs produce on PUs [60] and very little work considers how other PU interference can be modeled and how it would affect CR performance and decisions. There are also no measurements that consider important statistics that are necessary to fully characterize interference in a given band. Also, no work has been proposed that allows the interference to be synthesized with the desired characteristics and has been used to show that it can accurately simulate CR protocols under this interference.

This thesis provides results for a measurement campaign that aim at extracting interference statistics. The measurement campaign is the only known campaign to characterize the interference power density function, and the temporal and spatial correlations of the interference.

1.6 Contributions

The main research problem of this thesis is to assess the feasibility of using state of the art techniques such as CR for industrial WSNs especially in gas refineries operating at multiple bands that may have multiple interferers. This research problem can be broken down into 3 research questions that the thesis tries to answer. The first question is what broadcasting techniques are most resilient to interference and provide the required network coverage while meeting the strict timing and energy constraints of industrial networks. The second question is what interference model best characterizes the probability density, temporal correlation, and spatial correlation of PU interference signals, relates them to PU network parameters, and allows for the synthesis of these interference signals with the required statistics. The final question is how practical measurements of the industrial wireless propagation environment and interference that an industrial WSN is to experience would relate to analytical models and would help in the improved design of industrial WSNs. The following are a list of the contributions of this thesis:

1. Conducted a comparative study between two broadcasting techniques, namely flooding and NC, in order to find which has better performance in the presence of interference. The study aimed at finding which protocol had better timing and energy efficiency under PU interference with different network parameters.

2. Proposed the only known interference model that characterizes the probability density function of the interference power, the temporal correlation, and the spatial correlation. The model is the only one that allows for the synthesis of interference signals that relate to the network parameters of the PU causing it. The use of this synthesized interference was shown to produce results that are similar to results when simulated interference signals are used instead.

3. Conducted a multi-antenna measurement campaign to capture the statistics of the small-scale and large-scale channel propagation effects in a gas refinery. The results

have been published in a journal paper in IEEE Antennas and Wireless Propagation Letters [61].

4. Performed a measurement campaign that is the first to obtain interference power probability density function, temporal correlation, and the spatial correlation.

Chapter 2

CR Broadcasting Protocols

This chapter discusses the network simulations used to model a SU network in the presence of a PU network. The importance of this chapter will be to study the performance of SU networks at broadcasting in the presence of interference. The network simulation platform described in this chapter will also be used in the interference model validation in Chapter 3. This chapter has three sections. The first section will explain the network model and the techniques used in the network simulations. The second section will discuss the results obtained from the network simulations. The third will summarize the results of this chapter.

2.1 Network Model

The focus of this section will be to describe the network setup and the main techniques used in the network simulations in Section 2.2. The aim of the simulations will be to model a SU network that operates as a wireless mesh network within the ISM band and there will be another PU network operating at the same band. Signals from the PU nodes and SU nodes will be considered as interference from the point of view of a SU node. The performance of the SU network at broadcasting in the presence of PU network interference is the focus of this chapter. How to improve the efficiency of the broadcast process, in the presence of interference, is a very important question that this chapter will try to answer.

Another important point to make is that in the simulations in this chapter consider the operation of a PU and SU the same. In general, the difference between a PU and SU is when and how they decide to transmit. A SU usually transmits if it detects that a band is not in use and will usually not use an idle band for a long period of time to avoid interfering with a PU if it decides to transmit on the same band. A SU may also use power control to make sure that the SINR at all PUs does not

exceed a certain threshold. So, a SU tries to reduce usage of a band and reduce transmit power to minimize SINR at PUs. In the simulations in Chapter 2 and Chapter 3 the operation of the PUs and the SUs are assumed to be the same. There are two reasons for this. The first is that the interference model in Chapter 3 assumes interference from networks that use the same parameters, that include packet lengths and transmit powers. The second reason is that the focus of the work is more on the broadcast performance of the CR network than the operation of the CR network. The results in this chapter can be considered as the best-case performance, since the reduction of band usage or transmit power of the SU nodes would reduce the performance of the SU network.

This section has 6 subsections. Section 2.1.1 will describe the topology of the networks used in the simulations. Section 2.1.2 will explain the physical layer (L1) concepts specifically signal transmissions, the channel model, and reception of signals. Section 2.1.3 will discuss the MAC layer (L2) and the multiple access protocols the simulation uses. Section 2.1.4 will describe the network layer routing techniques used, namely flooding and NC. Section 2.1.5 will give assumptions made about higher levels of the network.

2.1.1 Topology

Figure 2.1 shows an example of the PU and SU networks. The inner circle is the area that holds SUs which are represented by small squares. The red square in the center is the source node that will broadcast its packets to all other nodes in the SU network. The outer circle holds PUs, represented by small triangles, and can exist within the inner circle as well. The diameter of the outer circle is L, and the diameter of the inner circle is $L/4$. The SU network size was chosen to be small enough, with respect to the PU network, to use the assumption that the PU network interference is stationary, and this will be discussed further in Section 3.1.2.

The node placement follows a Poisson Point Process (PPP) for both the PU and SU networks. A Point Process (PP), in probability theory, is a collection of points that are randomly located in a certain space which can be a line, two-dimensional plane, or a space with even more dimensions. In other words, it is a mathematical model that describes the distribution of elements or objects in

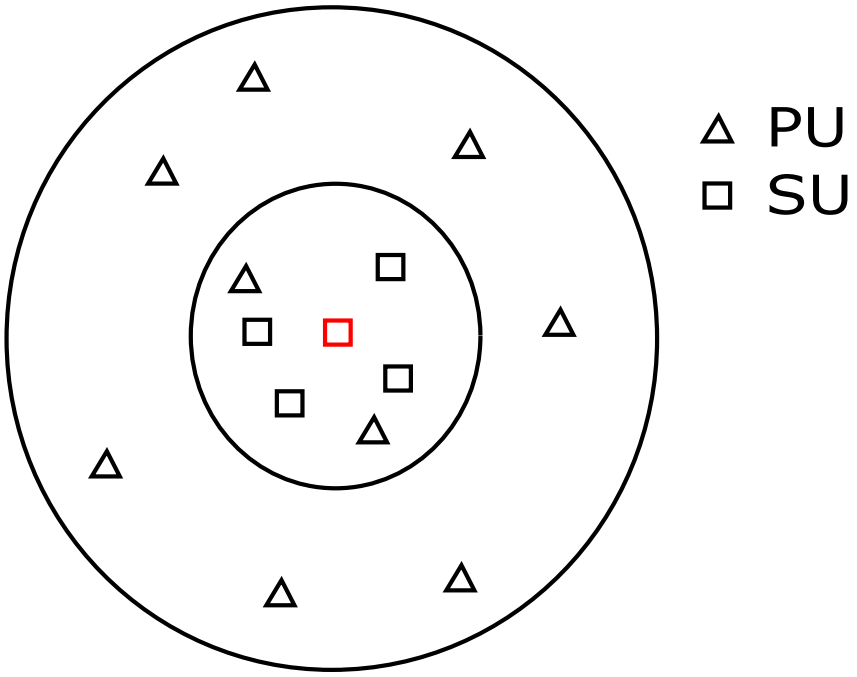

Figure 2.1: Network topology

an environment. There are many types of PPs, but the PPP is commonly used with node placement in wireless networks [62] and the reason for this is its ease in analysis. The PPP describes a random variable N, in a region R with area A_{R}, as having a value of n with a probability as shown in Equation 2.1, which follows a Poisson distribution.

$$P\{N=n\} = \frac{\lambda^{\mathrm{n}}}{n!}e^{-\lambda} \qquad \lambda > 0, n \geq 0 \tag{2.1}$$

There is a single parameter, λ, used to define this distribution and has units as number of nodes per network area, A_{R}. The parameter is known as the mean rate, intensity, or mean density and is normalized by the area of the network to give the mean number of nodes per network. In the thesis, this parameter will be referred to as the user density. If this parameter is a constant, over time and area, then the point process is said to be homogeneous or stationary. Another property that is important is that the points are uniformly distributed in any of the dimensions of the Cartesian coordinates.

2.1.2 Physical Layer

This subsection will describe the aspects that relate to the PHY layer such as the packet transmission, wireless channel, and the packet reception.

Channel

The simulation will use the simplified path loss model [63] given in Equation 2.2, where P_{r} is the received power at distance r, P_{t} is the transmit power, d_0 is a reference distance, α is the path loss exponent, and $a = P_{\mathrm{t}} K d_0^{\alpha}$. K is a unitless constant, given in Equation 2.3, used as the free space path gain at distance d_0, where c is the speed of light and f is the frequency of operation. The value of d must be greater than the reference distance d_0 which is used as 1 m.

$$P_{\mathrm{r}} = P_{\mathrm{t}} K \left(\frac{d_0}{r}\right)^{\alpha} = a r^{-\alpha} \quad , \quad r > d_0 \tag{2.2}$$

$$K = \left(\frac{c}{4\pi f d_0}\right)^2 \tag{2.3}$$

To obtain the signal power received by the receiving node from a certain transmitting node, the transmit power, P_{t}, transmitted is divided by the path loss. The transmitted and received power values here are not instantaneous but instead the average power over a time-slot, T_{s} seconds. The total received power by any given node is $P_{\mathrm{r}} = P_{\mathrm{r}}^{\mathrm{INT}} + P_{\mathrm{r}}^{\mathrm{SIG}}$, where $P_{\mathrm{r}}^{\mathrm{INT}}$ is the received interference power and can either be from a PU or SU or both, and $P_{\mathrm{r}}^{\mathrm{SIG}}$ is the power received from the desired SU. All signals from PUs will be considered as interference, while broadcast packets from SUs will be considered as desired signals and non-broadcast packets from SUs will be considered as interference. Equation 2.4 defines the average Signal to Interference plus Noise Ratio (SINR), where P^{N} is the noise power.

$$SINR = \frac{P_{\mathrm{r}}^{\mathrm{SIG}}}{P^{\mathrm{N}} + P_{\mathrm{r}}^{\mathrm{INT}}} \tag{2.4}$$

Packet Reception

The simulations use Binary Phase Shift Keying (BPSK) as the modulation. The packet is transmitted over a time that is always an integer multiple of time-slots. The packet transmission time in seconds, T_{f}, is always an integer multiple, s, of a time-slot, T_{s}, therefor $T_{\mathrm{f}} = sT_{\mathrm{s}}$. Each packet has N_{b} bits which will be constant for all simulations. The data rate, R_{b} will be varied to change the packet time T_{f}, where $T_{\mathrm{f}} = N_{\mathrm{b}}/R_{\mathrm{b}}$.

It is important to note that the decision for successful packet reception is not on a bit per bit basis but on the entire packet. The SINR values are recorded at every T_{s} and the average of these values is compared with γ. If the average value of SINR is greater than γ then the packet will be considered to have been received successfully. This approximation does simplify the simulation, but it also underestimates the probability of not receiving a packet. The reason for this is because the SINR may drop at a bit causing a bit error and therefor a frame error, even though the average SINR may be above γ. While a transmitting node sends a packet to a receiving node, a collision is defined as another node transmitting causing an average SINR at the receiver that is lower than γ. The fact that a simultaneous transmission happened does not mean failed packet reception, but what decides is the comparison of the average SINR value with γ. The aver

To calculate the SINR threshold, γ, the minimum frame error rate ($\mathrm{FER}_{\mathrm{min}}$) is assumed to be known and the minimum Bit Error Rate ($\mathrm{BER}_{\mathrm{min}}$) can be calculated from Equation 2.5. The use of BPSK and assuming Gaussian interference means the relation between BER and SINR can be approximated using Equation 2.6, where $erfc$ is the complementary error function. The SINR threshold, γ, can then calculated using Equation 2.7. The threshold calculated here assumes that if the instantaneous SINR drops below this value a single bit error will occur and therefore the packet will be dropped. The simulations, however, compare this threshold to the average SINR (over the

entire packet) and not the instantaneous one, and this will mean an underestimate of the dropped packets in the simulations.

$$\mathrm{FER_{min}} = 1 - (1 - \mathrm{BER_{min}})^{\mathrm{N_b}} \tag{2.5}$$

$$\mathrm{BER} = \frac{1}{2} erfc(\sqrt{\mathrm{SINR}}) \tag{2.6}$$

$$\gamma = (erfc^{-1}(2\mathrm{BER_{min}}))^2 \tag{2.7}$$

2.1.3 MAC Layer

The network simulation uses a multiple access control (MAC) layer with p-persistent Carrier Sense Multiple Access (CSMA) in the simulations as a multiple access protocol. This is a non-centralized random-access MAC protocol used in broadcasting. If a node has a packet to send, it will sense the channel and decide if it is busy or idle. If the channel is idle, it will send it with a probability of p called the transmission probability. If the channel is busy, it will continue to sense it until it becomes idle. In the network simulation, a node that has a packet to send will sense the channel every time-slot, T_s, and will continue to do this until the channel becomes idle. A node decides a channel is idle if the received power, P_r, is less than a threshold P_r^th. The receiver sensitivity is the lowest power level at which the receiver can detect an RF signal and support a minimum FER, FER_min.

Changing the value of p to zero makes this non-persistent CSMA where the node will send a packet if the channel is idle and if the channel is busy it will wait for a random time to sense the channel again. By changing the value of p to one then this becomes 1-persistent CSMA where the node will send the packet if the channel is idle and if it is busy it will continuously keep sensing the channel until it becomes idle. P-persistent CSMA takes the best of both worlds, where it is not as aggressive as 1-persistent CSMA, therefore reducing collisions, however, it is more efficient

than non-persistent CSMA. It is important to note that since broadcast transmissions will be the focus of the work, there will be no acknowledgement (ACK) packet sent after each transmission and there is also no form of automatic repeat request (ARQ).

The use of p-persistent CSMA is common especially in WiFi [64] and some work proposes its use in SU networks [65]. The use of p-persistence CSMA also makes more sense for broadcasting since there is no use for the Clear-To-Send (CTS) and Request-To-Send (RTS) packets. [66] analyzes the performance of broadcasting using p-persistent CSMA. The work in this thesis intends to build on the application of broadcasting using p-persistent CSMA for SU networks by studying its performance within a PU network.

2.1.4 Network Layer

This subsection will discuss the two broadcast protocols used and the metrics used to compare them.

Flooding

Flooding is the process by which a node sends a packet to every other node in the network. An application of flooding is sending control packets to all nodes in the network. Another application is to share routing information that a node may have such as its routing table or information about its neighboring nodes. Recently, the use of flooding has become very common in collaborative communications. Here, nodes share information, with other nodes in the network, such as channel states or statistics of PU usage of channels. It is very important that as many nodes as possible receive these packets since there are no ACK packets after each transmission.

There are many variations of flooding and examples are gossip [67] and Optimal Flooding Protocol (OFP) [68]. GOSSIP sets a probability for a node to send a packet it received which reduces the number of packet transmissions if compared to flooding. This reduction in packet transmissions comes at a cost of reduced network coverage. OFP further reduces packet transmissions, however,

it assumes a node knows its relative location with respect to neighboring nodes. However, current wireless standards such as IEEE 802.11, still use regular flooding due to its simplicity [64].

This work will focus on regular flooding since it is the most widely used form of broadcast. In the simulation, the node in the center of the network will broadcast N_{p} packets to every single node in the SU network. Once a node receives a packet for the first time it will send it once but will drop it if it receives more duplicates of it. This process will continue until the source node has transmitted all N_{p} packets and all other nodes have transmitted all non-repeated packets they received.

Random Linear Network Coding (RLNC)

The first work to suggest NC was to improve network capacity [35]. NC aims to improve network capacity, effective data rates and can even help avoid network attacks and eavesdropping. NC is a technique used to combine several packets in a single packet. The receiving node receives many such packets and uses them to decode them to obtain the original packets.

The main difference between NC techniques is in the procedures used to combine the packets. Linear NC uses a linear combination of packets for transmissions. Most NC protocols use linear combinations since the decoding of non-linear NC is complex. Digital NC (DNC) combines packets at a bit level, usually by XOR-ing bits from different packets together [69]. Analog NC (ANC) adds packets together as analog signals before demodulation takes place [70]. These two methods can combine more than one packet, but to decode them multiple mixed packets need to be available. For this reason, most applications of these methods mix up to two or three packets.

Random Linear NC (RLNC), first introduced in [71], is a form of NC that mixes many packets together using Galois field math with a parameter q that describes the Galois field size. If the receiver knows the coefficients used for the combinations it can decode the packets. Each combination packet sent must therefore hold, as overhead, the coefficients used in the combination process. RLNC was introduced to achieve higher network capacity, however, its power in broadcasting will be made use of in this thesis.

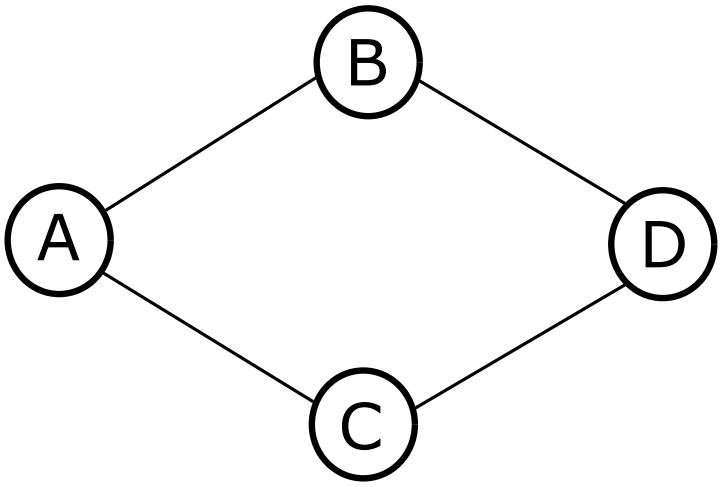

Figure 2.2: RLNC network example

A simple example can better explain how the simulations implement RLNC. Figure 2.2 shows a simple network with four nodes and the lines represent a wireless connection between the nodes it connects. Node A broadcasts two packets, F_1 and F_2, to all the other nodes in the network. Each packet has N_b bits which is divided into blocks, each of size q. Each block stands for an element of a Galois field of size 2^q and can be represented as bits, a polynomial, or an integer. For example, for $q = 3$ the 3 bits 101 can be represented as an integer, 5, or a polynomial, $x^2 + 1$. We will consider $F_1 = [F_{11} \quad F_{12}]$ and $F_2 = [F_{21} \quad F_{22}]$, where each packet has two blocks. Node A will send two packets $Y_{\mathrm{A}1}$ and $Y_{\mathrm{A}2}$ as shown in the equations below:

$$Y_{\mathrm{A}1}^{\mathrm{T}} = g_1 F_1^{\mathrm{T}} + g_2 F_2^{\mathrm{T}} = \begin{bmatrix} F_1^{\mathrm{T}} & F_2^{\mathrm{T}} \end{bmatrix} \begin{bmatrix} g_1 \\ g_2 \end{bmatrix} = \begin{bmatrix} F_{11} & F_{21} \\ F_{12} & F_{22} \end{bmatrix} \begin{bmatrix} g_1 \\ g_2 \end{bmatrix} = \begin{bmatrix} F_{11}g_1 + F_{21}g_2 \\ F_{12}g_1 + F_{22}g_2 \end{bmatrix} \tag{2.8}$$

$$Y_{\mathrm{A}2}^{\mathrm{T}} = g_3 F_1^{\mathrm{T}} + g_4 F_2^{\mathrm{T}} = \begin{bmatrix} F_1^{\mathrm{T}} & F_2^{\mathrm{T}} \end{bmatrix} \begin{bmatrix} g_3 \\ g_4 \end{bmatrix} = \begin{bmatrix} F_{11} & F_{21} \\ F_{12} & F_{22} \end{bmatrix} \begin{bmatrix} g_3 \\ g_4 \end{bmatrix} = \begin{bmatrix} F_{11}g_3 + F_{21}g_4 \\ F_{12}g_3 + F_{22}g_4 \end{bmatrix} \tag{2.9}$$

The first packet that node A sends holds, as overhead, the Galois field coefficients g_1 and g_2

and the second packet holds g_3 and g_4. Nodes B and C receive both packets $Y_{\mathrm{A}1}$ and $Y_{\mathrm{A}2}$, and will then generate their own coefficients and each will send two combined packets showed below:

$$Y_{\mathrm{B}1}^{\mathrm{T}} = g_5 Y_{\mathrm{A}1}^{\mathrm{T}} + g_6 Y_{\mathrm{A}2}^{\mathrm{T}} = (g_5 g_1 + g_6 g_3) F_1^{\mathrm{T}} + (g_5 g_2 + g_6 g_4) F_2^{\mathrm{T}} \tag{2.10}$$

$$Y_{\mathrm{B}2}^{\mathrm{T}} = g_7 Y_{\mathrm{A}1}^{\mathrm{T}} + g_8 Y_{\mathrm{A}2}^{\mathrm{T}} = (g_7 g_1 + g_8 g_3) F_1^{\mathrm{T}} + (g_7 g_2 + g_8 g_4) F_2^{\mathrm{T}} \tag{2.11}$$

$$Y_{\mathrm{C}1}^{\mathrm{T}} = g_9 Y_{\mathrm{A}1}^{\mathrm{T}} + g_{10} Y_{\mathrm{A}2}^{\mathrm{T}} = (g_9 g_1 + g_{10} g_3) F_1^{\mathrm{T}} + (g_9 g_2 + g_{10} g_4) F_2^{\mathrm{T}} \tag{2.12}$$

$$Y_{\mathrm{C}2}^{\mathrm{T}} = g_{11} Y_{\mathrm{A}1}^{\mathrm{T}} + g_{12} Y_{\mathrm{A}2}^{\mathrm{T}} = (g_{11} g_1 + g_{12} g_3) F_1^{\mathrm{T}} + (g_{11} g_2 + g_{12} g_4) F_2^{\mathrm{T}} \tag{2.13}$$

Node B sends the packets $Y_{\mathrm{B}1}^{\mathrm{T}}$ and $Y_{\mathrm{B}2}^{\mathrm{T}}$ while node C sends $Y_{\mathrm{C}1}^{\mathrm{T}}$ and $Y_{\mathrm{C}2}^{\mathrm{T}}$. The coefficients sent in these packets are the new combinations of the original packets. For example, the packet $Y_{\mathrm{B}1}^{\mathrm{T}}$ will have the coefficients $(g_5 g_1 + g_6 g_3)$ and $(g_5 g_2 + g_6 g_4)$ sent with it. Nodes B and C each received two packets and therefore they can also decode these packets. It is important to note that now node D will receive 4 packets even though it only needs 2 packets to be able to decode them. The extra packets are not redundant and can be used in case some packets are corrupted. It is in making use of multiple transmissions that lies the strength of RLNC.

To obtain the original packets, the received packets are decoded using Gauss-Jordan elimination since matrix inversion does not work with Galois field math. The fact that each node randomly generates coefficients, there is no guarantee that the final obtained coefficients will successfully decode the packets. This is equivalent to a matrix of coefficients not having a full rank in a system of linear equations. The higher the value of q, the higher the decoding probability is [72].

In the simulation, there is a single source node that broadcasts N_{p} packets each with N_{b} bits. N_{b} will be used as a multiple of q so that each packet can divided up evenly into blocks. If this is not the case, the use of zero padding can ensure this. If we consider the source node to be node 1, then let the data packets be will be $F_1 = [F_{11} \quad F_{12} \quad .. \quad F_{1\mathrm{N_b/q}}]$ to $F_{\mathrm{N_p}} = [F_{\mathrm{N_p}1} \quad F_{\mathrm{N_p}2} \quad .. \quad F_{\mathrm{N_pN_b/q}}]$ and

let the transmitted packets be mixtures of the data packets. The N_p transmitted packets will be Y_{11}, Y_{12}, .. and Y_{1N_p}, where $Y_{11}^T = [g_{11}F_1^T; \quad g_{12}F_2^T; \quad .. \quad g_{1N_p}F_{N_p}^T]$ and so on. Node 1 will randomly generate the coefficients each time. The other nodes will only send a packet every time they receive one irrespective of where it came from. They will each send a maximum of N_p packets and then stop. Any packet sent by a node is a combination of every single packet received thus far by that node. For example, consider a network with node 3 that is within the vicinity of node 1 and node 2. If it receives a packet from node 1, Y_{11}, it will immediately try and send a packet that will be $Y_{31} = g_{31}Y_{11}$. If it then receives another packet from node 1, Y_{12}, it will send $Y_{32} = g_{32}Y_{11} + g_{33}Y_{12}$. If it then receives a packet from node 2, Y_{21}, it will send $Y_{33} = g_{34}Y_{11} + g_{35}Y_{12} + g_{36}Y_{21}$. It is important to note that it generates each of its coefficients randomly. It also attaches the coefficients of the combinations of the original packets. For example, the coefficients that will be attached for Y_{31} are $g_{31}g_{11}$, $g_{31}g_{12}$, .. and $g_{31}g_{1N_p}$.

The main advantage that RLNC has over flooding is its ability to make use of repeated transmissions. The use of an example may help elaborate this point. In the case of flooding multiple packets, the first packet to be broadcast will spread through the network and we will call this the first wave of broadcasting. If a certain node does not get this packet in the first wave, then it has lost it and will not be able to recover it even if future broadcast packets are received multiple times by this node. With RLNC, if a node does not receive a combination packet in the first wave, it does not necessarily mean that it lost a data packet. If it does, however, receive many combination packets on future broadcast waves, the node benefits from this and can use these extra combination packets in the decoding of the original data packets.

With the advantages that RLNC has, there are some disadvantages as well. One is that the overhead in packets increases, since the coefficients used for mixing are attached to the packet. The other disadvantage is the increased processing involved in decoding the packet. The work in this thesis compared only transmission power and didn't consider extra energy required due to the extra overhead and the extra processing.

Flooding vs. RLNC

Here a more detailed description of the exact process that each node follows, in the simulation, will be explained regarding both flooding and RLNC. In general, both techniques assume no ACK or ARQ processes occur and therefore it is not necessary that 100% coverage is reached in every simulation. At a high-level observation, both simulations of the protocols behave in the exact same way and the only difference is what data is sent in each packet. Both the PU and SU networks will use a p-persistent MAC algorithm and every node will be assumed to have a packet to send at all times even if it is done with transmission of broadcast packets. However, if a node has a broadcast packet to send it will take priority over any other packets.

For flooding, we will differentiate between the source node and all other nodes. The source node will begin by having N_{p} packets to send. It will only send the first packet once it has access to the channel and once it does this it moves onto the next packet. It will keep doing this until it has transmitted all N_{p} packets. After this it will also try to access the channel but this time to send non-broadcast packets. Any other node will always try to access the channel as well. If it does not have any broadcast packets yet, it will send non-broadcast packets. Once it receives a broadcast packet, it will drop this packet if it has already received this packet before. If it is the first time to receive a packet, it puts it in a buffer that works on a First In, First Out (FIFO) basis. If this buffer has packets to be sent it will continue to try and send them and once its buffer is empty it will go back to trying to send non-broadcast packets. Each node may transmit only a maximum of N_{p} broadcast packets and it may be less than this if any packet is not received. Each node may receive and store a maximum of N_{p} broadcast packets and if any packet has not been received at least once by the end of the simulation then this will cause the network to not achieve 100% coverage.

For RLNC, the source node has N_{p} data packets to send. Every transmission it sends will be a combination of all these data packets. It will continue to access the channel and will send N_{p} broadcast packets that are each combinations of all data packets. Once it is done with this it will still try to access the channel but to send non-broadcast packets. The other nodes will send non-

broadcast packets until they receive a combination. Once they do they will be stored and remain in a buffer, however, unlike flooding every transmission will be a combination of each of the packets in the buffer. There is a counter that tracks the number of transmissions so far by this node. If the number of transmissions is less than the number of packets in the buffer, then it will keep transmitting until they are equal and will then go back to transmitting non-broadcast packets. This process will continue until the number of transmissions reaches N_{p} and then only non-broadcast packets will be sent. Another difference with RLNC is that each node can only decode the data packets when it has at least N_{p} packets in its buffer. For this reason, every packet received will be stored in the buffer and after it reaches a size of N_{p} it will try to decode the packets. If this fails it will attempt to decode when every new packet appears in the buffer. RLNC nodes will only send a maximum of N_{p} packets but may store an endless number of combination packets until successful decoding of the original broadcast packets has been done.

Broadcast Metrics

The main metric that will be used to compare between the two protocols is network coverage [66]. Network coverage is the average percentage of broadcast packets that arrived at each node in the network. For example, consider a network with a source node that will broadcast 10 packets in a network with 10 nodes other than itself. If all nodes receive all 10 packets, then that will be 100% coverage. If only a single node loses a single packet, then that will be 99% coverage.

In the results section, network coverage will be plotted against two other parameters, number of time-slots and energy per node. The coverage measured against time-slots will give the time efficiency of the protocol, i.e. how efficiently the broadcast will take place with respect to time. In other words, this will give an expectation of the number of time-slots needed to reach a certain network coverage. The coverage measured against the average energy used per node will give the energy efficiency, i.e. how much energy an average node in the network will use to broadcast. Similarly, this will give the expected energy a node will use to reach a certain network coverage.

Another metric that will be used is the 90% coverage time and 90% coverage energy per node.

This will be a more reasonable method to make comparisons since it may not be very straight forward to compare two plots and assess how similar or different they are to each other. This metric will be obtained from the plot by evaluating the values that correspond to 90% coverage on both the time-slot plots and energy per node plots.

2.1.5 Upper Layers

A few assumptions were made about the upper layers. One assumption is that any node will always have a packet to send, including the source node (after it finishes its N_{p} transmissions), but if a broadcast packet is available it will take the highest priority. This means that even though a node may have finished sending all the broadcast packets it was sending, it will try and access the channel again. Another assumption is that all sent packets occupy the channel for the same time, T_{f}, which will always be an integer number of time-slots. There is also no higher level acknowledge packet sent and no re-transmissions of packets.

2.2 Network Simulations

This section will present and discuss the network simulation results. There are two subsections. The first subsection will summarize the parameters that are used in the simulation. The second subsection will compare flooding and RLNC and study the effect of varying certain network parameters on the SU broadcasting performance.

Table 2.1 summarizes the parameters used in the simulation which are in accordance with the CR 802.22 standard [73]. The standard does specify operation within the TV bands, however, the frequency was assumed to be in the 2.4 GHz ISM band in the simulation. A path loss exponent value of 2.828 was used since this is what was measured in the gas refinery environment in Section 4.2.2. The maximum allowable transmission power depends on the country of operation; however, the standard specifies a transmission power range of at least 60 dB to allow for power control, and the maximum power must meet the regulatory limits. In the simulations, a fixed transmission

power was selected as 1 W (30 dBm) for all nodes. The noise power, $10\log(\sigma_n^2)$, was used as -82.83 dBm which is the same as the noise power measured at the ADC of the measurement equipment used in this thesis and was measured as descried in Section 4.3.2. The standard does not specify a value for P_r^{th} and it is dependent on receiver design but is usually chosen to be around 20 dB above receiver sensitivity [74]. A slightly stricter threshold was chosen as -70 dBm, about 12 dB above the average noise power. The value of the time-slot, T_s, was also chosen to be within the allowed ranges and such that the packet time, T_f, would be an integer multiple of the time-slot. A value of 1% for the FER_{min} was used as specified by the standard, and Equations 2.6 and 2.7 can be used to calculate the BER_{min} and γ respectively. The value of q was selected to give reasonable performance according to [72] and N_b was selected to be a multiple of q. All the results are averaged over 10000 simulations and each simulation generates a new realization of PU and SU networks.

The range of values used for p, T_f, and λ were selected to give reasonable network performance such that interference does not cause network coverage to drop significantly below 100%. The same network parameters were used for both the PU and SU networks.

The simulations will study the effect of varying the 3 network parameters, p, T_f, and λ for both the PU and SU networks, on network performance. The effect of network traffic is observed by varying p. The effect of the packet transmission time is observed by varying T_f. Finally, the effect of user density is observed by varying λ. For flooding, a broadcast wave for flooding will refer to a packet being sent from the source node in the center of the circle until the last node in the SU network sends this packet. For RLNC, a broadcast wave will refer to the start of a combination packet at a source node that will cause combination packets to be sent by every other node until the last node sends its respective combination packet. There is no ACK or ARQ mechanism implemented.

Table 2.1: Simulation parameters

Parameter	**Value**
L	100 m
f	2.4 GHz
α	2.828
P_{t}	30 dBm
$10\log(\sigma_{\mathrm{n}}^2)$	-82.83 dBm
$P_{\mathrm{r}}^{\mathrm{th}}$	-70 dBm
T_{s}	0.1024 ms
N_{b}	512
N_{p}	10
FER_{min}	1%
BER_{min}	$1.96\mathrm{x}10^{-5}$
γ	8.45 dB
RLNC block size	32
q	16

2.2.1 Effect of Network Parameters

This subsection will discuss the effect of changing network parameters on network coverage performance for flooding and RLNC. There are 3 subsections, one for each of the network parameters, namely p, T_{f}, and λ. T_{f} is always an integer multiple, s, of time-slots. Each of these subsections will discuss the effect of varying that parameter on flooding and RLNC for both timing and energy efficiency.

Effect of amount of traffic (p)

This simulation looks at the effect of p on the broadcast protocols. This parameter relates to the amount of traffic in the network. The closer the value is to 1 the more traffic and the closer it is to 0 the less traffic. This is true since every node is assumed to have a packet to send, even if it is not a broadcast packet, as described in the upper layers in Section 2.1.5. The values of s and λ are fixed at 5 and 10 nodes/A_{R}, respectively.

Figure 2.3 shows the coverage vs. time-slots plot for different values of p. The first observation is that RLNC is better than flooding for all cases of p and RLNC reaches 100% coverage while

flooding does not. The reason for this is that RLNC makes use of repetitions since they increase decoding probability, while for flooding, if a packet is not received, repetitions of other packets will not help with the lost packet. The second observation is that as p increases there is an increase in the number of transmissions and therefore faster coverage may be reached for both flooding and RLNC. The improvement by increasing p is reduced as you increase p since the number of collisions is increased. Lower values of p mean that the channel may be idle for longer periods of time which also reduces time efficiency for both protocols. An optimal value for p may be found for both RLNC and flooding that minimizes the number of time-slots needed to reach maximum coverage.

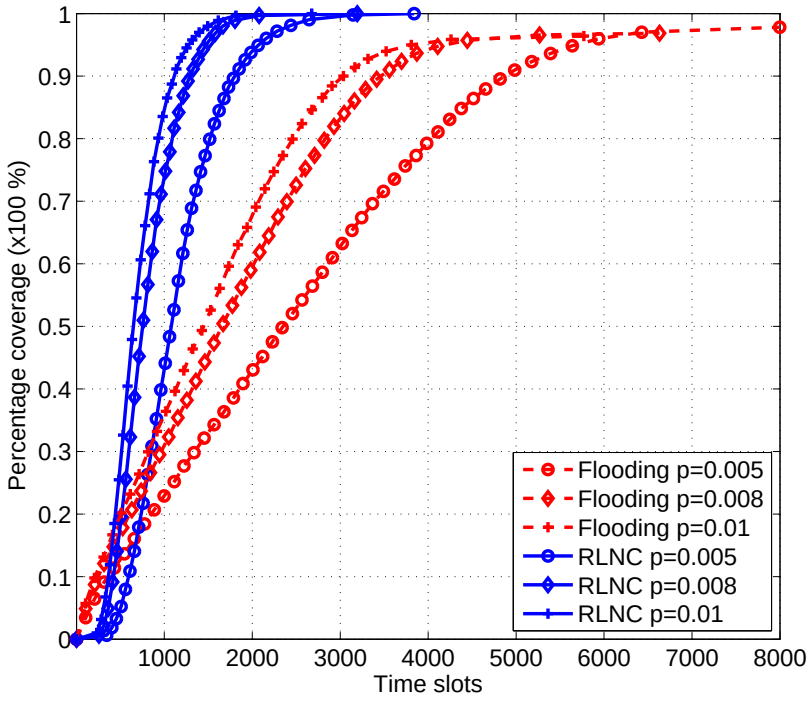

Figure 2.3: Effect of p on coverage vs. time-slots

Table 2.2 shows the average number of time-slots needed for 90% coverage. RLNC outperforms flooding in all cases of p and what is interesting in this comparison is that RLNC uses almost 36% of the time-slots that flooding uses and this value is independent of p. This will be referred

Table 2.2: Effect of p on time-slots for 90% coverage

p	0.005	0.008	0.01
Flooding	4805	3401	2972
RLNC	1716	1207	1061
Ratio	0.36	0.35	0.36

to as the RLNC efficiency ratio. This means that the RLNC efficiency ratio is not affected by the amount of traffic in the network given that T_{f} and λ are fixed.

Figure 2.4 shows a plot of coverage vs. energy per node. RLNC is also more efficient at broadcasting with less energy for all cases of p. There are 2 observations. One is that the shape of the curves for RLNC and flooding are different, and the other is that the energy efficiency is not a function of p. The slope of the curve is related to the energy efficiency, i.e. a larger slope means more coverage for less energy per node.

For RLNC, the curve has a small slope in the beginning, then it increases and finally decreases again towards the end of the simulation. In the beginning, there are many transmissions that will occur without resulting in any coverage increase since each node needs to collect at least N_{p} packets to start decoding. When the first node can successfully decode all N_{p} packets then a jump occurs in the coverage. It is for this reason flooding is better than RLNC in the beginning. After this point is reached, the slope is increased until towards the end of the simulation. The reason for this is that towards the end of the simulation, there may be nodes that have received N_{p} packets and it still may not be able to decode successfully, and more packets may be needed. These extra packets are extra energy that is used inefficiently to increase coverage, since more than N_{p} packets needed to be received to decode N_{p} packets.

For flooding, the relation between coverage and energy per node is almost linear. Here flooding differs from RLNC in that there is not much of a difference between the beginning of the simulation and the end. In the beginning, packet 1 is being broadcast and in the end packet N_{p} is being broadcast. If we consider there to be N_{CR} SU nodes, then in each broadcast wave there will be N_{CR}

transmissions given that each node receives this packet. This packet begins from the source node in the center of the area and slowly gets transmitted towards the edge of the circle in all directions. On average you will find that each of these transmissions adds to coverage equally and therefore the linear relation. This happens for every broadcast wave, whether it be in the beginning of the simulation or the end, and therefore it is almost linear at all coverage values.

For both RLNC and flooding, the energy efficiency decreases as p is increased. The reason for this is that as p increases, collisions increase and more transmissions, or energy per node, is necessary to attain the same coverage. Increasing p may cause quicker coverage but more energy per node will be needed for the same coverage.

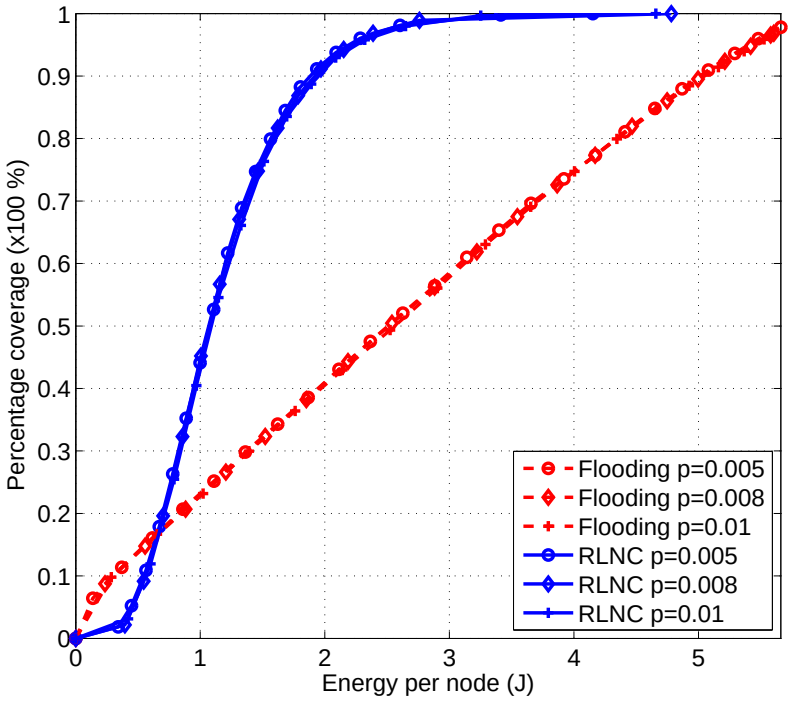

Figure 2.4: Effect of p on coverage vs. energy per node

Table 2.3 summarizes the average energy needed per node to reach 90% coverage. Again, RLNC is found to need only about 36% of the energy that is needed by flooding for 90% coverage.

Table 2.3: Effect of p on energy per node for 90% coverage

p	0.005	0.008	0.01
Flooding	5.02	5.04	5.05
RLNC	1.77	1.84	1.87
Ratio	0.35	0.37	0.37

This value is the same as that for the number of time-slots. This means that RLNC has an efficiency ratio which does not depend on the value of p.

To summarize, RLNC has better time and energy efficiency than flooding for all the cases of p. Regarding time efficiency, both RLNC and flooding improve as p increases but this improvement becomes less significant as p is increased. Regarding energy efficiency, both RLNC and flooding have lower efficiency as p is increased since more packets are lost in collisions. RLNC has a small slope in the beginning and towards the end of the simulation due to the way the decoding of packets works. For flooding energy efficiency, there is a linear relation between the coverage and energy per node. RLNC needs about 36% the number of time-slots and energy that flooding needs for 90% coverage and this value is independent of p.

Effect of packet transmission time (T_f)

Here we will look at the effect of packet transmission time on network coverage. The number of bits, N_b, will not change but R_b will and therefore T_f, since $T_\mathrm{f} = sT_\mathrm{s} = N_\mathrm{b}/R_\mathrm{b}$. T_f consists of an integer number of time-slots. The values of R_b used are 1, 0.5, and 0.33 Mbps to give s values of 5, 10, and 15, respectively. The value of T_f is varied for both the PU and SU networks. The values of p and λ are fixed at 0.005 and 10 nodes/A_R, respectively.

Figure 2.5 show that both techniques are very dependent on T_f and have better time efficiency for shorter packet times. The reason for this is that larger values for T_f mean that each transmission lasts longer, and full network coverage will take a longer time. The fact that the packet also lasts longer on the channel would mean that the probability of a collision occurring increases due to the hidden node problem. RLNC is more time efficient than flooding for all values of T_f.

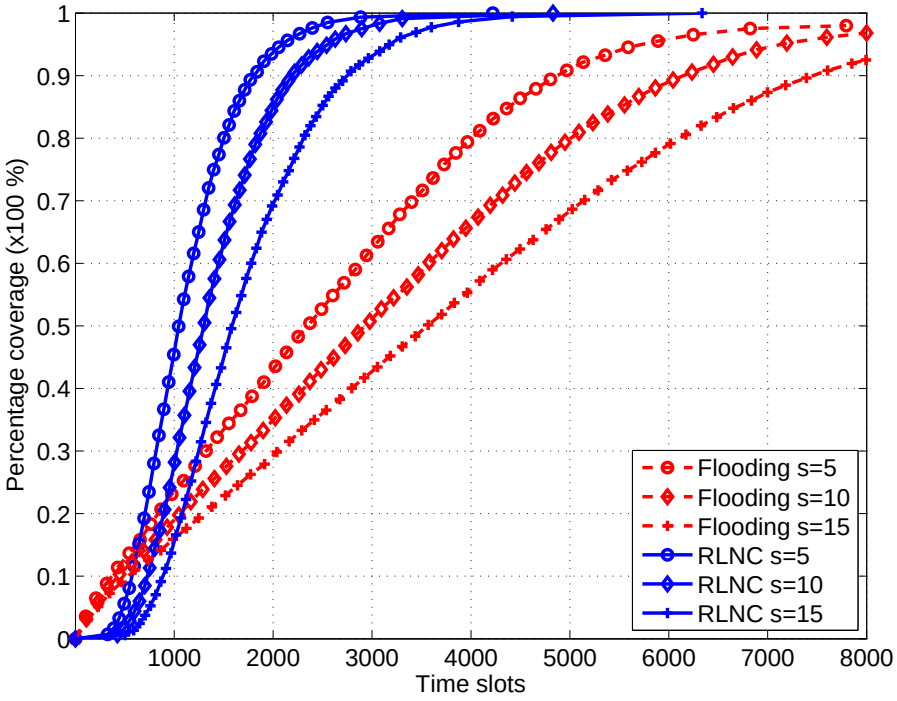

Figure 2.5: Effect of T_{f} on coverage vs. time-slots

Table 2.4: Effect of T_f on time-slots for 90% coverage

s	5	10	15
Flooding	4788	6097	7328
RLNC	1795	2157	2609
Ratio	0.37	0.35	0.36

Table 2.5: Effect of T_f on energy per node (J) for 90% coverage

s	5	10	15
Flooding	5.02	10.06	15.15
RLNC	1.89	3.69	5.55
Ratio	0.38	0.37	0.37

Table 2.4 also shows that RLNC always reaches 90% coverage at about 36% the number of time-slots it takes flooding, and this is not a function of T_f.

Figure 2.6 shows that RLNC and flooding are very dependent on T_f and are more energy efficient for shorter packet times. The reason for this is because the transmit power, P_t, is fixed and therefore increased packet times means that more energy is needed for the transmission of the same number of packets. Again, we see that the slope for RLNC depends on where you are in the simulation and flooding again has a linear relation for coverage and energy per node with a slope that is dependent on T_f.

Another observation that can be made from Table 2.5 is that when the packet length is doubled, from 5 to 10, or tripled from 5 to 15, the energy per node needed for 90% coverage doubles or triples for flooding. It is also a reasonable approximation to say the same happens for RLNC. This is because the number of transmissions needed for full coverage do not change but the power needed to send a single packet is proportional to its length in time.

Table 2.5 also shows that RLNC needs only about 36% of the energy flooding needs and it is not dependent on changes in T_f.

In summary, RLNC is more time and energy efficient than flooding for all values of T_f. Both

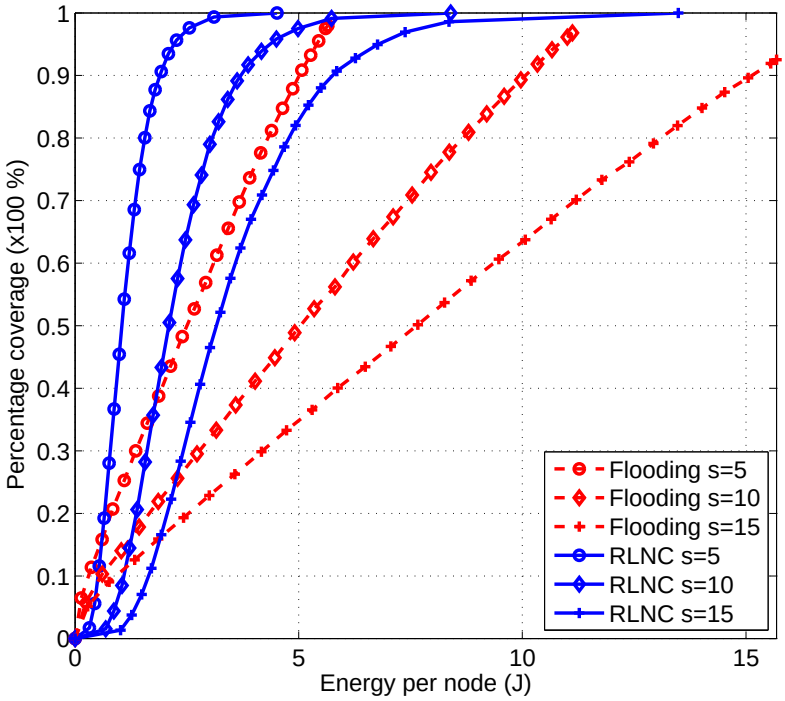

Figure 2.6: Effect of T_f on coverage vs. energy per node

protocols are very dependent on the value of T_f and are more time and energy efficient for smaller packet times. RLNC needs about 36% the number of time-slots and energy that flooding needs for 90% coverage and this value is independent of T_f.

Effect of node density (λ)

Here we discuss the effect of user density, λ, on the network coverage. The node density is changed for both the PU and SU networks. Increasing node density has very different effects on RLNC and flooding. Increasing node density means more interfering nodes competing for the channel and means more PU and SU nodes. The values of p and s are fixed at 0.005 and 5, respectively.

Figure 2.7 shows the effect that varying λ has on the time efficiency for both protocols. If we increase node density, the time efficiency for flooding reduces while for RLNC it increases. Increasing λ will cause more nodes to be in the network and closer to each other and a single transmission would mean more nodes receive that broadcast packet. There will be the same number of broadcast transmissions as there are SU nodes for each wave of broadcasts for both RLNC and flooding. For RLNC, each of these transmissions is a different combination of the original data packets and multiple packets received in the same wave of broadcasts adds to coverage. For flooding, the same packet keeps getting transmitted by different nodes for the same broadcast wave, meaning that a single broadcast wave takes longer, since each SU node must send the packet it receives in each wave. Each wave takes longer without adding to coverage significantly since the nodes are closer to each other and most nodes may have received it from the first few transmissions in the wave. It is important to note that for flooding, the time it takes for the N_p broadcast waves is not proportional to the user density since the second broadcast wave starts while the first is still occurring as described in Section 2.1.4. The effect increasing user density has is that it increases the time it takes for a broadcast wave which improves RLNC performance but reduces flooding performance.

Table 2.6 shows that increasing λ reduces the ratio of time-slots that RLNC needs with respect

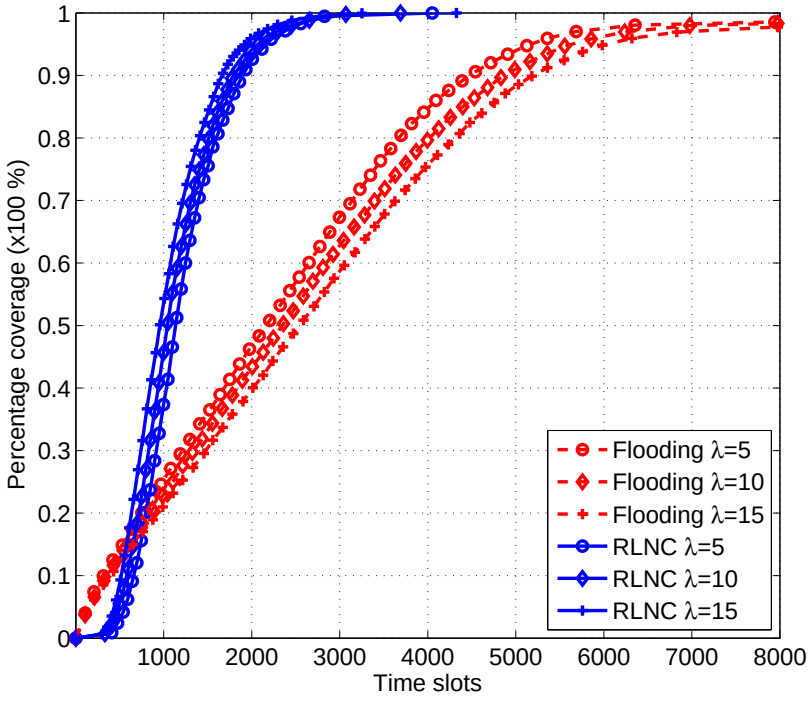

Figure 2.7: Effect of λ on coverage vs. time-slots

Table 2.6: Effect of λ on time-slots required for 90% coverage

λ	5	10	15
Flooding	4413	4878	5217
RLNC	1899	1769	1589
Ratio	0.43	0.36	0.30

Table 2.7: Effect of λ on energy per node (J) for 90% coverage

λ	5	10	15
Flooding	5.17	5.00	4.87
RLNC	2.21	1.86	1.47
Ratio	0.43	0.37	0.30

to flooding. Meaning that the RLNC efficiency ratio for time-slots increases as the node density increases.

Figure 2.8 shows the comparison for coverage vs. energy per node when λ is varied. Flooding also has a linear relation and there is a slight improvement in energy efficiency when node density is increased. When the user density is increased, more SU nodes will mean more transmissions per broadcast wave but the same energy per node will be needed, which will mean longer times for broadcast waves but the same energy per node is used for a broadcast wave. However, the fact that the SU nodes are closer to each other, slightly improves chances of more nodes getting the packets in the broadcast wave.

For RLNC, the energy efficiency is very dependent on λ and increases as the density increases. The reason for this is that each transmission adds to coverage more when there are more nodes to receive it. However, RLNC differs from flooding in that repeated packets add to coverage.

Table 2.7 also shows that the RLNC efficiency ratio for energy per node is improved as the node density increases.

To summarize, RLNC has better time and energy efficiency than flooding for all values of λ. Increasing λ improves the time and energy efficiency of RLNC, however, for flooding, increasing

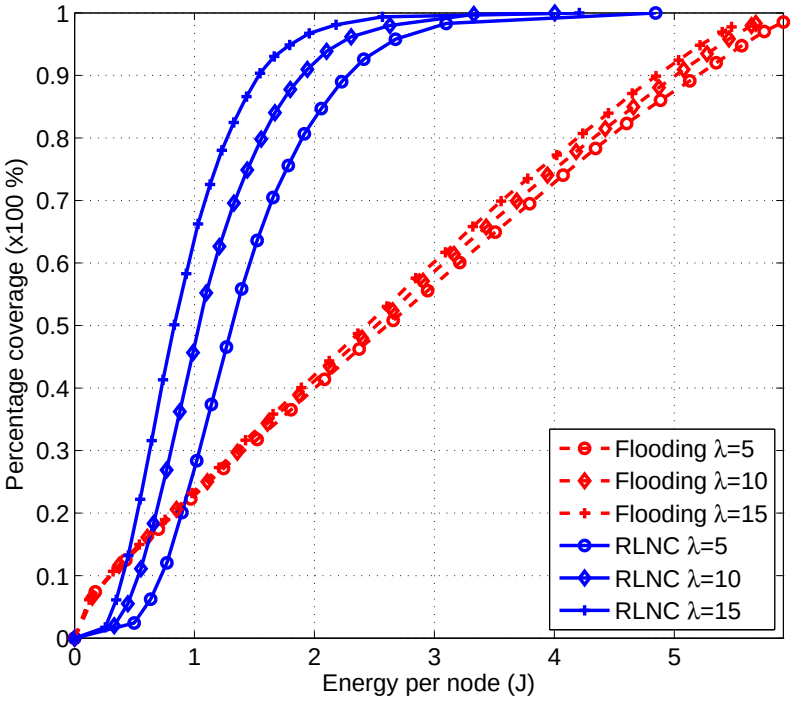

Figure 2.8: Effect of λ on coverage vs. energy per node

λ reduces time efficiency but slightly improves energy efficiency. The efficiency that RLNC has over flooding is increased as the node density is increased.

2.3 Conclusion

This section will summarize the conclusions reached by the simulation results. There are two main metrics used to compare RLNC and flooding, namely time and energy efficiency.

For time efficiency the following conclusions can be made:

1. RLNC outperforms flooding for all values of p, T_{f} and λ.
2. Increasing p improves time efficiency but this improvement becomes less significant the larger p becomes.
3. Both RLNC and flooding operate better for shorter frame times, T_{f}.
4. As λ increases, the timing efficiency for RLNC is improved while that of flooding is reduced.
5. The RLNC efficiency ratio for time-slots is only dependent on λ and increases as λ increases.

For energy efficiency the following conclusions can be made:

1. RLNC outperforms flooding for all values of p, T_{f} and λ.
2. The relation for coverage and energy per node is linear for flooding.
3. Flooding energy efficiency is only slightly reduced as values of p and λ are increased, however, it is almost linearly dependent on frame time, T_{f}.
4. RLNC energy efficiency is reduced for larger values of p and T_{f}, however, increases for higher values of λ.

5. The RLNC efficiency ratio for energy per node is only dependent on λ and increases as λ increases.

Chapter 3

Modeling PU Network Interference

Most work on CRs is more concerned with the effect that a SU network has on a PU network, which may be due to the strict requirements of a SU to minimize its interference on PU network. Little work has considered the PU network as an interference source with respect to the SU network, characterized this interference and studied the effects it would have on the performance of a SU network. Chapter 2 focused on the performance of the SU network at broadcasting in the presence of a PU network operating on the same band. This chapter will investigate the interference experienced by the SU network due to the PU network and propose a model that can synthesize this interference.

This chapter consists of five sections. The first section will describe the interference as a stochastic process and discuss the statistics that can be used to characterize it. The second section will give an overview of interference modeling and discuss related work. The third section will propose a model to synthesize interference signals produced by the PU network. The forth section is the results sections of this chapter. The last section will summarize the results in this chapter and discuss the most important conclusions.

3.1 Interference as a stochastic process

This section will describe the interference experienced by a SU network, due to a PU network, as a stochastic process. The section has 3 subsections. Section 3.1.1 will discuss the first and second order statistics of the interference. Section 3.1.2 will discuss the assumptions made about stationarity and ergodicity of the interference process. Section 3.1.3 will define the important interference statistics that will be continued to be used for the rest of the thesis.

Figure 3.1 shows two networks. On the left, there is a SU network represented by squares and

a PU network represented by triangles while there is only a SU network on the right. Both PU and SU networks are assumed to operate at the same band. The aim of this chapter is to model the interference experienced by SU nodes and synthesize their corresponding interference signals Z_1, Z_2, and Z_3 such that both SU networks, on the left and right, would have the same performance.

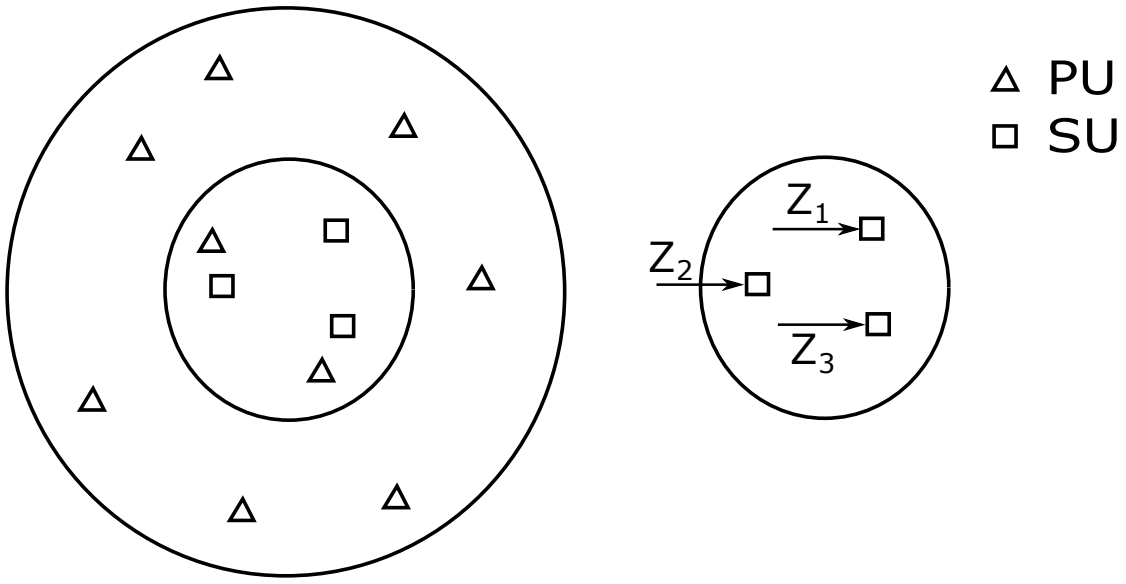

Figure 3.1: Real vs. synthesized interference

3.1.1 First and second order statistics

A node (PU or SU), i, will have location $(x_\mathrm{i}, y_\mathrm{i})$ where $i = 1, 2, .., N_\mathrm{CR}, N_\mathrm{CR}+1, .., N_\mathrm{CR}+N_\mathrm{PR}$. Equation 3.1 shows the received interference signal at SU nodes, $Y_\mathrm{i}(t)$ at node i, where α_ij is the pathloss between node i and node j, $S_\mathrm{j}(t)$ is the transmitted signal from node j, and $N_\mathrm{i}(t)$ is the Additive White Gaussian Noise (AWGN) at node i. At any given time, a SU node can receive interference that is from a PU node, SU node, or a combination of both. We will consider these signals to be stochastic processes with each signal being a realization from an ensemble of signals. The average power received by node i over a period, T seconds, is given by Equation 3.2 which is also a stochastic process. It is common to deal with averaged received power and examples that use this are metrics such as the Received Signal Strength Indicator (RSSI) and the Signal to

Interference plus Noise Ratio (SINR). For this reason, the signals that will be dealt with in this chapter are the average power received over a time T and this signal in general is continuous.

$$Y_{\mathrm{i}}(t) = \sum_{\mathrm{j}=1}^{N_{\mathrm{CR}}+N_{\mathrm{PR}}} \alpha_{\mathrm{ij}} S_{\mathrm{j}}(t) + N_{\mathrm{i}}(t), \quad i = 1,2,...,N_{\mathrm{CR}} \tag{3.1}$$

$$Z_{\mathrm{i}}(t) = \frac{1}{T} \int_{t-T}^{\mathrm{t}} |Y_{\mathrm{i}}(v)|^2 dv, \quad i = 1,2,...,N_{\mathrm{CR}} \tag{3.2}$$

The signal received by a SU may be the desired signal from another SU or just interference, from another PU or SU. Given that the received signal is interference, the process $Z(t)$ is the stochastic process describing the average interference power received by any given SU node from both the PU and SU networks. This interference is a function of the SU node's location (x_{i},y_{i}), the network realization, ζ, and time, t. The interference process should then be written as $Z_{\mathrm{i}}(\zeta,t)$. A network realization will be defined as a fixed number of nodes at fixed locations for both PU and SU networks. The use of ensemble averages will remove the dependence on ζ and therefore this term will be removed, and the interference will be written as $Z_{\mathrm{i}}(t)$.

The process $Z_{\mathrm{i}}(t)$ has a first order density function, denoted by $f_{\mathrm{i}}(z,t)$, which gives the relative probability for the average interference power value, z, occurring at a certain time instant, t. The density function in general may change with time, meaning that $f_{\mathrm{i}}(z,t_1)$ may be different from $f_{\mathrm{i}}(z,t_2)$, and it also depends on the location of the node i, $(x_{\mathrm{i}}, y_{\mathrm{i}})$. Density functions can be used to extract many statistical functions such as the first order moment or the mean of the stochastic process, shown in Equation 3.3, where $E[*]$ denotes the expected value or statistical average. This integral gives an ensemble average by integrating through all interference values of z for a given SU node's location $(x_{\mathrm{i}}, y_{\mathrm{i}})$ and a time t.

$$\mu_{\mathrm{i}}(t) = E[Z_{\mathrm{i}}(t)] = \int_{-\infty}^{\infty} z f_{\mathrm{i}}(z,t) dz \tag{3.3}$$

The entire ensemble of the stochastic process can be sampled at two separate times and at two separate locations giving the second order density function $f_{\mathrm{i}_1,\mathrm{i}_2}(z_1,z_2;t_1,t_2)$. Higher order

density functions exist but usually the first two orders are enough to characterize a stochastic process. The second order density function can be used to extract second order statistics such as the correlation, covariance, and the correlation coefficient. The correlation function, defined in Equation 3.4, measures the similarity between two samples of the stochastic process $Z_{i_1}(t_1)$ and $Z_{i_2}(t_2)$ at different locations, i_1 and i_2, and different times, t_1 and t_2. This gives a measure of the rate of change expected to occur between these two signals. If the calculation is made at the same node location, then it will be referred to as the auto-correlation, $R_i(t_1,t_2)$, while the term cross-correlation will refer to the correlation calculated at different node locations. It is important to note that usually the power of the signal at node i at time t_1 is $R_i(t_1,t_1)$, but in this case the signal we are dealing with is already a power signal and therefore this meaning cannot be attached to the auto-correlation.

$$\begin{aligned} R_{i_1,i_2}(t_1,t_2) &= E[Z_{i_1}(t_1)Z_{i_2}(t_2)] \\ &= \int_{-\infty}^{\infty}\int_{-\infty}^{\infty} z_{i_1} z_{i_2} f_{i_1,i_2}(z_{i_1},z_{i_2};t_1,t_2)\,dz_{i_1}\,dz_{i_2} \end{aligned} \tag{3.4}$$

The covariance is similar to the correlation, but the means are subtracted from their respective signals as shown in Equation 3.5. This usually gives clearer information about the expected rate of change than the correlation does. For zero mean signals, the correlation and the covariance are the same. If the calculation is made at the same node location, then $C_i(t_1,t_2)$ will be used and this will be referred to as the auto-covariance while cross-covariance will be used to mean the calculation was performed for different node locations.

$$\begin{aligned} C_{i_1,i_2}(t_1,t_2) &= E[(Z_{i_1}(t_1)-\mu_{i_1}(t_1))(Z_{i_2}(t_2)-\mu_{i_2}(t_2))] \\ &= R_{i_1,i_2}(t_1,t_2) - \mu_{i_1}(t_1)\mu_{i_2}(t_2) \end{aligned} \tag{3.5}$$

The correlation coefficient, defined in Equation 3.6, is obtained by dividing the covariance by the standard deviation of each signal, which is defined in Equation 3.7. The correlation coefficient has a value between -1 and 1, where 1 means perfect positive correlation, -1 means perfect negative

correlation, and 0 means uncorrelated. Again, if the calculation is made at the same node location, it will be referred to as the auto-correlation coefficient $\rho_{\mathrm{i}}(t_1,t_2)$, while cross-correlation coefficient will mean the calculation was performed on different node locations. It is important to note that all the second order coefficients are functions of t_1, t_2, x_{i_1}, y_{i_1}, x_{i_2}, and y_{i_2} but will be written in terms of t_1, t_2, i_1, and i_2 for simplicity.

$$\rho_{\mathrm{i}_1,\mathrm{i}_2}(t_1,t_2) = \frac{C_{\mathrm{i}_1,\mathrm{i}_2}(t_1,t_2)}{\sigma_{\mathrm{i}_1}(t_1)\sigma_{\mathrm{i}_2}(t_2)} \tag{3.6}$$

$$\sigma_{\mathrm{i}}^2(t) = E[Z_{\mathrm{i}}^2(t)] - \mu_{\mathrm{i}}^2(t) \tag{3.7}$$

3.1.2 Stationarity and Ergodicity

The statistics discussed above were all a function of time, t, and location, i, and therefore there are two dimensions we will consider when dealing with stationarity and ergodicity. The definition of stationarity depends on which statistics are independent of time or space. A process is Strict Sense Stationary (SSS) in time or space, if all higher order density functions, and therefore higher order moments as well, are independent of time or space, respectively. Another definition of stationarity is for a Wide Sense Stationary process (WSS) process in time or space, where only the mean and covariance are independent of time or space, respectively.

Let us consider a process that is WSS in time, then and the mean and standard deviation can be written as μ_{i} and σ_{i}, respectively. The second order statistics would not be functions of t_1 and t_2 but only the time difference, $\tau = t_2 - t_1$. The correlation, covariance, and correlation coefficient would become $R_{\mathrm{i}_1,\mathrm{i}_2}(\tau)$, $C_{\mathrm{i}_1,\mathrm{i}_2}(\tau)$, and $\rho_{\mathrm{i}_1,\mathrm{i}_2}(\tau)$, respectively.

For a process that is WSS in space, the first order statistics will be independent of location, and the mean and standard deviation can be written as $\mu(t)$ and $\sigma(t)$, respectively. The second order statistics would not be a function of node locations i_1 and i_2 but of the distance between them,

$d = \sqrt{(x_{i_1} - x_{i_2})^2 + (y_{i_1} - y_{i_2})^2}$. The correlation, covariance, correlation coefficient would become $R(d, t_1, t_2)$, $C(d, t_1, t_2)$, and $\rho(d, t_1, t_2)$, respectively.

If the process is WSS in both time and space, then the first order statistics would all become independent of time and location and the second order statistics would only be dependent on the differences in time and distance. This would mean that the first order statistics would become μ and σ, and the second order statistics would become $R(d, \tau)$, $C(d, \tau)$, and $\rho(d, \tau)$. The stationarity assumption simplifies calculations of the statistics since they can be performed at any time and at any location for first order statistics, and only consider time differences and relative node distances for second order statistics.

Ergodicity can also be defined for time and space for the interference process. The definition of ergodicity is made with regards to a specific statistic, for example, a process can be ergodic in the mean, or ergodic in the correlation etc. For a process to be considered ergodic for a specific statistic, then it is necessary but not sufficient for it to be stationary for that statistic. In general, a process is time ergodic in a specific statistic if the that statistic is stationary in time and can be calculated by either averaging over all ensembles or averaging over a large enough time for a single realization from the network ensemble. Ergodicity in space for a certain statistic would mean that the statistic is stationary in space, and the statistic can be calculated by taking an ensemble average or by averaging in space over all node locations for a single realization from the network ensemble. Slutsky's theorem provides a sufficient condition for a process to be ergodic for a particular statistic.

For the interference process, each network realization would have a different number of nodes and locations. The ergodicity definition does not hold because no matter how long a single fixed network operates for, it will never produce all possible interference signal values. If a single network realization was defined as a network that varies in time with regards to the number of nodes and their locations, then this would be a different case. However, since ergodicity does not hold for time and space, averages over time alone or space alone will not be correct.

The work in [75] and [76] has shown that when a homogenous PPP is used for node placement then the interference generated by this network is stationary both in time and space for infinitely large networks. The simulations performed in this chapter will not have infinitely large networks and therefore are not exactly stationary. To minimize the effect of the limited network size, the SU network is chosen to be small enough with respect to the PU network. This was done by choosing a SU network size that causes no significant difference in the interference experienced by a node at the center of the SU network and one at its edge. A SU network with a radius half of that of the PU network was enough to have a difference in the mean between a node at the center and edge to be less than 0.5 dB. The stationarity assumption will be shown to be reasonable one in this subsection, and this will simplify calculations of the interference statistics.

In this subsection, network simulations will be used to test the stationarity assumptions in time and space. Simulations will be performed exactly as described in Section 2.2 with the parameters $p = 0.005$, $s = 5$ and $\lambda = 10$ nodes/A_{R}, and PU and SU networks will be operating and causing interference except that there will be no central node broadcasting packets. Additionally, there will be 21 listening nodes placed in the SU region and will only record the interference they observe. Node 1 will be placed in the center of the network and the remaining 20 nodes will be randomly placed in the SU network region. Two statistics will be estimated from the simulations, namely the mean $\mu_{\mathrm{i}}[n]$ and the auto-correlation $R_{\mathrm{i}}[n_1, n_2]$. In this chapter, the interference observed by a node i at location $(x_{\mathrm{i}}, y_{\mathrm{i}})$ will be stored in an MxN matrix, $\mathbf{I}_{\mathrm{i}}$, where M is the number of simulations and N is the number of time-slots per simulation. The number of simulations used in this subsection are $M = 1000000$ and each simulation will be performed for $N = 100$ time-slots. There will be two test scenarios performed, one to test for stationarity in time and the other stationarity in space.

Testing for Stationarity in Time

To test the stationarity in time, only the interference signal of first listening node $i = 1$ will be used, $\mathbf{I}_1$. The mean in Equation 3.3 can be estimated using $\hat{\mu}_1[n] = \frac{1}{M}\sum_{m=1}^{M}\mathbf{I}_1(m,n)$, which

is a 1xN vector that represents the mean at location 1 calculated at N different time-slots. The value of the estimated mean plotted against time-slots is shown in Figure 3.2. There are two main observations that can be made. The first is that the mean, $\mu_1[n]$, does not vary significantly with time, remaining within a range of 0.5 dB, and can be assumed to be stationary with time. The mean can therefore be written as $\hat{\mu}_1 = \frac{1}{MN}\sum_{m=1}^{M}\sum_{n=1}^{N}\mathbf{I}_1(m,n)$ and can be calculated by averaging over all time-slots and all simulations. The second is that there is a transient time at the beginning of the simulation which is caused by the fact that the first time-slot, unlike any other time-slot, will always be considered idle for all nodes. Therefore, all statistics extracted from simulations in this chapter will be only be considered after 20 time-slots to ensure the transient period has passed.

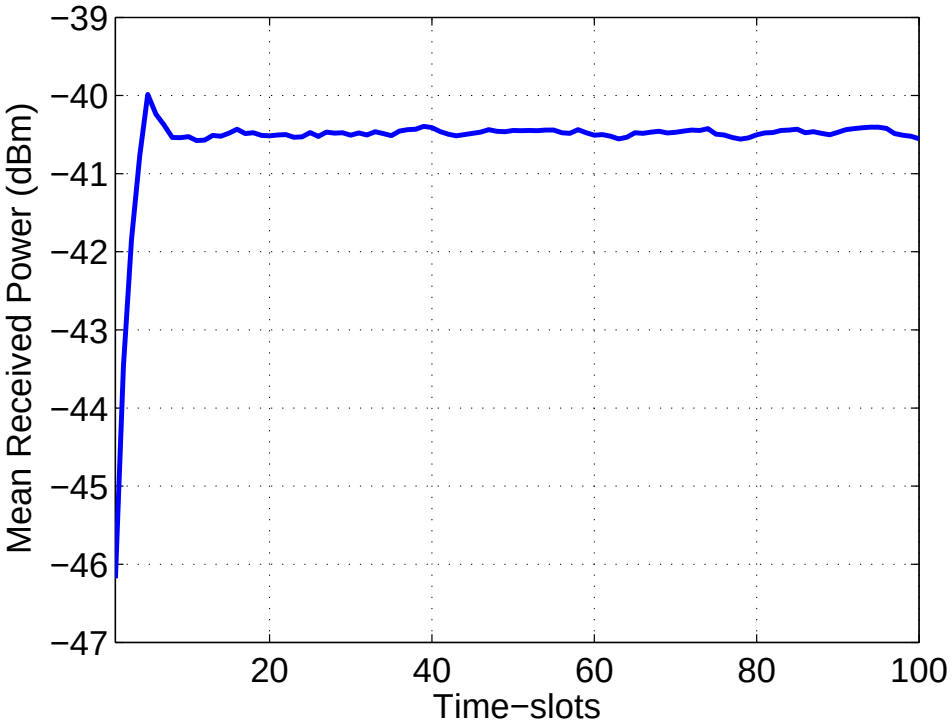

Figure 3.2: Stationarity of mean with time

The second statistic will be the auto-correlation coefficient for node 1 and an estimate of Equation 3.6 is the Pearson estimate given by $\hat{\rho}_1[n_1,n_2] = \frac{1}{M}\sum_{m=1}^{M}(\mathbf{I}_1(m,n_1)\mathbf{I}_1(m,n_2) - \hat{\mu_1}^2)/\hat{\sigma_1}^2$. The variance, given in Equation 3.7, is also assumed to be stationary with time, like the mean, and

can be estimated using $\hat{\sigma_1}^2 = \frac{1}{MN}\sum_{m=1}^{M}\sum_{n=1}^{N}\mathbf{I}_1^2(m,n) - \hat{\mu_1}^2$. A mesh plot of $\hat{\rho}_1[n_1,n_2]$ is shown in Figure 3.3 for the values of n_1 and n_2 from 20 to 40 to avoid the transient period. For the auto-correlation coefficient to be stationary with time, the auto-correlation coefficient must not change for any constant value $n_1 - n_2 = \tau$. This is the same as saying that all slices of the plot, $n_1 - n_2 = \tau$, are the same, and this can be said to be a reasonable assumption. The auto-correlation coefficient can therefore be estimated for node $i = 1$ as $\hat{\rho}_1[\tau] = \frac{1}{M(N-\tau_m)}\sum_{m=1}^{M}\sum_{n=1}^{N-\tau+1}(\mathbf{I}_1(m,n)\mathbf{I}_1(m,n+\tau) - \hat{\mu_1}^2)/\hat{\sigma_1}^2$. The auto-correlation function, if sliced at any $n_1 - n_2 = \tau$, will give a triangular shaped function.

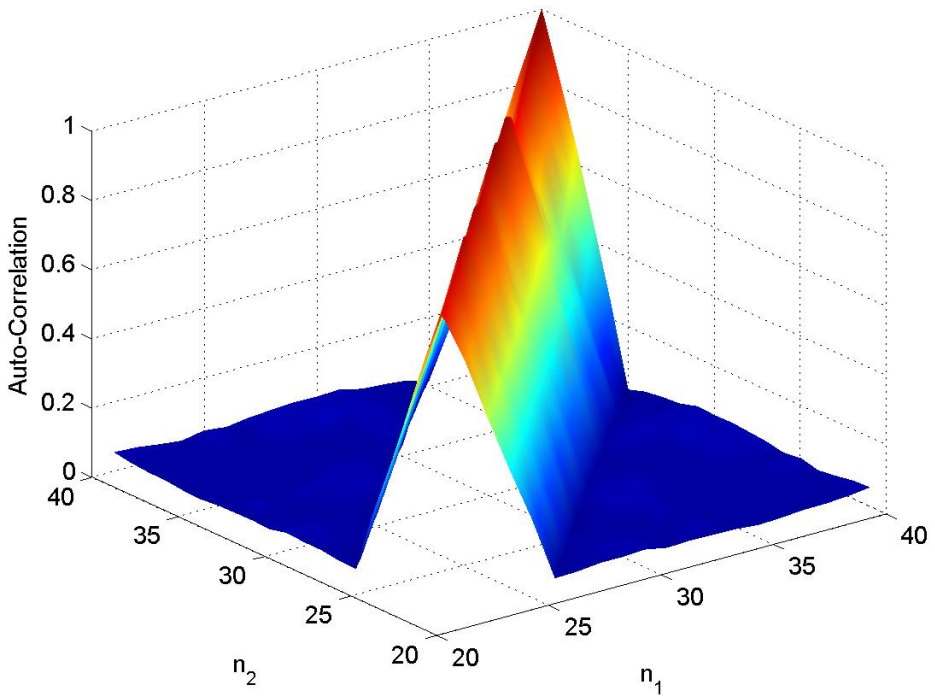

Figure 3.3: Stationarity of auto-correlation coefficient with time

Testing for Stationarity in Space

This section will build on the assumption that the mean and auto-correlation coefficient are

stationary in time. The means $\hat{\mu_2}$, $\hat{\mu_3}$, .., $\hat{\mu_{21}}$, are calculated for the remaining 20 randomly placed nodes (excluding node 1), using $\mathbf{I}_2$, $\mathbf{I}_3$, .., $\mathbf{I}_{21}$. The mean value obtained by each node is plotted against the node number in Figure 3.4. The mean value does not change drastically for a change in node location and remains within 0.5 dB which means that the assumption that the mean is not a function of node location is a reasonable one. This simplifies calculations and allows the mean to be calculated at any node location and at any time-slot.

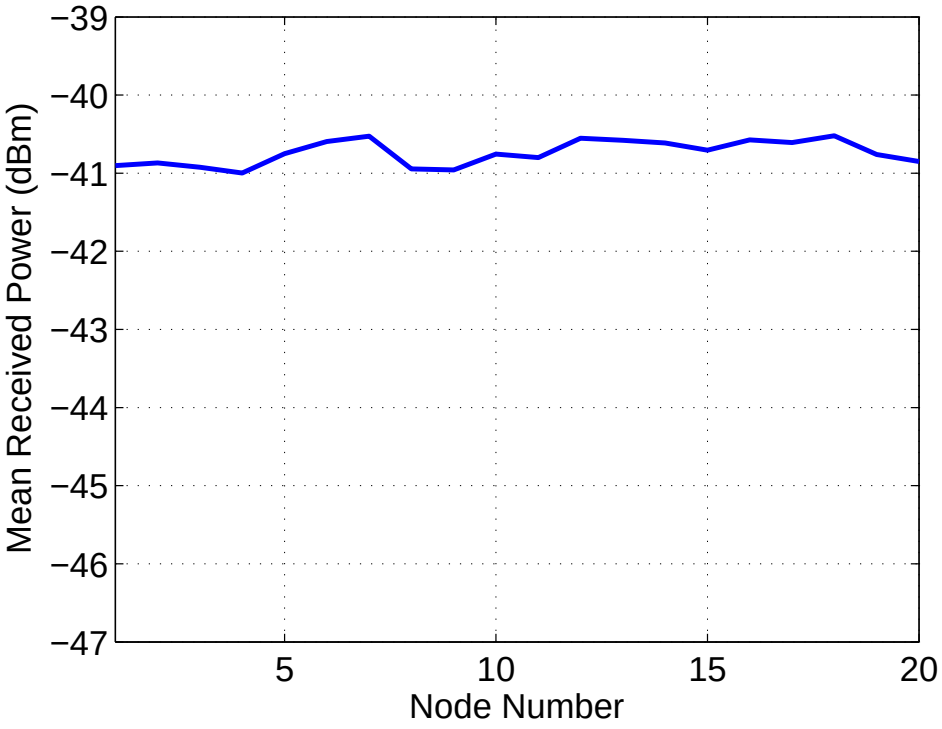

Figure 3.4: Stationarity of mean with space

The stationarity of the auto-correlation coefficient in time will be built on here and it will only be calculated in terms of τ, the lag between the signals. The auto-correlation coefficient was calculated for all 21 nodes and all these functions were plotted in Figure 3.5. The auto-correlation is seen to not change depending on the location of the node and the auto-correlation coefficient can be assumed to be stationary in space. Another important conclusion that can be made is that the

auto-correlation coefficient can be approximated to be a triangular function with the width having a value of s, the number of time-slots the packet occupies.

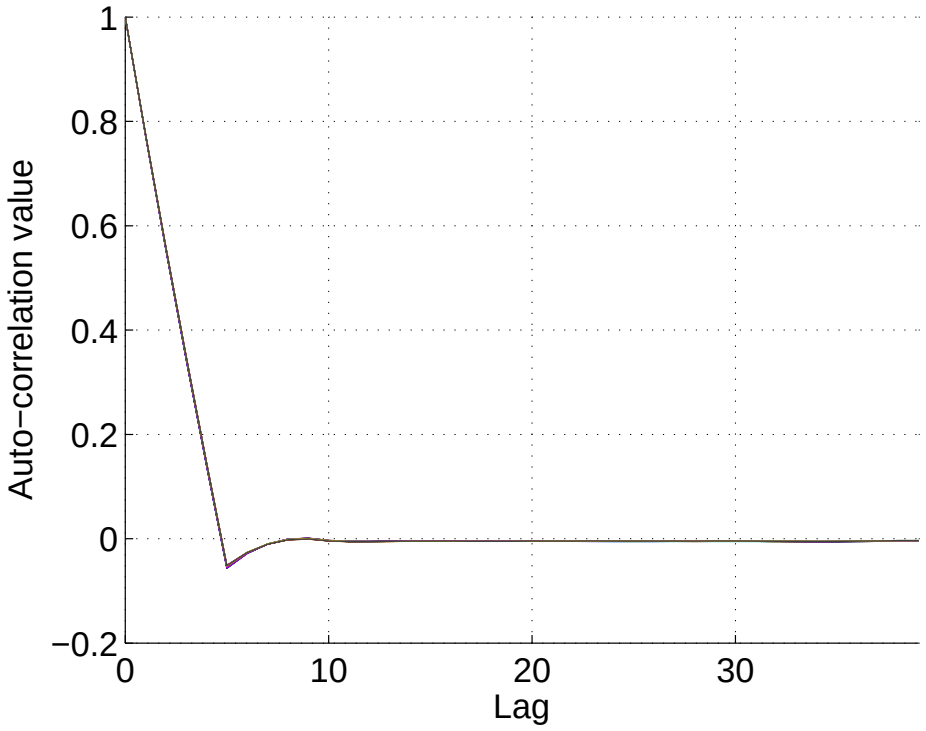

Figure 3.5: Auto-correlation coefficient for all nodes

Another test for stationarity of the auto-correlation coefficient in space will be done by comparing the auto-correlation coefficient of node 1, $\hat{\rho}_1[\tau]$, to all other nodes, 2 to 21. The Mean Square Error (MSE) between the auto-correlation coefficient of node 1 and every other node will be calculated and plotted against node number in Figure 3.6. The value of the MSE can be assumed to not change depending on node location which means that irrespective of where the auto-correlation coefficient was calculated, a maximum variation is expected. The value of the MSE is not meant to indicate anything since there is noise in the interference signals used, however, the important point is that the value of the MSE does not significantly change with location.

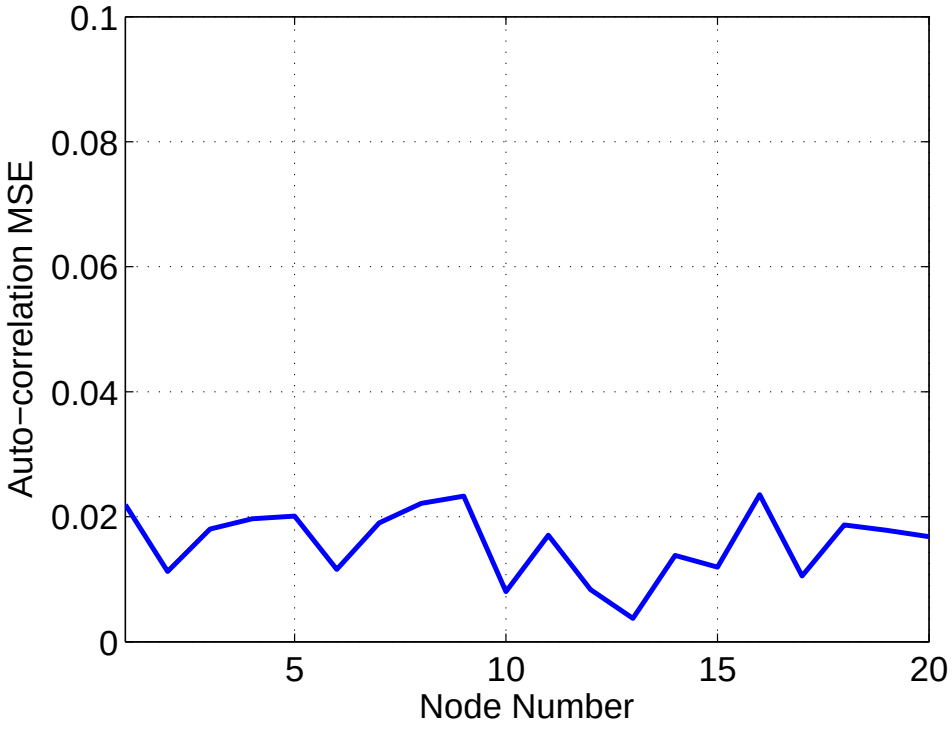

Figure 3.6: MSE between auto-correlation coefficients

3.1.3 Interference statistics of interest

The interference process, in general, is a continuous time signal as seen by the average interference power in Equation 3.2. The simulations in this chapter will deal with discrete signals and so the interference will now be defined as the average received interference power over the previous time-slot, T_s, shown in Equation 3.8. The interference will be changed to a discrete-time stochastic process where n will be an integer counter used to describe time as $t = nT_s$ and the interference can be written as $Z_i[n]$. The interference will be assumed to WSS in time and space and this was shown to be a reasonable assumption in Section 3.1.2 and therefore all interference statistics will independent of location and time (i, and n).

$$Z_i[n] = \frac{1}{T_s} \int_{(n-1)T_s}^{nT_s} |Y_i(v)|^2 dv, \quad i = 1, 2, ..., N_{CR} \tag{3.8}$$

There are 3 main interference statistics that are going to be used in the rest of this thesis. The first interference statistic is the first order density function, $f(z)$, defined in Section 3.1.1, and the term Probability Density Function (PDF) will refer to this. This is the probability that any SU node would receive a certain interference power. The second statistic is the correlation coefficient, defined in Equation 3.6, calculated at the same node location, $d = 0$. The term Auto-Correlation coefficient Function (ACF) will be used and it will be estimated using Equation 3.9, where τ_m is the maximum lag, M is the number of simulations used, N is the number of time-slots used in each simulation, the mean is given in Equation 3.11, and the variance is given in Equation 3.12. The ACF is a discrete function that is only a function of the integer lag between the signals. This function is assumed to be stationary in time and space and therefore the node index is dropped from it. This represents the temporal correlation between an interference signal and itself. The third statistic is the correlation coefficient calculated at $\tau = 0$ and between two nodes that have a distance d between them. The term Cross-Correlation coefficient Function (CCF) will be used to refer to this and it is given by Equation 3.10 and it is continuous and is only a function of the relative distance between the two nodes. This represents the spatial correlation between different

interference signals and the stationarity in space assumption means the function will only be a function of relative distance and the calculation can be made irrespective of the locations of nodes i_1 and i_2. The PDF, ACF and CCF will be referred to as the statistical functions of the interference process.

$$\hat{\rho}_{\mathrm{a}}[\tau] = \hat{\rho}[d=0,\tau] = \frac{1}{M(N-\tau_{\mathrm{m}})} \sum_{m=1}^{M} \sum_{n=1}^{N-\tau_{\mathrm{m}}+1} (\mathbf{I}(m,n)\mathbf{I}(m,n+\tau) - \hat{\mu}^2)/\hat{\sigma}^2 \tag{3.9}$$

$$\hat{\rho}_{\mathrm{c}}(d) = \hat{\rho}(\tau=0,d) = \frac{1}{MN} \sum_{m=1}^{M} \sum_{n=1}^{N} (\mathbf{I}_{\mathrm{i}_1}(m,n)\mathbf{I}_{\mathrm{i}_2}(m,n) - \hat{\mu}^2)/\hat{\sigma}^2 \tag{3.10}$$

$$\hat{\mu} = \frac{1}{MN} \sum_{m=1}^{M} \sum_{n=1}^{N} \mathbf{I}(m,n) \tag{3.11}$$

$$\hat{\sigma}^2 = \frac{1}{MN} \sum_{m=1}^{M} \sum_{n=1}^{N} \mathbf{I}^2(m,n) - \hat{\mu}^2 \tag{3.12}$$

3.2 Modeling Interference

Section 3.1 discussed the statistics of the interference process and discussed the stationarity assumption of the interference process. This section has 2 subsections and will give an overview of the importance of modeling interference, in Section 3.2.1, and will also give a discussion on related work, in Section 3.2.2.

3.2.1 Overview

Wireless network simulations are used often to test network protocols and study network performance. Models exist for many aspects of the network such as node placement, inter-arrival times of packets, packet lengths, noise, and interference. The more accurate the models for any given aspect, the closer the simulated network performance will be to practical network performance. Accuracy is important, but simplicity is also very important in deciding the usability of the model.

Simulating a SU network under the effect of PU interference would mean simulating a PU network with all its protocols just to create interference. This is possible, but if an accurate model allowed interference signals to be synthesized to produce the same SU performance then that would simplify simulations. The aim of the proposed interference model is to synthesize interference signals for a simulation with multiple SU nodes taking into the consideration the parameters of the PU network creating the interference. To our knowledge, no interference model exists that allows this.

The effectiveness of the interference model will be decided by comparing the synthesized interference to interference that has been produced by a simulated PU network. The network performance of a SU network using the synthesized interference should be like the performance if interference from a simulated PU network was used instead. The comparison metrics here will be the same coverage plots (in Chapter 2) for broadcast protocols for a SU network.

The PDF is critical in reproducing any stochastic process. Creating a signal, given that the PDF is known, is a straightforward process. Each sample of the signal would be produced by selecting a value from the PDF with its respective probability of occurring. The true PDF of a stochastic process is usually complicated and therefore a mathematical model will often be used to approximate the true PDF. Any value of interference at a given time could have been a result of a single, multiple or no transmission and therefore the PDF is expected to depend on the PU network parameters.

The importance of the PDF of a process may be more obvious when it comes to synthesizing interference, however, the ACF of the synthesized interference and how it relates to the PU network parameters is also very important. A good ACF model is necessary to ensure that a simulation of complex protocols using the synthesized interference yields realistic results. The temporal correlation of the interference will dictate how long a node can utilize a channel and therefore would affect its throughput.

The CCF is also a very important statistical function and it greatly affects the network perfor-

mance of a SU network with synthesized interference. The reason for this is that nodes within the same proximity should have correlated interference. Most of the time they should simultaneously observe close interferers and keep silent or simultaneously observe idle channels and attempt to send packets. If the interference they receive is uncorrelated their responses would be unrealistic and so would the network performance. The model will allow the synthesis of multiple interference signals that each individually meet the required PDF and ACF, while being correlated with each other according to their relative distances and the CCF and relate these statistical functions to the parameters of the PU network causing the interference.

3.2.2 Related Work

Extensive research exists on the PDF of interference received from a group of interfering nodes. A famous distribution is the Middleton model [39]. Another famous distribution used for characterizing this interference is a stable distribution [40–42]. In [77], the interference distribution was simplified by only considering the most dominant interfering node. Other distributions that have been used include Gaussian [43], K-distribution [44] and log-normal [45]. These models vary in complexity, but they just model the PDF and make it difficult to simultaneously consider other statistical functions such as the ACF and the CCF.

Most work on interference modelling has been on the PDF of the process. There has been less work done on modelling the ACF of the interference. The work in [46] considered the autocorrelation of interference. In [47] they derived a temporal correlation coefficient in an ALOHA network. The work in [38] also produced a temporal correlation coefficient. However, these coefficients have complex integrals and are not easy to produce. Current ACF models have an issue with their usability in synthesizing real interference and simultaneously using it with other interference statistical functions.

Little work has been done on the correlation of interference signals with distance in a random-access network. An analytical model for the cross-correlation of the shadowing experienced between nodes as a function of the relative distance between them was given in [78]. The work in [47]

produced a spatial-temporal correlation coefficient. The work in [38] also produced a spatial and time correlation coefficient that was later used for a cooperative CR spectrum sensing algorithm. Also, these coefficients are extremely complex to calculate. They also do not give a method to produce interference signals that follow these correlation coefficients and simultaneously model the other statistical functions.

There is a gap in previous research on the simultaneous modeling of all 3 statistical functions. There are also no proposed methods to synthesize network interference that take into consideration the 3 statistical functions and relate them to the parameters of the network creating them. There is also a lack in research available on how interference models affect simulated performance of certain network protocols. This chapter will propose an interference model that synthesizes interference that meet the required PDF, ACF, and CCF and relate them to the parameters of the PU network. These interference signals will be shown to produce SU network performance that is similar to that of a SU network with interference signals from simulated PU networks. The reason there is difficulty in synthesizing interference with the desired PDF, ACF and CCF, is that using methods such as filtering or Cholesky decomposition, to attain the required ACF or CCF would result in the PDF being distorted. The proposed model will resolve this issue.

To understand the difficulties that arise when trying to model multiple statistical functions simultaneously, a few examples will be given. For a given node i_1 and 1 simulation realization, the interference could be stored in the 1xN vector, $\mathrm{I}_{\mathrm{i}_1}$. A known method where you can produce a signal with a required PDF and ACF is described in [79]. This method works by making each value in this vector follow a certain PDF, and randomly swapping two samples, in the vector, and calculating the new ACF and comparing it to the desired ACF. Any swap that gets you closer to the desired ACF is kept and if it does not, then the swap is taken back. This process will be repeated until a reasonable level of error is reached. This process is considerably slow; however, it is possible to create interference for each SU node that has the desired PDF and ACF simultaneously. This, however, does not allow for each signal to have the cross-correlation between them that

corresponds to the relative distance between the respective nodes. A slow solution to this is to place all interference vectors, one for each node, horizontally in a matrix and using two-dimensional swapping. After each swap you would simultaneously test the CCF between each row and the ACF of each row and deciding whether to keep this swap or not. This method was implemented, and an error criterion created to in-cooperate both the ACF and CCF, but the process was found to be extremely slow and impractical.

Another method that could work on the PDF and ACF simultaneously is the use of a Weiner filter [80]. The Weiner filter allows you to create a signal with the desired ACF, however, it requires that the signal used have a Gaussian PDF. If you do use the Gaussian PDF assumption it still does not solve the CCF requirement between each signal. A more complex two-dimensional filtering process that will simultaneously keep the PDF unaffected, reach the desired ACF of each row and have each row correlated with a value that corresponds to the relative node distances was not found.

3.3 Proposed Interference Model

This section will explain the proposed interference model for a random-access network. There are 2 subsections. The first will describe the different parameters of the model and describe the algorithm by which the model synthesizes interference. The second will have derivations for the necessary parameters used in the model.

3.3.1 Model Implementation

This subsection describes the proposed interference model by first giving a high-level explanation of the model and then each part will be discussed in detail. The model uses the Chi-squared distribution as the PDF of the interference power and therefore this distribution will first be discussed. The reason for this will be shown to be the ability it gives in creating multiple correlated signals. A Chi-squared distribution with k degrees of freedom is obtained by summing the square of k Gaussian random variables that have a PDF shown in Equation 3.13. If general Gaussian random

variables with the same mean of μ and standard deviation σ are used, then the PDF of the Chi-squared distribution is given in [81]. This general PDF is complicated and can be simplified by assuming zero mean Gaussian random variables which results in a PDF shown in Equation 3.15. The mean and the second non-central moment of the Chi-squared random variable, Q, is given by Equation 3.16 and Equation 3.17 respectively.

$$f(x) = \frac{1}{\sqrt{2\pi\sigma_{\mathrm{x}}^2}} e^{-\frac{(x-\mu_{\mathrm{x}})^2}{2\sigma^2}} \tag{3.13}$$

$$Q = \sum_{i=1}^{\mathrm{k}} G_{\mathrm{i}}^2 \tag{3.14}$$

$$f(x;k) = \frac{x^{\frac{\mathrm{k}}{2}-1} e^{-\frac{\mathrm{x}}{2\sigma^2}}}{\sigma^{\mathrm{k}} 2^{\frac{\mathrm{k}}{2}} \Gamma(\frac{k}{2})}, \qquad x > 0 \tag{3.15}$$

$$E(Q) = k\sigma^2 \tag{3.16}$$

$$E(Q^2) = 2k\sigma^4 + k^2\sigma^4 \tag{3.17}$$

If we consider the simple network shown in Figure 3.1, the aim of the model is to synthesize the interference signals $Z_1(t)$, $Z_2(t)$, and $Z_3(t)$. Figure 3.7 shows a simplified example of interference power signals synthesized that can be used to explain the model. The model assumes that the interference signals consist of alternating transmission and idle times that occur at the same time for all interference signals. Transmission times occur for a period of T_{f} sampling times while the idle times occur for T_{i} sampling times.

During transmission times, the signal will be assumed to consist of interference and noise $Z = Q_{\mathrm{i}} + Q_{\mathrm{n}}$, while only noise will exist during idle periods, $Z = Q_{\mathrm{n}}$. The random variable Q_{i} represents the part of the interference that is from interferers and is a Chi-squared distribution with k degrees of freedom and its value is fixed for the T_{f} sampling times. The random variable Q_{n} is

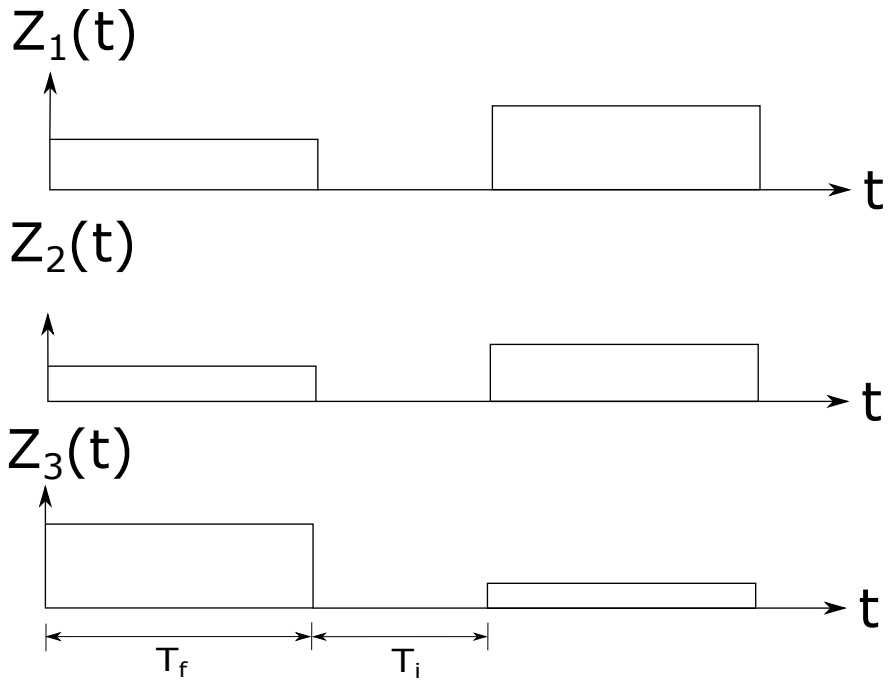

Figure 3.7: Example of interference signals from 3 SU nodes

the noise value that will follow a Chi-squared distribution with $k = 2$ degrees of freedom, since we are dealing with the power of the interference signal, and it will have the same mean as the receiver noise power. The value of the noise represents the average noise measured over the previous time-slot its value will change every sampling time T_s. The PDF of the interference signal is generated as a Chi-squared distribution which consists of a sum of k squared Gaussian random variables. The standard deviation, σ_o, of these Gaussian random variables used to create Q_i will be used to control the Chi-squared distribution and fit it to the desired PDF. Similarly, the standard deviation, σ_n, of the Gaussian random variables in Q_n, will correspond to the receiver noise floor.

The ACF will be modeled by fixing transmission times for a period of T_f samples which will be shown to produce an ACF with a shape that is close to a triangular function which was seen in Section 3.1.2. The idle time T_i is selected from a Poisson distribution to ensure a certain channel utilization or probability that the channel is busy, P_b. The probability that the channel is idle on

average is given by $P_{\mathrm{i}} = 1 - P_{\mathrm{b}}$. This process is repeated until there are N time-slots for each signal this allows the control of the PDF, ACF and P_{b}.

To meet the CCF requirements, the interference signals must be correlated with each other with values that correspond to their relative distances. The interference signals consist of transmission periods that are correlated, by choosing values for Q_{i} for each signal that are correlated, and idle periods that are uncorrelated. Creating random variables Q_{i} for each transmission period for each interference signal that are correlated is possible by using Gaussian random variables that are correlated with each other. The main idea of the model will be to generate correlated Gaussian random variables to create correlated Chi-squared random variables that will simultaneously produce the desired PDF and the correlations that correspond to the relative distances between the nodes.

The mean and second moment of the interference signals are important factors that will be used in the model. Any characteristic of the signal that will be considered during transmission times and will have the superscript $()^{\mathrm{trans}}$, during the idle period will have the superscript $()^{\mathrm{idle}}$, and for the entire signal and will have the superscript $()^{\mathrm{total}}$. The mean will have 3 values, namely $E(Z)^{\mathrm{trans}}$, $E(Z)^{\mathrm{idle}}$, and $E(Z)^{\mathrm{total}}$. Similarly, the second moment will have 3 values , namely $E(Z^2)^{\mathrm{trans}}$, $E(Z^2)^{\mathrm{idle}}$, and $E(Z^2)^{\mathrm{total}}$. The Chi-squared random variables created during transmission and idle times will be created to produce the desired mean and second moments.

Similarly, correlation can also be defined for different times. If we consider two nodes i and j with a distance of $d_{\mathrm{i,j}}$ between them, the correlation between their interference signals will be $\rho_{\mathrm{i,j}}(d_{\mathrm{i,j}})$. This value will be written as $\rho_{\mathrm{i,j}}^{\mathrm{total}}$ and will also have corresponding values $\rho_{\mathrm{i,j}}^{\mathrm{trans}}$ and $\rho_{\mathrm{i,j}}^{\mathrm{idle}}$. Since the correlation during idle times is 0, then the correlation during transmission, $\rho_{\mathrm{i,j}}^{\mathrm{trans}}$, will cause the desired total correlation, $\rho_{\mathrm{i,j}}^{\mathrm{total}}$. The Chi-squared random variables during transmission times will be created to produce the desired correlation. This will mean that the Gaussian random variables used will have to be correlated in a way to make this possible.

A high-level explanation of the synthesis algorithm is given here but derivations of each of the

parameters will be given in Section 3.3.2. The process of synthesizing the interference signals can be summarized into 3 main steps:

1. Calculate average idle time, T_{i}, that will correspond to the desired P_{b}
2. Calculate variances of Gaussian random variables, σ_{o}^2, used to create Chi-squared random variables during transmissions
3. Create Chi-squared random variables for each transmission time for each interference signal that are correlated according to the relative distance between the nodes

The first step requires the knowledge of T_{i} that will be derived in Section 3.3.2. This will allow for the creation of the interference signals that alternate between transmission times that are fixed for T_{f} samples and idle times that are a Poisson random variable with mean T_{i}. This signal structure allows the synthesis of interference signals with the required ACF and channel utilization, P_{b}.

The second step needs the knowledge of means and second moments during transmission and idle times, namely $E(Z)^{\mathrm{trans}}$, $E(Z)^{\mathrm{idle}}$, $E(Z^2)^{\mathrm{trans}}$, and $E(Z^2)^{\mathrm{idle}}$. The values during idle times easily relate to the noise power and the values during transmission times will be derived in Section 3.3.2. Once the values of σ_{o}^2 and σ_{n}^2 are known, Chi-squared random variables can be created to produce signals with the desired means and second moments.

The third step involves the creation of N_{CR} signals, one for each SU node that corresponds to the relative distance between them. This process involves finding a relation between the distance between nodes and the correlation of the Gaussian random variables used to create the desired Chi-squared random variables. This relation will be derived in Section 3.3.2. This relation starts at the relative distances between nodes which can be stored in a matrix $\mathbf{D}$ where $\mathbf{D}(i,j) = d_{\mathrm{i,j}}$. The corresponding correlation between the total interference signals will then be obtained and stored in $\mathbf{C}^{\mathrm{total}}$ where $\mathbf{C}^{total}(i,j) = \rho_{\mathrm{i,j}}^{total}$. Since the signal contains correlated and uncorrelated times, the correlation during transmission times would be calculated and stored in $\mathbf{C}^{\mathrm{trans}}$, where $\mathbf{C}^{\mathrm{trans}}(i,j) = \rho_{\mathrm{i,j}}^{\mathrm{trans}}$. This will correspond to the desired correlation of the Chi-squared random

variables. Finally, the correlation between the Gaussian random variables that is needed to make this possible would be calculated and stored in $\mathbf{C}^{\text{gauss}}$. The main goal is to relate the distance matrix, $\mathbf{D}$, to the correlation matrix of the Gaussian random variables, $\mathbf{C}^{\text{gauss}}$. Since the Gaussian random variables also must have a variance σ_o^2, the covariance matrix of the Gaussian random variables will be $\Sigma = \sigma_o^2 \mathbf{C}^{\text{gauss}}$.

Once the covariance matrix for the Gaussian random variables is known, the Gaussian random variables can be created using the Cholesky decomposition. This allows the creation of correlated Gaussian random variables with a required covariance matrix, from uncorrelated Gaussian random variables that have an identity covariance matrix. This can be achieved using $\mathbf{Q} = \mathbf{LG}$, where $\mathbf{G}$ is a N_{CR}x1 vector of uncorrelated Gaussian random variables with identity covariance matrix, $\mathbf{L}$ is a N_{CR}xN_{CR} lower triangular matrix obtained by the Cholesky decomposition such that $\mathbf{L}\mathbf{L}^T = \Sigma$, and $\mathbf{Q}$ is a N_{CR}x1 vector of correlated Gaussian random variables with covariance matrix Σ. This process is used for each transmission time to produce interference values that have the desired correlation.

3.3.2 Parameter Estimation

This section will provide the derivations of all the parameters discussed in the previous subsection. The derivations will be organized in the order of the steps given for the proposed model in Section 3.3.1 and they will be related to the parameters of the PU network assumed to be creating the interference. This section will be divided into 4 subsections. The first will provide the main assumptions made for the model. The second will derive T_{i}, which is the first step in the model. The third derives the variance, σ_o^2, of the Chi-squared random variables, which is the second step in the model. The final subsection provides the derivations that will produce the relation between the distances between nodes and the correlation of the Gaussian random variables used to create the interference, and this is the third step in the model.

Model Assumptions

Figure 3.8 shows the region around a SU node, where only PU nodes in this range will be assumed to interfere. The path loss model is used and the received interference power is given by $Z(r) = P_t K(d_0/r)^{\alpha} = ar^{-\alpha}$ which is the same as the received power given by Equation 2.2. The transmit power from the PUs and SUs is assumed to be constant. The next subsection will provide derivations of the mean and second moment of the received interference. A problem arises when using integrals with this path loss model since it is a singular model, meaning infinite values are reached when the distance approaches zero in the integral. The model used instead will be $Z(r) = max(a\varepsilon^{-\alpha}, ar^{-\alpha})$, where ε is assumed to be a very small value. This non-singular model does solve the problem of the infinite values for parameters but creates a new problem where all parameters are very sensitive to the choice of the value of ε. To solve this problem, the value used for ε in analytical equations derived will be the same value used in simulations, where no node will be allowed to be closer than this distance to the SU nodes.

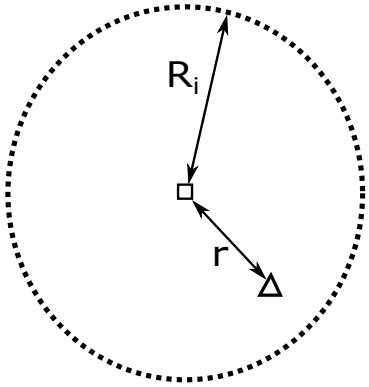

Figure 3.8: Reception region for a node

The model assumes that only interfering nodes within a radius of R_i, given by Equation 3.18, will interfere on a SU node. This is obtained by assuming that interference powers that are received less than the threshold for received power, P_r^{th}, will not be considered as interference. The other assumption that the model makes is that only interference from the dominant interfering node will be considered. This was shown to be a reasonable assumption in [77]. Even though interference

is considered only from the most dominant node, it will be assumed that there are N_{i} interfering nodes, given by Equation 3.19, competing for the channel, which will be shown to affect T_{i}. The node density parameter is multiplied by 2 since there are SU and PU nodes causing interference in this region. The nodes are placed according to a PPP with a node density parameter, λ. The node distribution follows a PPP which means that the node distribution is uniform in the Cartesian coordinates. The node distribution in polar coordinates gives a uniform angular distribution and the radial distribution is given by Equation 3.20 [82].

$$R_{\mathrm{i}} = \left(\frac{a}{P_{\mathrm{r}}^{\mathrm{th}}} \right)^{1/\alpha} \tag{3.18}$$

$$N_{\mathrm{i}} = 2\lambda \pi R_{\mathrm{i}}^2 \tag{3.19}$$

$$f_{\mathrm{r}}(r) = \frac{2r}{R_{\mathrm{i}}^2} \quad , \quad 0 \leq r \leq R_{\mathrm{i}} \tag{3.20}$$

Step 1 - Obtaining T_{i}

The desired ACF and channel utilization will be obtained by using transmission times for T_{f} time-slots and then using idle times from a Poisson random variable of mean T_{i} time-slots. The channel utilization, or the probability a channel is busy, is defined as $P_{\mathrm{b}} = T_{\mathrm{f}}/(T_{\mathrm{f}} + T_{\mathrm{i}})$, where T_{i} is the average time the channel remains idle. The probability that a channel remains idle is defined as $P_{\mathrm{i}} = 1 - P_{\mathrm{b}} = T_{\mathrm{i}}/(T_{\mathrm{f}} + T_{\mathrm{i}})$. The values of P_{b}, P_{i} and T_{i} will be derived in terms of the parameters (p, T_{f}, and λ) of the network creating the interference.

To derive the channel utilization model, a Markov chain will be created to define states that exist in changes between the channel being idle and busy. The channel being busy will be defined as there being at least a single interferer transmitting at a given time-slot, within a radius of R_{i}, given by Equation 3.18. The channel being idle is defined as there being no interfering nodes transmitting at a given time-slot in this region. The average number of nodes in this region is N_{i} and is given by Equation 3.19. Figure 3.9 shows the state transitions in the Markov chain.

State S_0 means that the channel is idle in the current time-slot. When the current state is S_0, the probability of the next state being S_0 is $(1-p)^{N_i}$ (no node transmits), where p is the probability of a single node transmitting in an idle time-slot. The probability of transitioning to state S_1 from S_0 is $1-(1-p)^{N_i}$ (a node begins its transmission). The states S_1 to S_{T_f} are the state of being in the first time-slot of a transmission until the last time-slot of a transmission. The state transitions here to the next state happen with probabilities of 1 since the transmission will continue uninterrupted. When at the state S_{T_f}, the next state could be S_0, which would be an idle time-slot, with probability $(1-p)^{N_i}$. Another possibility is that a new transmission starts immediately, and this could happen with a probability $1-(1-p)^{N_i}$.

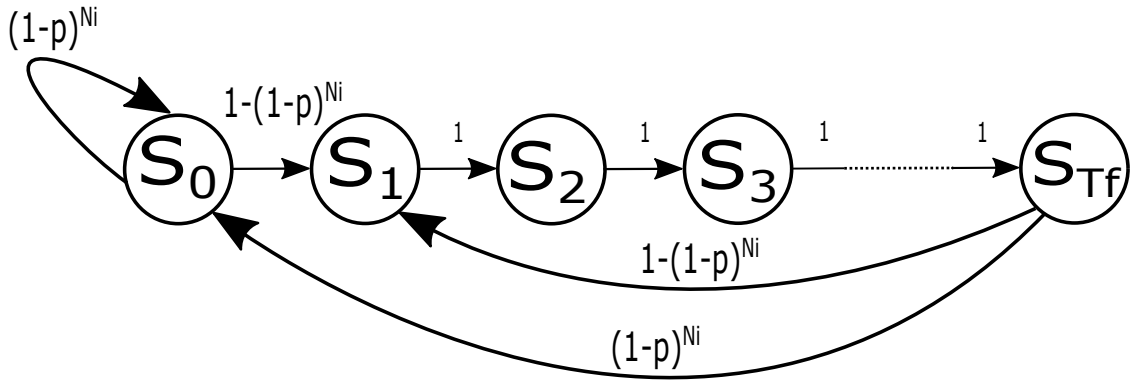

Figure 3.9: Markov chain for state transitions

The state transition matrix for a general packet size, T_f is shown in the matrix in Equation 3.21. This matrix has dimensions (T_f+1) x (T_f+1). The only state where the channel is idle is S_0 and the remaining states all occur during transmissions.

$$P = \begin{pmatrix} (1-p)^{N_i} & 1-(1-p)^{N_i} & 0 & 0 & \cdots & 0 \\ 0 & 0 & 1 & 0 & \cdots & 0 \\ \vdots & \vdots & 0 & 1 & & \vdots \\ 0 & 0 & \vdots & & \ddots & 1 \\ (1-p)^{N_i} & 1-(1-p)^{N_i} & 0 & 0 & \cdots & 0 \end{pmatrix} \tag{3.21}$$

The steady state vector for this Markov chain is $\pi = [\pi_0 \quad \pi_1 \quad \cdots \quad \pi_{T_f}]$. The first term, π_0, would therefore tell us how long the channel stays idle. To find the probability of each state at steady state, the Equations 3.22 and 3.23 need to be solved. The first equation is composed of $T_f + 1$ equations and the second is only one equation. Since there are $T_f + 1$ unknowns then one equation could be dropped. The $T_f + 2$ equations obtained are shown in 3.24.

$$\pi P = \pi \tag{3.22}$$

$$\sum_{i=0}^{T_f} \pi_i = 1 \tag{3.23}$$

$$\begin{aligned}
(\pi_0 + \pi_{T_f})(1-p)^{N_i} &= \pi_0 \\
(\pi_0 + \pi_{T_f})[1-(1-p)^{N_i}] &= \pi_1 \\
\pi_1 &= \pi_2 \\
\pi_2 &= \pi_3 \\
\vdots &= \vdots \\
\pi_{T_f - 1} &= \pi_{T_f} \\
\pi_0 + \pi_1 + ... + \pi_{T_f} &= 1
\end{aligned} \tag{3.24}$$

There is one observation which could simplify solving this, that all the states except S_0 are equal i.e. $\pi_1 = \pi_2 = \cdots = \pi_{T_f}$. This reduces the number of unknowns 3 equations remain shown in 3.25.

$$\begin{aligned}
(\pi_0 + \pi_1)(1-p)^{N_i} &= \pi_0 \\
(\pi_0 + \pi_1)[1-(1-p)^{N_i}] &= \pi_1 \\
\pi_0 + T_f \pi_1 &= 1
\end{aligned} \tag{3.25}$$

Solving these equations leads to the probability a channel is idle or busy and this is shown in Equations 3.26 and 3.27. It important to note that the probabilities P_{i} and P_{b} are dependent on p, T_{f} and λ (through N_{i}).

$$P_{\mathrm{i}} = \pi_0 = \frac{(1-p)^{\mathrm{N_i}}}{T_{\mathrm{f}} - (1-p)^{N_{\mathrm{i}}}(T_{\mathrm{f}}-1)} = \frac{T_{\mathrm{i}}}{T_{\mathrm{i}}+T_{\mathrm{f}}} \tag{3.26}$$

$$P_{\mathrm{b}} = \sum_{i=1}^{T_{\mathrm{f}}} \pi_{\mathrm{i}} = \frac{T_{\mathrm{f}}[1-(1-p)^{N_{\mathrm{i}}}]}{T_{\mathrm{f}} - (1-p)^{N_{\mathrm{i}}}(T_{\mathrm{f}}-1)} = \frac{T_{\mathrm{f}}}{T_{\mathrm{i}}+T_{\mathrm{f}}} \tag{3.27}$$

After the channel utilization and idle probabilities, P_{b} and P_{i}, have been calculated this can be used to calculate the average time a channel is idle for given in Equation 3.28. The idle time, T_{i}, as expected is not a function of the frame length T_{f} unlike the channel utilization, P_{b}. The idle time is only dependent on p and λ (through N_{i}), and not T_{f}.

$$T_{\mathrm{i}} = \frac{T_{\mathrm{f}}(1-P_{\mathrm{b}})}{P_{\mathrm{b}}} = \frac{P_{\mathrm{i}}T_{\mathrm{f}}}{1-P_{\mathrm{i}}} = \frac{(1-p)^{N_{\mathrm{i}}}}{1-(1-p)^{N_{\mathrm{i}}}} \tag{3.28}$$

Step 2 - Obtaining σ_{o}^2

This section will start by deriving the mean interference during transmissions, $E(Z)^{\mathrm{trans}}$. The aim will be to use this to derive the necessary variance, σ_{o}^2, of the Gaussian random variables that will be used to synthesize interference with this mean. The main aim is to obtain a closed form equation for σ_{o}^2 in terms of the parameters (p,T_{f}, and λ) of the network causing the interference.

The mean of the interference signal during transmission, $E(Z)^{\mathrm{trans}}$, is derived in 3.29. There are two equations depending on the value of the path loss exponent. The second order non-central moment of the interference during transmissions, $E(Z^2)^{\mathrm{trans}}$, is derived in 3.30. There are also two equations depending on the value of the path loss exponent. Finally, the variance of the interference signal is given by Equation 3.31. It is important to note that the mean of the interference signal during transmissions, $E(Z)^{\mathrm{trans}}$, is dependent on the frequency of operation, f, and the transmit power, P_{t}, which are included in constant a from Equation 2.2. It is also dependent on the received threshold power, $P_{\mathrm{r}}^{\mathrm{th}}$, which is included in the term R_{i} from Equation 3.18. It is independent of the

PU network parameters p, T_{f} and λ because of the dominant interference assumption. However, the dependence of the PU network parameters will be in-cooperated into the network in the derivations for the mean of the total interference signal, $E(Z)^{\mathrm{total}}$, which will depend on these parameters.

$$\begin{aligned} E(Z)^{\mathrm{trans}} &= \int_{\varepsilon}^{R_{\mathrm{i}}} Z(r) f_{\mathrm{r}}(r) dr = \int_{\varepsilon}^{R_{\mathrm{i}}} a r^{-\alpha} \frac{2r}{R_{\mathrm{i}}^2} dr = \frac{2a}{R_{\mathrm{i}}^2} \int_{\varepsilon}^{R_{\mathrm{i}}} r^{(1-\alpha)} dr \\ &= \begin{cases} \frac{2a}{R_{\mathrm{i}}^2} ln\left(\frac{R_{\mathrm{i}}}{\varepsilon}\right) & , \quad \alpha = 2 \\ \frac{2a(R_{\mathrm{i}}^{|2-\alpha|} - \varepsilon^{|2-\alpha|})}{R_{\mathrm{i}}^{\alpha}|2-\alpha|} & , \quad o.w \end{cases} \end{aligned} \tag{3.29}$$

$$\begin{aligned} E(Z^2)^{\mathrm{trans}} &= \int_{\varepsilon}^{R_{\mathrm{i}}} Z^2(r) f_{\mathrm{r}}(r) dr = \int_{\varepsilon}^{R_{\mathrm{i}}} a^2 r^{-2\alpha} \frac{2r}{R_{\mathrm{i}}^2} dr = \frac{2a^2}{R_{\mathrm{i}}^2} \int_{\varepsilon}^{R_{\mathrm{i}}} r^{(1-2\alpha)} dr \\ &= \begin{cases} \frac{2a^2}{R_{\mathrm{i}}^2} ln\left(\frac{R_{\mathrm{i}}}{\varepsilon}\right) & , \quad \alpha = 1 \\ \frac{a^2(R_{\mathrm{i}}^{|2-2\alpha|} - \varepsilon^{|2-2\alpha|})}{R_{\mathrm{i}}^{2\alpha}|1-\alpha|} & , \quad o.w \end{cases} \end{aligned} \tag{3.30}$$

$$Var(Z)^{\mathrm{trans}} = E(Z^2)^{\mathrm{trans}} - [E(Z)^{\mathrm{trans}}]^2 \tag{3.31}$$

During the transmission periods a Chi-squared variable, Q_{i}, with k degrees of freedom is added to the Chi-squared noise, Q_{n}, with 2 degrees of freedom. During idle times there is only the noise variable, Q_{n}. The mean and second non-central moment of Chi-squared distributions are given in Equations 3.16 and 3.17. Equations 3.32, 3.33, and 3.34 give the mean, second non-central moment, and variance of the interference signal during transmission times, respectively. Equations 3.35, 3.36, and 3.37 give the mean, second non-central moment and variance of the interference signals synthesized using the Chi-squared distribution during idle times, respectively. The value of σ_{o}^2 can be calculated using Equation 3.38 such that $E(Z)^{\mathrm{trans}}$ is obtained from Equation 3.29. This will be the variance used for all Gaussian random variables used to create the Chi-squared random variables such that we obtain our required PDF.

$$E(Z)^{\text{trans}} = E(Q+N) = E(Q) + E(N) = k\sigma_{\text{o}}^2 + 2\sigma_{\text{n}}^2 \tag{3.32}$$

$$\begin{aligned} E(Z^2)^{\text{trans}} &= E[(Q_{\text{i}} + Q_{\text{n}})^2] = E(Q_{\text{i}}^2) + 2E(Q_{\text{i}})E(Q_{\text{n}}) + E(Q_{\text{n}}^2) \\ &= [2k\sigma_{\text{o}}^2 + k^2\sigma_{\text{o}}^2] + 2[k\sigma_{\text{o}}^2][2\sigma_{\text{n}}^2] + [2(2)\sigma_{\text{n}}^2 + (2)^2\sigma_{\text{n}}^2] \end{aligned} \tag{3.33}$$

$$Var(Z)^{\text{trans}} = E(Z^2)^{\text{trans}} - [E(Z)^{\text{trans}}]^2 \tag{3.34}$$

$$E(Z)^{\text{idle}} = E(Q_{\text{n}}) = 2\sigma_{\text{n}}^2 \tag{3.35}$$

$$E(Z^2)^{\text{idle}} = E(Q_{\text{n}}^2) = 2(2)\sigma_{\text{n}}^2 + (2)^2\sigma_{\text{n}}^2 \tag{3.36}$$

$$Var(Z)^{\text{idle}} = E(Z^2)^{\text{idle}} - [E(Z)^{\text{idle}}]^2 \tag{3.37}$$

$$\sigma_{\text{o}}^2 = \frac{E(Z)^{\text{trans}} - 2\sigma_{\text{n}}^2}{k} \tag{3.38}$$

The process of obtaining σ_{o}^2, using Equation 3.38, can end here since $E(Z)^{\text{trans}}$ was derived in 3.29. If instead of the mean and second moment during transmission, we have the total interference mean, $E(Z)^{\text{total}}$, then a relation between them must be available to calculate $E(Z)^{\text{trans}}$ and therefore σ_{o}^2. The relation between $E(Z)^{\text{total}}$ and $E(Z)^{\text{trans}}$ is given in Equation 3.39, and one can be obtained from the other using the values of P_{b} (Equation 3.27), and P_{i} (Equation 3.26). The second non-central moment and the variance of the total signal can be obtained using Equations 3.40 and 3.41, respectively.

$$E(Z)^{\text{total}} = E(Z)^{\text{trans}}P_{\text{b}} + E(Z)^{\text{idle}}P_{\text{i}} \tag{3.39}$$

$$E(Z^2)^{\text{total}} = E(Z^2)^{\text{trans}}P_{\text{b}} + E(Z^2)^{\text{idle}}P_{\text{i}} \tag{3.40}$$

$$Var(Z)^{\text{total}} = E(Z^2)^{\text{total}} - [E(Z)^{\text{total}}]^2 \tag{3.41}$$

Step 3 - Obtaining L from D

The last step in the process is to use the distance matrix, **D**, to obtain the Cholesky matrix, **L**, that will be used to correlate the Gaussian random variables used to create the interference. The

correlation coefficient between two nodes during a transmission from an interferer as a function of distance will now be derived. Figure 3.10 shows 3 cases where 2 SU nodes, node 1 and node 2, are separated by a distance d. The correlation coefficient between them is $\rho_{1,2}^{\text{trans}}(d)$ this will be derived and related to the parameters (p, T_{f}, and λ) of the network creating the interference. The assumptions that only interferers within a radius of R_{i} can interfere and that only the most dominant interferer will be made use of in this derivation. In the first case, when the distance between them is $2R_{\text{i}}$, there is no interferer location that will cause interference at both nodes. Here the correlation coefficient will be zero and will remain zero for any distance larger than $2R_{\text{i}}$ between them. In case 2, the nodes are exactly on each other and the distance between them is zero and the correlation will be 1.

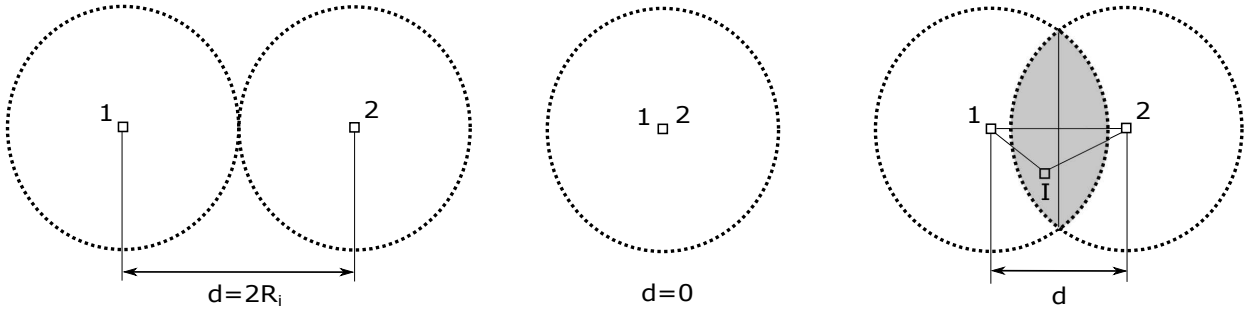

Figure 3.10: Cases for correlation as a function of distance

Case 3 is the general case where the distance between them is greater than zero and less than $2R_{\text{i}}$. Here, the only region where an interfering node can interfere on both nodes simultaneously and cause non-zero interference, is in the two segments that are in the intersection of both circles. Let the area of the intersection be A which can easily be derived and is given by Equation 3.42. Given that the interfering node is transmitting, and at least one node can hear it, then only the region within both circles will be considered. The entire area where the interferer can be located in is $2\pi R_{\text{i}}^2 - A$. Since the interfering nodes are assumed to be uniformly distributed, the probability of the node being within the intersecting area, A, is $A/(2\pi R_{\text{i}}^2 - A)$. In this region the correlation coefficient will be approximated to 1. The probability of the node being outside this region is

$(2\pi R_{\mathrm{i}}^2 - 2A)/(2\pi R_{\mathrm{i}}^2 - A)$. In this region the correlation coefficient will be approximated to 0. The average correlation coefficient will be given by Equation 3.43. The expected value of the correlation coefficient as a function of distance, is the sum of the multiplication of the probability of a node being in each region with the expected correlation in each region. If all node locations were known and the distances obtained and stored in $\mathbf{D}$, then by calculating the values of $\rho_{\mathrm{i,j}}^{\mathrm{trans}}(d_{\mathrm{i,j}})$, the matrix $\mathbf{C}^{\mathrm{trans}}$ can be created.

$$A(d_{\mathrm{i,j}}) = 2R_{\mathrm{i}}^2 cos^{-1}(\frac{d_{\mathrm{i,j}}}{2R_{\mathrm{i}}}) - d_{\mathrm{i,j}}\sqrt{R_{\mathrm{i}}^2 - \frac{d_{\mathrm{i,j}}^2}{4}} \tag{3.42}$$

$$\begin{aligned}\rho_{\mathrm{i,j}}^{\mathrm{trans}}(d_{\mathrm{i,j}}) &= \frac{A(d_{\mathrm{i,j}})}{2\pi R_{\mathrm{i}}^2 - A(d_{\mathrm{i,j}})}(1) + \frac{2\pi R_{\mathrm{i}}^2 - 2A(d_{\mathrm{i,j}})}{2\pi R_{\mathrm{i}}^2 - A(d_{\mathrm{i,j}})}(0) \\ &= \frac{A(d_{\mathrm{i,j}})}{2\pi R_{\mathrm{i}}^2 - A(d_{\mathrm{i,j}})}\end{aligned} \tag{3.43}$$

The derived correlation coefficient in 3.43 is for the correlation of the signals during transmission. The Chi-squared random variables during transmission times will be required to have this same correlation and this is what is required to create the matrix $\mathbf{C}^{\mathrm{trans}}$. If, however, the total correlation between the signals is known instead, $\mathbf{C}^{\mathrm{total}}$, then the relation between correlation coefficients of the total signal, $\rho_{\mathrm{i,j}}^{\mathrm{total}}$, and only during transmission, $\rho_{\mathrm{i,j}}^{\mathrm{trans}}$, can be obtained using the 3 equations, 3.44, 3.45, and 3.46. To summarize this point, if the distance between the nodes is known, then 3.43 can be used to calculate $\rho_{\mathrm{i,j}}^{\mathrm{trans}}$ and the matrix $\mathbf{C}^{\mathrm{trans}}$ can be created and this is what is needed to create the Chi-squared random variables. If instead, the total correlation coefficients between the signals, $\rho_{\mathrm{i,j}}^{\mathrm{total}}$, are already known, then Equations 3.44 to 3.46 can be used to calculate $\rho_{\mathrm{i,j}}^{\mathrm{trans}}$ and therefore the matrix $\mathbf{C}^{\mathrm{trans}}$ can be created.

$$\rho_{\mathrm{i,j}}^{\mathrm{total}} = \frac{cov(Z_1, Z_2)^{\mathrm{total}}}{\sqrt{Var(Z_1)^{\mathrm{total}} Var(Z_2)^{\mathrm{total}}}} = \frac{E(Z_1 Z_2)^{\mathrm{total}} - [E(Z)^{\mathrm{total}}]^2}{Var(Z)^{\mathrm{total}}} \tag{3.44}$$

$$E(Z_1 Z_2)^{\mathrm{total}} = E(Z_1 Z_2)^{\mathrm{trans}} P_{\mathrm{b}} + E(N^2) P_{\mathrm{i}} \tag{3.45}$$

$$E(Z_1 Z_2)^{\mathrm{trans}} = \rho_{\mathrm{i,j}}^{\mathrm{trans}} Var(Z)^{\mathrm{trans}} + [E(Z)^{\mathrm{trans}}]^2 \tag{3.46}$$

The derived values in $\mathbf{C}^{\mathrm{trans}}$ are also the correlation between the Chi-squared variables used to create each interference signal. This correlation is controlled by the correlation between the Gaussian random variables used to create the Chi-squared variables. A relation between the Chi-squared correlation (correlation during transmission), ρ^{trans}, and the Gaussian correlation, ρ^{gauss}, will now be derived. Consider two Chi-squared random variables, with k degrees of freedom, $Q_{\mathrm{i}} = G_{\mathrm{i1}}^2 + G_{\mathrm{i2}}^2 + ... + G_{\mathrm{ik}}^2$ and $Q_{\mathrm{j}} = G_{\mathrm{j1}}^2 + G_{\mathrm{j2}}^2 + ... + G_{\mathrm{jk}}^2$. The Gaussian random variables are $N(0, \sigma_{\mathrm{o}}^2)$ and the correlation between the Chi-squared random variables, Q_{i} and Q_{j}, is $\rho_{\mathrm{i,j}}^{\mathrm{trans}}$ and the correlation coefficient between the Gaussian pairs, G_{i1} and G_{j1} until G_{ik} and G_{jk}, is $\rho_{\mathrm{i,j}}^{\mathrm{gauss}}$. The derivation starts in 3.47 and aims to obtain a relation between $\rho_{\mathrm{i,j}}^{\mathrm{trans}}$ and $\rho_{\mathrm{i,j}}^{\mathrm{gauss}}$.

$$\begin{aligned} \rho_{\mathrm{i,j}}^{\mathrm{trans}} &= \frac{cov(Q_{\mathrm{i}}, Q_{\mathrm{j}})}{\sqrt{Var(Q_{\mathrm{i}}) Var(Q_{\mathrm{j}})}} = \frac{k[cov(G_{\mathrm{i1}}^2, G_{\mathrm{i2}}^2)]}{Var(Q_{\mathrm{i}})} \\ &= \frac{k[E(G_{\mathrm{i1}}^2 G_{\mathrm{i2}}^2) - E(G_{\mathrm{i1}}^2) E(G_{\mathrm{i1}}^2)]}{E(Q_{\mathrm{i}}^2) - E(Q_{\mathrm{i}})^2} \end{aligned} \tag{3.47}$$

In this derivation it is necessary to calculate the expected value of the multiplication of the square of two Gaussian random variables, $E(G_{\mathrm{i1}}^2 G_{\mathrm{i2}}^2)$. This will be obtained by writing the second Gaussian variable in terms of the first such that $G_{\mathrm{i2}} = cG_{\mathrm{i1}} + aX$ where X is independent of G_{i1} and is $N(0, \sigma_{\mathrm{o}}^2)$ and also let $a^2 = 1 - c^2$. First the value of c will be derived in 3.48 and is shown to be the same as the correlation, $\rho_{1,2}^{\mathrm{gauss}}$, between the Gaussian random variables, G_{i1} and G_{i2}.

$$\begin{aligned}\rho_{1,2}^{\text{gauss}} &= \frac{cov(G_{\text{i}1}, G_{\text{i}2})}{\sqrt{Var(G_{\text{i}1})Var(G_{\text{i}1})}} = \frac{E(G_{\text{i}1}G_{\text{i}2}) - E(G_{\text{i}1})E(G_{\text{i}2})}{Var(G_{\text{i}1})} \\ &= \frac{E(G_{\text{i}1}(cG_{\text{i}1} + aX)) - 0}{\sigma_{\text{o}}^2} \\ &= \frac{cE(G_{\text{i}1}^2) + aE(G_{\text{i}1}X)}{\sigma_{\text{o}}^2} \\ &= \frac{c\sigma_{\text{o}}^2 + 0}{\sigma_{\text{o}}^2} = c \end{aligned} \tag{3.48}$$

The expected value of $G_{\text{i}1}^2 G_{\text{i}2}^2$ is derived in 3.49.

$$\begin{aligned} E(G_{\text{i}1}^2 G_{\text{i}2}^2) &= E(G_{\text{i}1}^2(cG_{\text{i}1} + aX)^2) = E(G_{\text{i}1}^2(c^2 G_{\text{i}1}^2 + 2acG_{\text{i}1}X + a^2X^2)) \\ &= c^2 E(G_{\text{i}1}^4) + 2acE(G_{\text{i}1}^3)E(X) + a^2 E(G_{\text{i}1}^2)E(X^2) \\ &= c^2(3\sigma_{\text{o}}^4) + 2ac(0)E(0) + a^2(\sigma_{\text{o}}^2)(\sigma_{\text{o}}^2) \\ &= (3c^2 + a^2)\sigma_{\text{o}}^4 = (2c^2 + 1)\sigma_{\text{o}}^4 \end{aligned} \tag{3.49}$$

Finally, the relation between $\rho_{1,2}^{\text{trans}}$ and $\rho_{1,2}^{\text{gauss}}$ is given in 3.50. It is important to note that this relation is independent of the values of k and σ_{o}^2. Using this relation, the matrix $\mathbf{C}^{\text{trans}}$ can be used to obtain the correlation matrix $\mathbf{C}^{\text{gauss}}$ of the Gaussian random variables used to create the Chi-squared random variables. The covariance matrix of the Gaussian random variables is $\Sigma = \sigma_{\text{o}}^2 \mathbf{C}^{\text{gauss}}$.

$$\begin{aligned}\rho_{1,2}^{\text{gauss}} &= \frac{k[E(G_{\text{i}1}^2 G_{\text{i}2}^2) - E(G_{\text{i}1}^2)E(G_{\text{i}1}^2)]}{E(Q_{\text{i}}^2) - E(Q_{\text{i}})^2} \\ &= \frac{k[(2c^2 + 1)\sigma_{\text{o}}^4 - \sigma_{\text{o}}^4]}{2k\sigma_{\text{o}}^4 + k^2\sigma_{\text{o}}^4 - k^2\sigma_{\text{o}}^4} \\ &= \frac{2kc^2\sigma_{\text{o}}^4}{2k\sigma_{\text{o}}^4} = (\rho_{1,2}^{\text{trans}})^2 \end{aligned} \tag{3.50}$$

The last step will be to create correlated Chi-squared random variables using Gaussian random variables with covariance matrix Σ. These correlated Gaussian random variables will be created by

first using independent Gaussian random variables with an identity covariance matrix. To create a Chi-squared random variable, k Gaussian random variables are created and squared and added. As an example, let us assume two correlated Chi-squared random variables, $Q_{\mathrm{i}} = G_{\mathrm{j1}}^2 + G_{\mathrm{i2}}^2 + ... + G_{\mathrm{ik}}^2$ and $Q_{\mathrm{j}} =_{\mathrm{j1}}^2 + G_{\mathrm{j2}}^2 + ... + G_{\mathrm{jk}}^2$. First you calculate the desired covariance matrix of the Gaussian variables, $\Sigma = \sigma_{\mathrm{o}}^2 \mathbf{C}^{\mathrm{gauss}}$, that will be used to create the Chi-squared random variable. The first Gaussian random variables would be calculated using $[G_{\mathrm{i1}}; G_{\mathrm{j1}}] = \mathbf{L}[X_1; X_2]$, where X_1 and X_2 are uncorrelated Gaussian random variables, $N(0,1)$. This process is repeated for the pairs G_{i2} andG_{j2} until G_{ik} and G_{jk}. Finally, the Gaussian random variables are squared and added. This process is repeated for every transmission time to obtain correlated Chi-squared variables for each SU node.

The steps below will summarize this process that is repeated for each transmission time:

1. Calculate covariance matrix of the Gaussian random variables, $\Sigma = \sigma_{\mathrm{o}}^2 \mathbf{C}^{\mathrm{gauss}}$
2. Calculate lower triangular Cholesky matrix such that $\mathbf{L}\mathbf{L}^T = \Sigma$
3. Create vector of independent Gaussian random variables $[X_1; X_2; ..; X_{N_{\mathrm{CR}}}]$ with identity covariance matrix
4. Create vector of correlated Gaussian random variables with covariance matrix Σ, using $[G_{11}; G_{12}; ..; G_{1\mathrm{N_{CR}}}] = \mathbf{L}[X_1; X_2; ..; X_{N_{\mathrm{CR}}}]$
5. repeat steps 3 and 4 until there are k vectors of correlated Gaussian random variables $[G_{11}; G_{12}; ..; G_{1\mathrm{N_{CR}}}]$, $[G_{21}; G_{22}; ..; G_{2\mathrm{N_{CR}}}]$, .., $[G_{\mathrm{k1}}; G_{\mathrm{k2}}; ..; G_{\mathrm{kN_{CR}}}]$
6. Create the correlated Chi-squared random variables by squaring and adding the respective Gaussian random variables, using $Q_1 = G_{11}^2 + G_{21}^2 + ... + G_{\mathrm{k1}}^2$, $Q_2 = G_{12}^2 + G_{22}^2 + ... + G_{\mathrm{k2}}^2$, .., $Q_{\mathrm{N_{CR}}} = G_{1\mathrm{N_{CR}}}^2 + G_{2\mathrm{N_{CR}}}^2 + ... + G_{\mathrm{kN_{CR}}}^2$

3.4 Results

This section will provide results that are used to validate the model. The results will compare the performance of a SU network in the presence of a PU network and the performance of a SU network with synthesized interference using the proposed model. The similarity of performance of the 2 SU networks will be the main validation criterion. The effect of the network parameters on RLNC and flooding as protocols will not be discussed here since this was done in Section 2.2.

3.4.1 Model Validation

Figure 3.1 can be used to summarize the simulations used in this section. For each set of network parameters, 2 simulations scenarios are considered. The first scenario, on the left, is of a SU network operating with a PU in the same band. Interference on the SU network comes from other PUs and SUs and Section 2.2 described this scenario in detail and results were provided. The second scenario, on the right, only has SU nodes and the interference for each node is synthesized as described in Section 3.3. The decision that a SU node takes on whether the channel is idle or whether a packet was successfully received is based on only observing the synthesized interference signal since the model considers the interference to originate from both PU and SU nodes. This was in cooperated into the model using double the node density parameter in Equation 3.19. The coverage vs. time-slot and energy per node plots are compared for both scenarios for range of network parameters and the results averaged over 10,000 simulations.

Figures 3.11 - 3.16 show the effect of varying p, T_{f} and λ are on the model when comparing the SU network performance with interference from the model and simulated interference. The required time-slots and energy per node for 90% coverage are available in Tables 3.1 - 3.6.

The SU network performance is better in all the cases when using model interference as compared to simulated interference. This means that less time-slots and energy per node are expected when using the interference model. It is also apparent in the fact that flooding does not reach 100% coverage when using simulated interference, but it does when using modeled interference.

Table 3.1: Effect of p on model for time to 90% coverage

p	0.005	0.008	0.01
Flooding Sim	4805	3401	2972
Flooding Model	4666	3239	2784
RLNC Sim	1716	1207	1061
RLNC Model	1680	1159	997

The reason this is that the model assumes only a single dominant interferer causing the interference at any given time, which may not be the case when simulated interference is being used. On average, smaller interference values are expected when using modeled interference.

Another reason for this is the difference in the interference signal structure between the model and simulated interference. The model assumes transmission periods in time of length T_{f} samples and then idle times of length T_{i} samples. During transmission periods all SU nodes will sense there is a transmission and fewer lost packets will occur during this time. This is not the case with simulated interference since the hidden node problem can occur.

Another observation is that using modeled interference is more accurate when using lower values p, T_{f} and λ. The reason for this is that when any of these values increase, it means that the likelihood of multiple interfering nodes at a given time increases, as explained in Section 2.2.1, which would cause stronger simulated interference signals. The more this happens the less accurate the single interferer assumption of the model becomes.

The final observation is that the model is most accurate when being used to predict the energy per node performance of flooding in all cases. The reason for this is that the energy per node is almost entirely dependent on the value of T_{f}, and little dependence p and λ. The single interferer assumption is most affected by increasing values of p and λ but less so when T_{f} increases, as seen in the results of Section 2.2.1. In other words, since the energy efficiency of flooding is mostly dependent on the packet time, and less on the number of interferences, then the model's single interference assumption has a less effect.

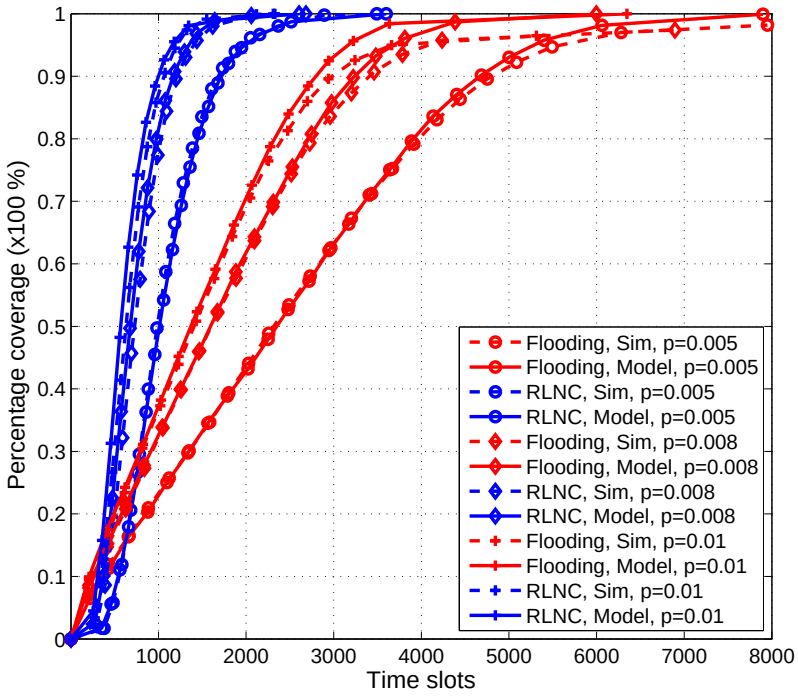

Figure 3.11: Effect of p on model for coverage vs. time-slots

Table 3.2: Effect of p on model for energy per node (J) for 90% coverage

p	0.005	0.008	0.01
Flooding Sim	5.02	5.04	5.05
Flooding Model	4.96	4.97	4.99
RLNC Sim	1.77	1.84	1.87
RLNC Model	1.77	1.78	1.80

Table 3.3: Effect of T_{f} on model for time to 90% coverage

s	5	10	15
Flooding Sim	4788	6097	7328
Flooding Model	4691	5859	6984
RLNC Sim	1795	2157	2609
RLNC Model	1721	2000	2469

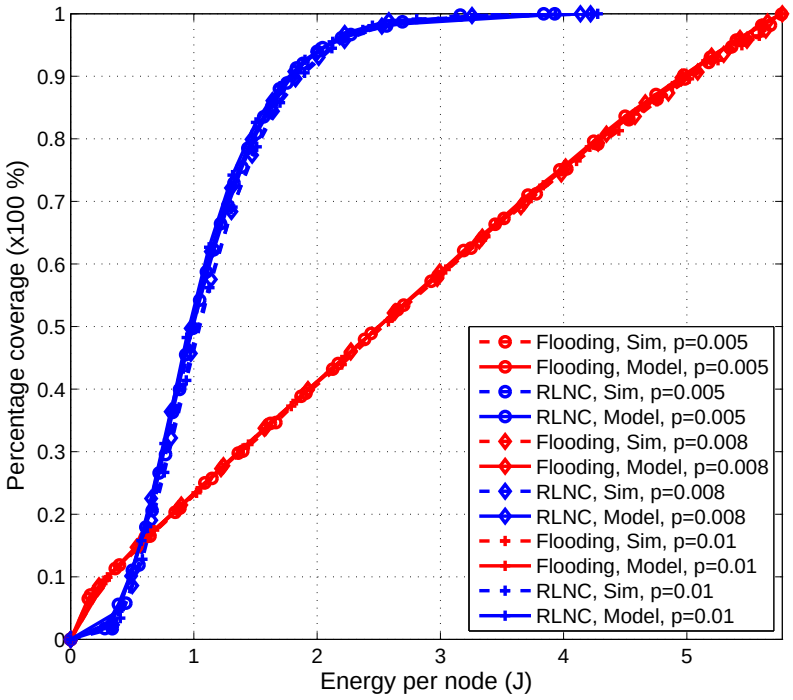

Figure 3.12: Effect of p on model for coverage vs. energy per node

Table 3.4: Effect of T_{f} on model for energy per node (J) for 90% coverage

s	5	10	15
Flooding Sim	5.02	10.06	15.15
Flooding Model	4.97	9.98	14.98
RLNC Sim	1.89	3.69	5.55
RLNC Model	1.81	3.45	5.38

Table 3.5: Effect of λ on model for time to 90% coverage

λ	5	10	15
Flooding Sim	4413	4878	5217
Flooding Model	4364	4694	5050
RLNC Sim	1899	1769	1589
RLNC Model	1763	1663	1547

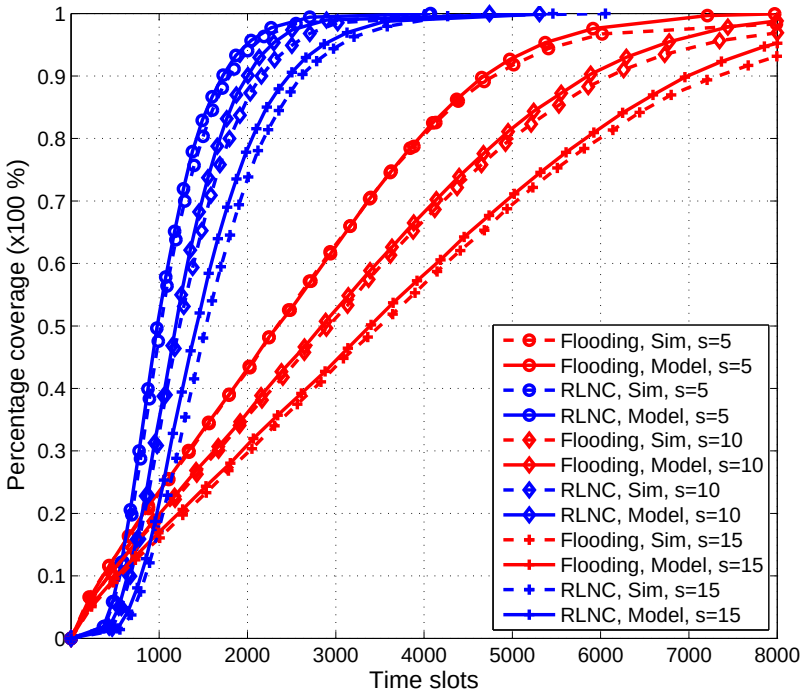

Figure 3.13: Effect of T_{f} on model for coverage vs. time-slots

Table 3.6: Effect of λ on model for energy per node (J) for 90% coverage

λ	5	10	15
Flooding Sim	5.17	5.00	4.87
Flooding Model	5.16	4.97	4.82
RLNC Sim	2.21	1.86	1.47
RLNC Model	2.13	1.75	1.42

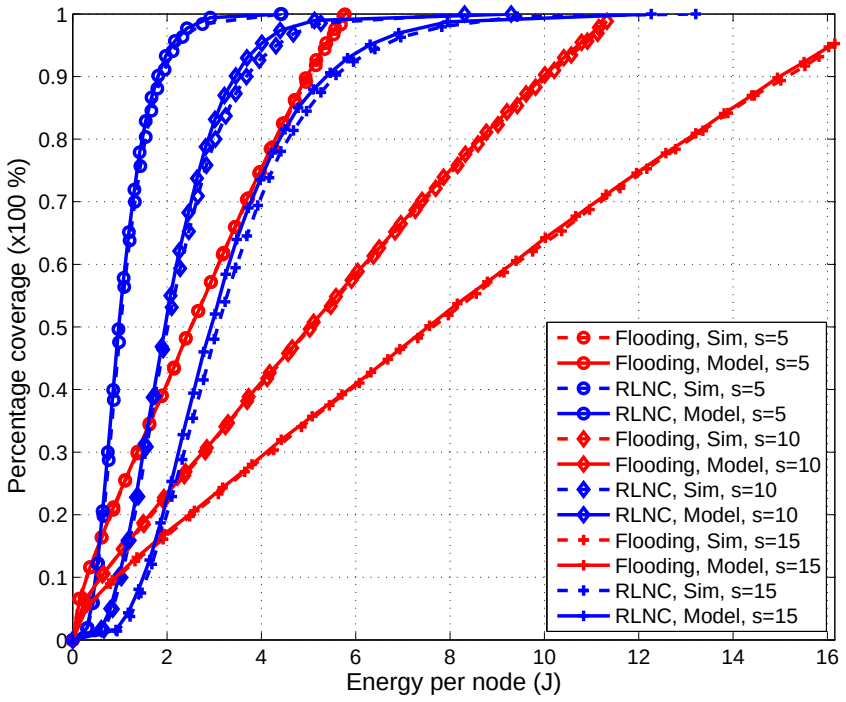

Figure 3.14: Effect of T_{f} on model for coverage vs. energy per node

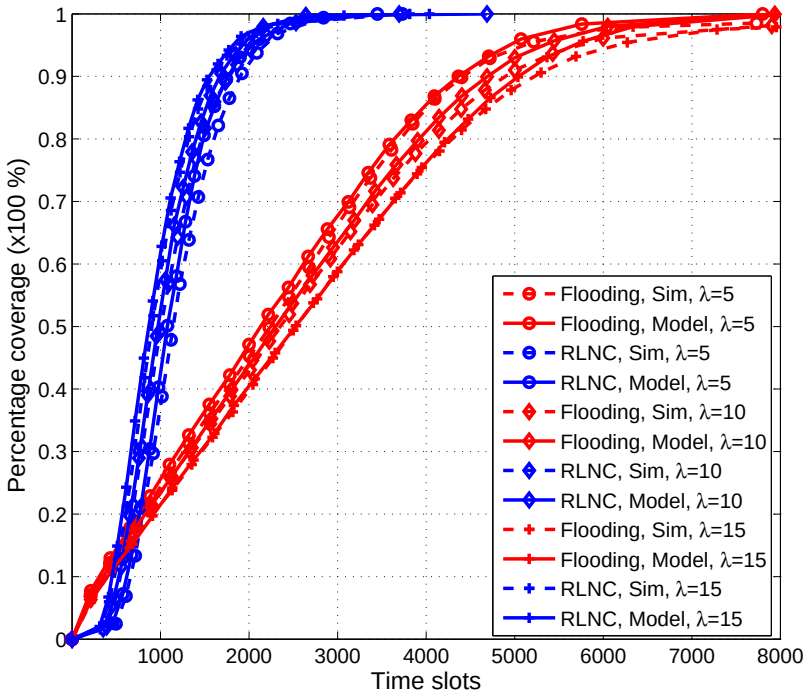

Figure 3.15: Effect of λ on model for coverage vs. time-slots

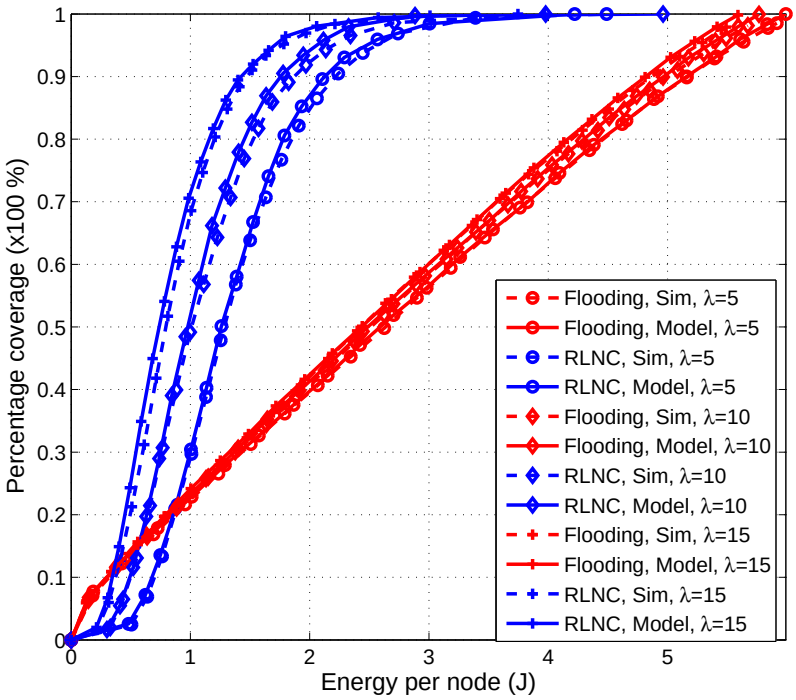

Figure 3.16: Effect of λ on model for coverage vs. energy per node

3.5 Conclusion

This chapter studied the interference produced by random access networks and considered it as a stochastic process. The first and second order statistics were described, and the stationarity assumption of the interference was discussed. The process was assumed to be WSS in both time and space and this was shown to be a reasonable assumption. The important statistical functions were defined, namely the PDF, ACF and CCF.

The proposed interference model is the first to simultaneously model the PDF, ACF, and CCF. The model used a Chi-squared PDF that allowed the synthesis of multiple interference signals that were correlated according to the relative distances of the SU nodes they are being synthesized for. The important model parameters were all derived and related to the network parameters of the network causing the interference. Finally, the model was used as interference for a SU network broadcasting using flooding and RLNC. The performance produced was compared to that of a SU network operating under a simulated PU network causing the interference. The model was found to be accurate, however, it did produce network performance that was slightly more time and energy efficient than when compared to use of simulated interference. The accuracy of the model was found to reduce as higher values for the network parameters were used, since the single interfering node assumptions becomes less applicable.

Chapter 4

Channel and Interference Measurement Campaigns

This chapter discusses the measurement campaigns that were performed in this thesis. The work includes 2 measurement campaigns. The first campaign was the first to measure the channel propagation effects in a gas refinery. The work and results of this campaign were published in a journal paper in the IEEE Antennas and Wireless Propagation Letters [61]. The second measurement campaign was the first to extract all 3 of the statistical functions (PDF, ACF, and CCF) of the interference created by WiFi. The chapter is divided into 4 sections. Section 4.1 will describe the hardware that was used and the measurements. Section 4.2 will discuss measurement setup and the results of the first measurement campaign. Section 4.3 will discuss the measurement setup and the results of the second measurement campaign. Finally, Section 4.4 will summarize the important results reached in this chapter.

4.1 Hardware and Software Radio Overview

All the measurement campaigns in this chapter made use of a Software Defined Radio (SDR). An SDR is a communication system that can send and/or receive wireless signals and uses components that are implemented in software rather than in hardware. The main idea of an SDR is to push the ADC of a receiver (or DAC of transmitter) as close as possible to the antenna and have most of the components implemented in software (or digitally). This makes the SDR re-programmable and can allow for multiple communication standards to be implemented on the same device. This concept made it possible to perform the measurement campaigns in this chapter.

The SDR used is the Universal Software Radio Peripheral (USRP) N210 Software Radio [83] which is used to implement and design radio systems. Table 4.1 summarizes the specifications of the USRP N210 with the SBX daughterboard. The USRP N210 uses an added-on SBX daugh-

terboard that allows it to send and receive signals at a center frequency in the range of 400 MHz-4.4 GHz. Industrial wireless networks and SU networks extensively use the ISM band at the 2.4 GHz band, and for this reason this band was selected for the measurements. The center frequency is programmable and was set to 2.4724 GHz for the measurement campaigns. The sampling frequencies of the ADC and DAC were set to 25 MHz which corresponds to a sampling time of 40 ns.

Table 4.1: USRP specifications

DC Input	6 V
Current Consumption	2.3 A
ADC Sampling Rate	25 MS/s
ADC Resolution	14 bits
DAC Sampling Rate	25 MS/s
DAC Resolution	16 bits
Dimensions (l x w x h)	22x16x5 cm
Weight	1.2 Kg

Figure 4.1 shows a simplified block diagram of the USRP transmitter. The software radio has an FPGA which sends data to a 16-bit DAC. The DAC converts this signal to an analog signal and the mixer upconverts the signal to the center frequency and finally the signal is amplified before being sent to the antenna. The blocks that have been shown in the figure are programmable and have initialization registers that control their modes of operation. The FPGA was used to initialize these registers to control operating parameters such as the DAC sampling frequency, mixer center frequency and amplifier gain. The FPGA is also used create the required signals that are to be sent to the DAC and the FPGA was coded using Verilog.

Figure 4.2 shows the USRP receiver block diagram, which has a programmable amplifier, mixer, and ADC. The FPGA is also used to send the initialization registers to these components and performs any further processing on received signals. A 10 Mbps Ethernet module, programmed in Verilog onto the FPGA, is used to send the processed data to be stored onto a computer or a

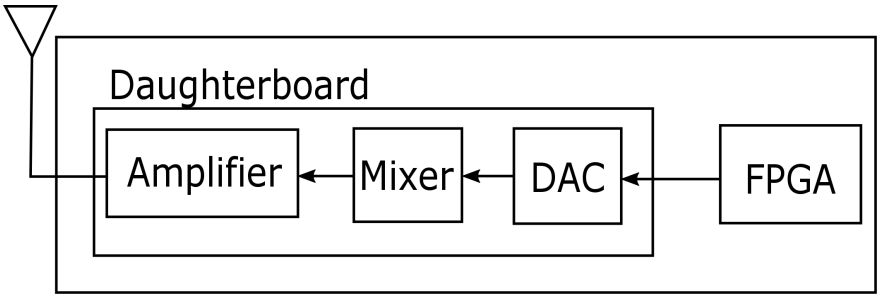

Figure 4.1: Simplified transmitter block diagram of USRP

Beaglebone Black [84]. The Ethernet module used was an opensource module from OpenCores [85].

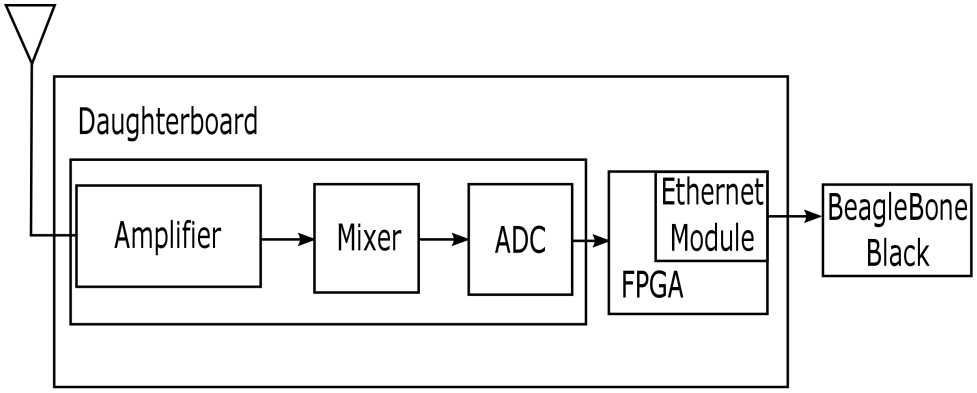

Figure 4.2: Simplified receiver block diagram of USRP

Figure 4.3 shows the measurement equipment, which in this case consists of two transmitters (one for each antenna) and a single receiver. The first measurement campaign will use two transmitters and a receiver, and the second will use two receivers. The USRP N210 needs a 6 V DC input that can be from an adaptor using a 110 V AC source. Some measurement environments did not have access to AC sources, and for this reason the devices used were all powered using 22.2 V, 21000 mAH Lithium Polymer (LIPO) batteries. Regulators were used to ensure that the necessary voltages and currents were available for each device. LIPO batteries can deliver substantial amounts of instantaneous current therefore fuses were used to ensure that no fires or damage to the

equipment occurred. In certain measurements the use of a computer for storage was not possible or practical, therefore a BeagleBone Black was used to store the data that was sent from the radio via Ethernet.

SIM940 rubidium clocks [86] were used to provide two synchronized reference signals to the radios which allows for the synchronization of multiple radios even if they are separated by a large distance. When multiple transmitters and/or receivers were used, the reference signals used had to be synchronized. The clocks are connected for a while and left to synchronize and then can be separated and will remain synchronized and provide synchronized reference signals for the duration of the measurement. One reference signal from the clock is the 10 MHz input source and the second signal is the Pulse Per Second (PPS) which is used to synchronize specific events for multiple radios. The SDRs have their own internal 10 MHz clocks which can be used if no synchronization is necessary which was not the case in any of the campaigns.

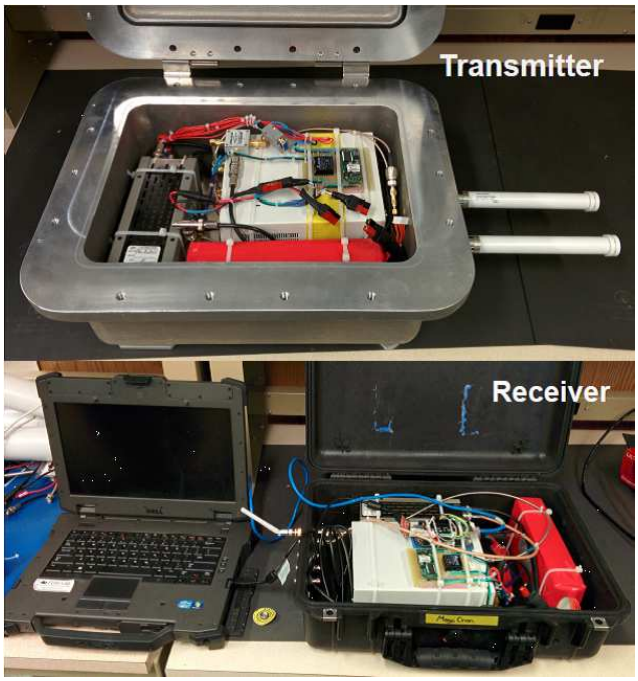

Figure 4.3: Measurement equipment

4.2 Wireless Propagation Measurement Campaign

This section will discuss the first measurement campaign and it is divided into 2 subsections. The first will describe the measurement setup used and the second will discuss the results obtained.

4.2.1 Measurement Setup

This is among the first measurement campaigns to measure the propagation channel effects at a gas refinery. The aim of this measurement campaign is to characterize the propagation channel in an industrial environment where a WSN may be used which would result in better WSN design. A multiple antenna measurement was used to obtain large-scale and small-scale channel effects in a gas refinery wireless channel. Two transmitters were used that each send a Pseudo-Noise (PN) sequence and a single receiver is used to receive these signals which allowed for the extraction of the required channel characteristics. The measured propagation channel characteristics can be used to create more realistic network simulations of such environments and for better network design.

The measurement was performed at a Shell Canada gas refinery, like that shown in Figure 4.4. The explosive nature of the environment, due to flammable vapors in the air, required that the equipment meet Class 1/Division 1 (C1/D1) standards [87] that are set by the Canadian Standards Association (CSA) [88]. Class 1 refers to a location made hazardous by the presence of flammable gases or vapors that may be present in the air in quantities sufficient to produce an explosive or ignitable mixture. Division 1 refers to a location where a classified hazard exists or is likely to exist under normal conditions. The C1/D1 requirements entail properly packaging and insulating equipment to ensure that no sparks occur that may cause an explosion. This is the reason the metallic enclosure, shown in Figure 4.3, was used to package the equipment. To work on-site, safety courses had to be taken which included a H2S Alive course and a Shell specified safety orientation. The difficulty to access such sites, due to the strict requirements, causes a barrier for research.

The campaign consisted of 80 measurements taken at possible sensor/actuator locations. A

Figure 4.4: Gas refinery

map showing the area where the measurements were taken is shown in Figure 4.5. There are three main regions that can be found in the map. Region 1 consists of tall metallic vessels (10-30 m high) and piping like what can be seen in Figure 4.4. Region 2 has buildings or equipment that are solid and/or metallic which were opaque to radio signals. Region 3 consisted of roadways that had overhead piping and conduit about 2.5 m above the ground. The transmitter was moved around to the 80 locations in a C1/D1 zone, where sensors would be expected to be, and are represented by the black circles, and therefore the transmitter needed to be C1/D1 compliant for these measurements. The receiver was placed in the central process control building and is represented by the star. This location was outside the C1/D1 zone and therefore did not need to be compliant with the standard. This measurement setup was designed to obtain the propagation channels for a many-to-one WSN in such an environment.

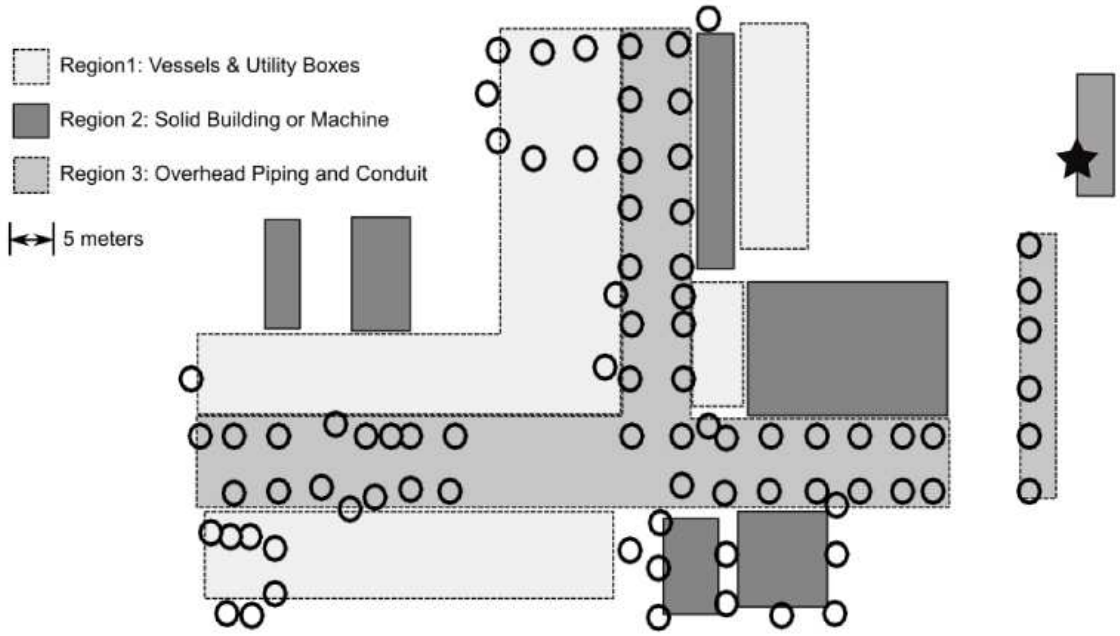

Figure 4.5: Measurement environment

Figure 4.6 shows the block diagram of one of the two transmitters used in the 2x1 MISO system to measure channel impulse responses. Each transmitter has its own radio and its separate antenna

which is a PCTEL MH024004NM dipole antenna [89] and the antenna separation was set at 16 cm. Both transmitters are in the same enclosure, powered by the same battery and had the same rubidium clock providing reference signals. Both transmitters send PN sequences at 25 Mchips per second which are created in the FPGA and sent to the DAC. The PN sequences have a maximal length of 2^{19-1} chips [90]. They both have a time offset difference of 2^{18} chips, which means that both sequences $P_1[n]$ and $P_2[n]$ will be orthogonal. The signals were transmitted at a 3 dB double sided bandwidth of 25 MHz, a 6 dBm Equivalent Isotropically Radiated Power (EIRP) and at a center frequency of 2.4724 GHz.

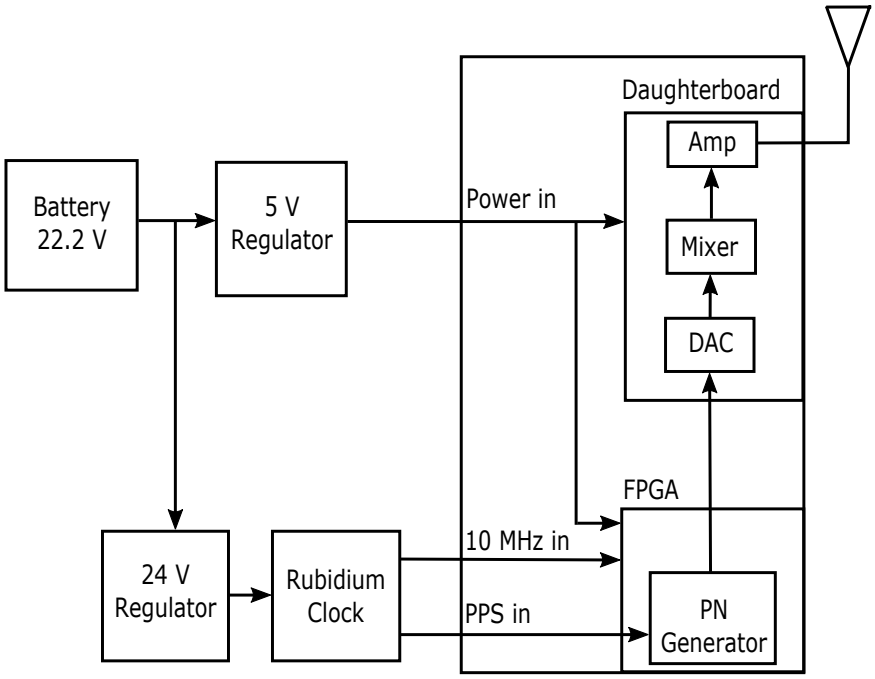

Figure 4.6: Transmitter block diagram for propagation measurements

Figure 4.7 shows the receiver block diagram that consists of one radio that is connected to a rubidium clock and both these devices are powered by a single battery. The receiver radio receives signals at a center frequency of 2.4724 GHz and the correlation with the two PN sequences is performed in the FPGA. A correlation window of 69 chips is used and this window is shifted over 100,000 chips which corresponds to a measurement capture rate of 250 Hz over a 4 ms period.

For this correlation to be successful and accurate, the transmitters and receiver all need to be synchronized in time. This is achieved using the rubidium clock references, one connected to both the transmitters and the other to the receiver, and only after both clocks have been left to synchronize can the measurements start.

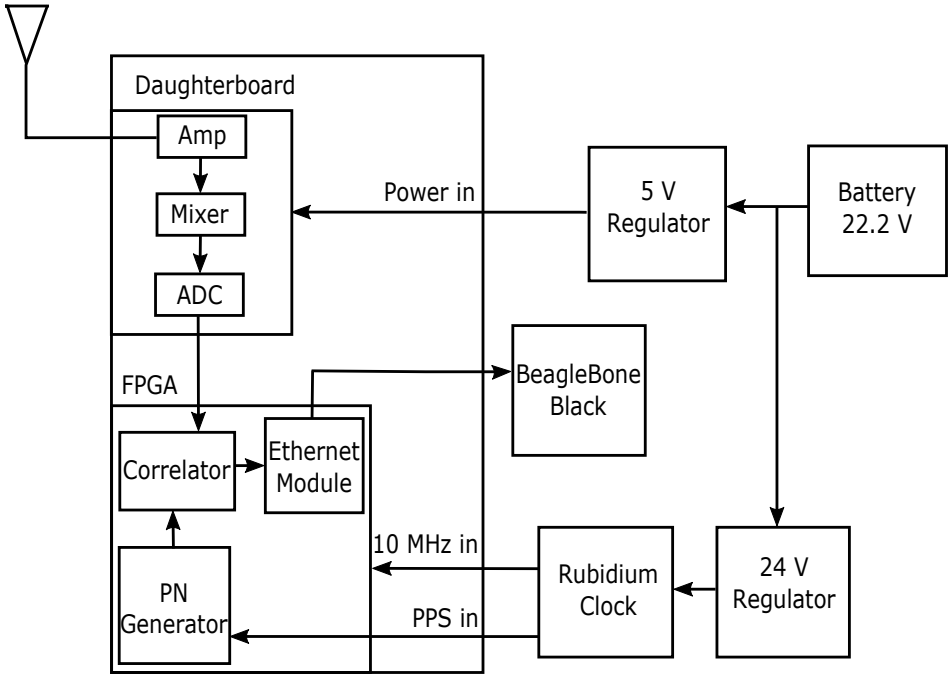

Figure 4.7: Receiver block diagram for propagation measurements

4.2.2 Results

This section will show and discuss the results of the first measurement campaign which aims to characterize the wireless propagation channel in a gas refinery. The results will be divided into 2 parts, the large-scale channel effects, and the small-scale channel effects.

The campaign consisted of 80 measurements, each at possible sensor/actuator locations. Each measurement consists of N captured channel impulse responses with L discrete channel taps from each antenna i, represented by $h_{\mathrm{i}} \in C^{\mathrm{NxL}}$, which has a normalized total energy. The element in row n and column l for antenna i is denoted by $h_{\mathrm{i}}(n, l)$. There are two main channel characteristics that

were measured, namely the large-scale and the small-scale channel effects. Large-scale channel effects are those that occur over a spatial distance of many wavelengths, hundreds or more. Two large-scale effects are calculated, the path loss exponent and the shadowing distribution. Small-scale fading is mostly a result of multi-path fading and has been found to occur in the spatial distance of about half a wavelength. For the small-scale channel effects three parameters are calculated; namely the coherence bandwidth, K-factor, and the antenna correlation coefficient.

Large-scale Channel Effects

Fading refers to the rapid fluctuations in received signal strength. Large-scale fading describes the variation of received signal strength over large distances. The two main large-scale fading factors are the path loss exponent and the shadowing distribution. The path loss exponent describes how quickly this received power is expected to decay as the distance from the transmitter increases. Different measurements taken at a fixed distance between the receiver and transmitter will have varying received powers from what is expected from the path loss. These variations follow a distribution known as the shadowing distribution.

The path loss exponent is a very important factor that has a major part in the analysis and design of the link budget of communications systems. Calculating this factor in a gas refinery allows for better simulations and designs of WSNs in these environments. It is also essential for analysis of link budgets and the calculation of the required node transmit powers. Sensor nodes usually run on batteries and transmission power is a major part of the power consumption of the batteries of nodes in a network. Having accurate power loss exponents would help analyze and simulate network performance and therefore facilitate the implementation of WSNs.

To determine the large-scale channel effects, an average attenuation is calculated for each location r using $A_{\mathrm{r,i}} = \frac{1}{N}\sum_{\mathrm{n}}\sum_{\mathrm{l}}|h_{\mathrm{i}}(n,l)|^2$, which is basically the difference between the transmit power and the averages of the received signal from antenna i over the N measurements. The average attenuation is taken for all measurements that were within a 0.5 m x 0.5 m spatial region

to get an average attenuation at that location. Averaging over all these measurements removes the small-scale effects in each measurement.

The path loss exponent is calculated by plotting the log-attenuation at each location versus the log-distance of each location from the central building that has the receiver. The slope of the best fit line will give the path loss exponent as done in [54]. Figure 4.8 shows the attenuation versus log-distance plot and the path loss exponent was calculated and found to be 2.828. This path loss is above that of an indoor environment which falls in the range of 1.6-1.8 and within the range of urban environments which have a range of 2.7-3.5 [93].

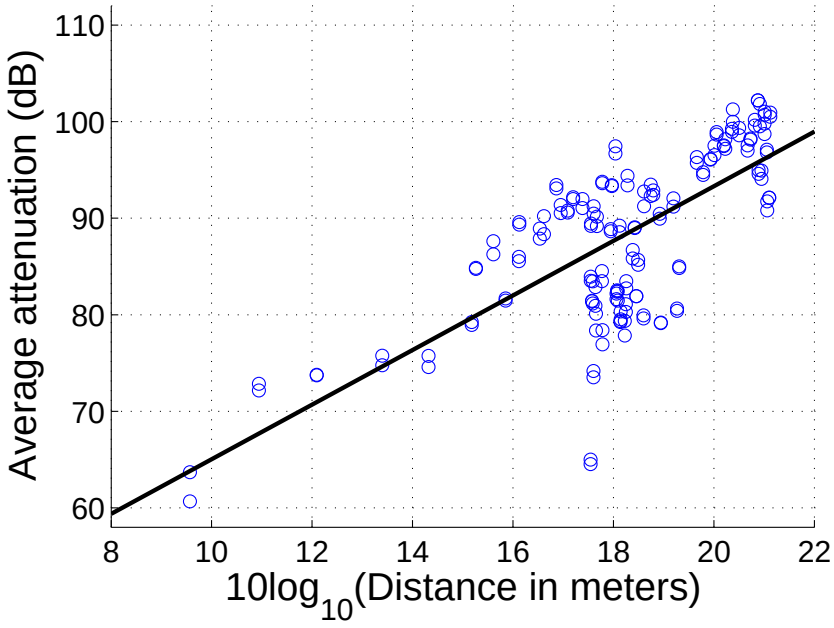

Figure 4.8: Log average attenuation versus log distance

The other large-scale channel effect is shadowing. Path loss shows the average reduction in received power as a function of distance from receiver. There are deviations from this average value due to multi-path effects. The value of the deviation from this average has a distribution which will be obtained. The importance of measuring the shadowing distribution is to know the

variance about the mean received power to have more accurate link budget calculations for links in a WSN.

Shadowing is the deviation of each average received power from the best fit line in the attenuation versus log-distance plot. These values of deviation are used to plot the PDF of the shadowing distribution. It has been shown that indoor wireless channels show shadowing distributions that are close to log-normal [94]. Figure 4.9 shows the shadowing distribution measured at the gas refinery which does not conform to the log-normal distribution of indoor environments. It is also not symmetric about 0 dB. We can assume that this is due to a lack of random changes, but not due to the lack of scattering events caused by the large number of metallic objects in the environment. These metallic obstacles we assume will scatter the signal but in a less random manner than would be the case in other environments such as indoor environments.

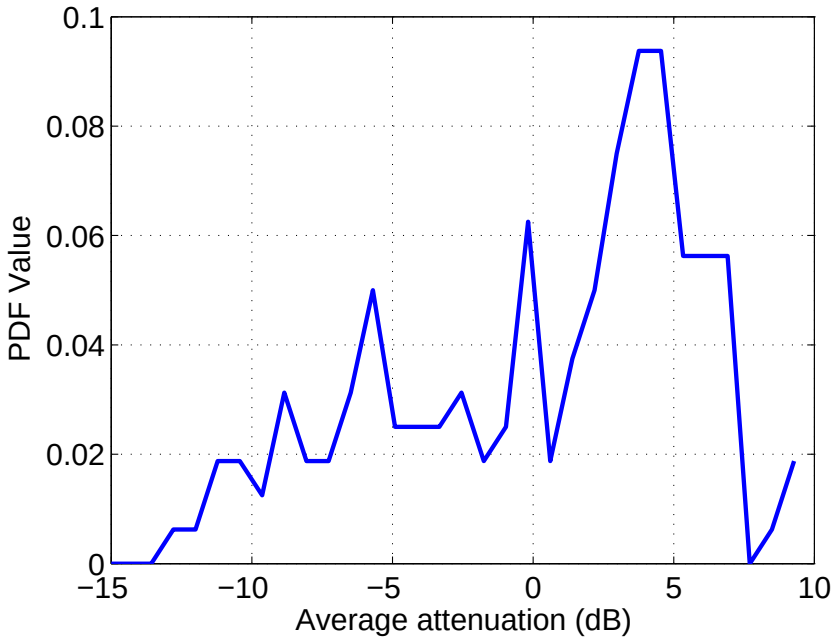

Figure 4.9: Shadowing distribution

Small-Scale Channel Effects

The small-scale analysis includes calculating parameters like the coherence bandwidth, K-factor, and antenna correlation. The coherence bandwidth is defined as the range of frequencies over which the channel can be considered flat. The larger the coherence bandwidth, the larger the signal bandwidth that can be used such that it experiences flat fading. Frequency selective fading causes distortions in the received signal. Calculating the coherence bandwidth gives insight into what would be considered as acceptable channel separations and therefore in choosing which communication standard could be used in this environment. It also helps decides what channel separation would be acceptable for use of frequency diversity techniques.

The 50% coherence bandwidth is calculated, and it is defined as the frequency separation of 2 sinusoids such that their correlation is 0.5. It is calculated as $1/5T_{\text{rms}}$ where T_{rms} is the RMS delay spread which is calculated from the power delay profile (PDP) which is obtained by averaging the power of h_{i} over the n axis [54]. The CDF of the coherence bandwidth is shown in Figure 4.10 and the mean coherence bandwidth is calculated to be 1.36 MHz which corresponds to a mean RMS delay spread of 147.04 ns. The industrial wireless network standard ISA 100.11a [95] uses the Zigbee 802.15.4 physical layer which uses a channel separation of 5 MHz. This means that the use of such standards with this channel separation would have little distortion to signals. This also means that channels in this environment, neighboring channels can be considered independent of each other allowing for the use of frequency diversity techniques.

The fading distribution refers to the distribution of the received signal envelope. The type of fading distribution describes the fading channel at the gas refinery. Two famous distributions are the Rayleigh and Rician fading channels and the K-factor is important in differentiating between them. The K-factor is the ratio between the Line-Of-Sight (LOS) and the non-LOS components. Zero or close to zero K-factors mean the fading distribution is Rayleigh and this would mean that there are no LOS components and all or most of the power arrives at the receiver through scattering components in the environment. Higher K-factors would mean that the power of the

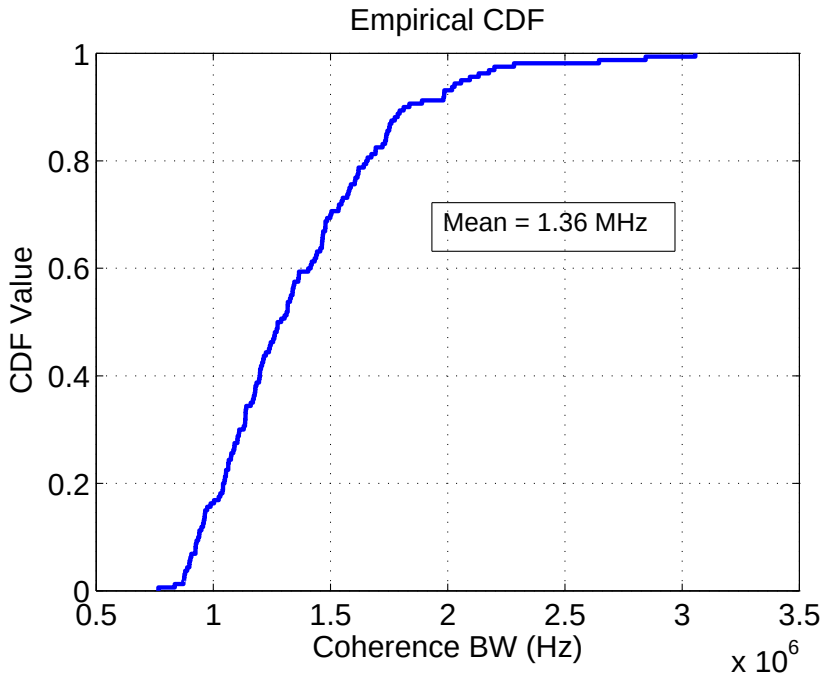

Figure 4.10: CDF of coherence bandwidth

LOS components is a lot larger than that of the scattered components and this would give a Rician fading distribution.

To estimate the K-factor, the method of moments is used as in [96]. This method entails using a time varying channel response that is narrowband. This means that the channel frequency response is first calculated, and only independent channel bands are used to ensure the narrowband condition remains. The Fourier Transform for each antenna of the channel, h_{i}, is taken along the l axis to give us the channel response matrix which is defined as $H_{\mathrm{i}} \in C^{\mathrm{NxL}}$ where $H_{\mathrm{i}}(n, w)$ is the matrix element in the n^{th} row and w^{th} column. To find the number of independent frequency response bands we use $R = \lfloor W_{\mathrm{sig}}/W_{\mathrm{coh}} \rfloor$ where W_{coh} is the coherence bandwidth calculated before and W_{sig} is the signal bandwidth. For each measurement, there are R independent frequency points taken and since there are N fading values captured we can create a fading vector for the i^{th} antenna of size $1\mathrm{x}NR$ and defined as $e_{\mathrm{i}} = [|H_{\mathrm{i}}(0,0)|\ |H_{\mathrm{i}}(1,0)|\ \ldots\ |H_{\mathrm{i}}(N-1,0)|\ |H_{\mathrm{i}}(W_{\mathrm{coh}},0)|\ \ldots\ |H_{\mathrm{i}}(W_{\mathrm{coh}},N-1)|$

... $|H_{\mathrm{i}}(RW_{\mathrm{coh}},0)|$ ... $|H_{\mathrm{i}}(RW_{\mathrm{coh}},N-1)|$]. Since there are 80 measurement locations and 2 antennas, there will be 160 fading vectors.

We first assume that each of these elements, in e_{i}, has been taken from a Rician distribution. The elements are then used to plot a histogram of their true distribution using X bins which will depend on the desired degrees of freedom in the Chi-squared goodness of fit test. Using maximum-likelihood distribution fitting, the closest Rician distribution is found also for the same X bins. A Chi-squared goodness of fit test is applied to each of these vectors as in [97]. The number of bins, X, is selected to have a reasonable number of degrees of freedom which was chosen to be 50. Since there are 3 degrees of freedom used up (i) sum of bins is X, (ii) the v parameter is used to define the Rician distribution and (iii) the s parameter is used to define the Rician distribution, that makes us use $X = 53$ bins. In the goodness of fit test, the observed values are those from the measured histogram and the expected values are those from the best fit Rician distribution. A significance level of 10% is used in the Chi-squared goodness of fit test, which means that 10% of the measurements that are Rician will be discarded. Only those vectors that satisfy the Chi-square test will be considered Rician and only their K-factors will be used.

The K-factors that passed the Chi-squared goodness of fit were used to plot the CDF of the K-factors in Figure 4.11. Those that passed the Chi-squared test are 144 which is 90% of all the locations. The mean of the K-factors was calculated to be -2.95 dB which is low, and this leads us to believe that the fading distribution is Rayleigh, which makes sense since there are a lot of surrounding buildings that will cause scattering and reflections. The many metallic buildings in the environment will also mean that the power of the reflected signals is large as compared to LOS components that may exist.

The antenna correlation, for a given antenna separation, describes the similarity of the received signals by each antenna. The correlation of received signals from multiple antennas is dependent on the environment. Having a large correlation would mean that using spatial diversity techniques to improve performance would not be helpful. This usually occurs in environments with very little

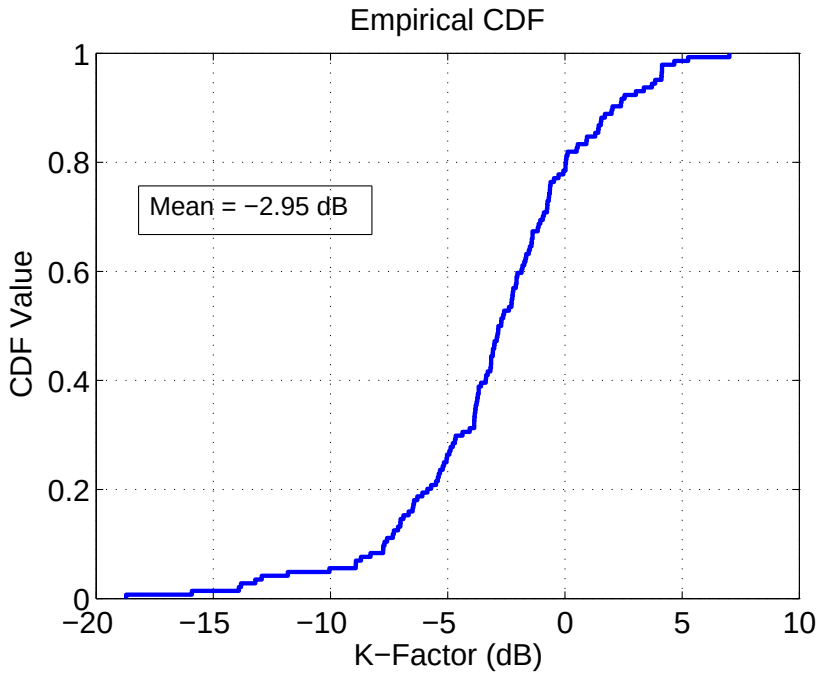

Figure 4.11: CDF of K-Factors

obstacles causing scattering and therefore the antenna spacing would need to be large to obtain low correlation values, which becomes impractical for nodes in a WSN. Calculating the correlation helps assess if the use of multiple antenna techniques would be practical.

To calculate the correlation between the antennas, with a separation of 0.16 m, the correlation coefficient between e_1 and e_2 are calculated for all measurements even if it does not satisfy the Chi-Square goodness of fit for a Rician distribution. This is because calculating the antenna correlation is independent of the type of the fading distribution of the channel. The CDF of the correlation values is plotted and shown in Figure 4.12 and the mean value of the correlation coefficient is found to be 0.077. This is very low and means that multiple antenna techniques will be effective for diversity or spatial multiplexing since the channels between the antennas can be considered independent. The use of multiple antennas, however, will depend on the size and cost allowed for the sensor nodes.

To conclude, this measurement campaign characterized the wireless propagation channel in a

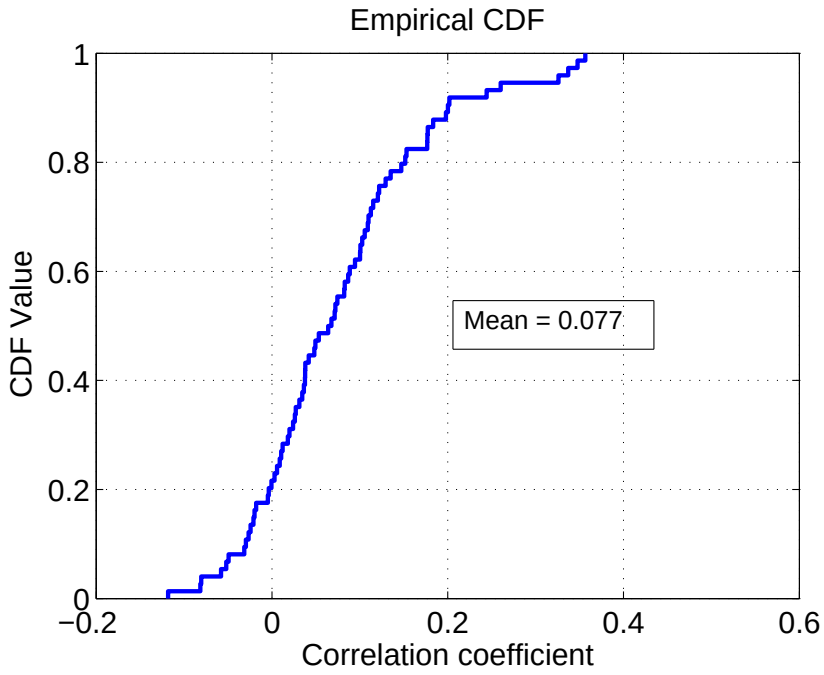

Figure 4.12: CDF of antenna correlation coefficient

gas refinery and measured large-scale and small-scale channel effects. Regarding the large-scale effects, the path loss exponent and the shadowing distribution were measured and found to be 2.828, which is higher than indoor environments and in the lower range of urban environments. The shadowing distribution did not follow the known log-normal distribution and was also asymmetric about 0 dB. In the small-scale channel effects, the coherence bandwidth, K-factor, and antenna correlation were measured. The mean coherence bandwidth was found to be 1.36 MHz, which is reasonable for the Zigbee channel separation of 5 MHz and makes the environment suitable for the use of frequency diversity techniques. The mean K-factor was calculated to be -2.95 dB, which means the signals experience Rayleigh fading. The mean antenna correlation for a spacing of 16 cm was found to be 0.077, which is very low and means that multiple antenna diversity and spatial multiplexing techniques can be used in this environment.

4.3 Interference Statistical Functions Measurement Campaign

This section will discuss the second measurement campaign and it is divided into 2 subsections. The first will describe the measurement setup used and the second will discuss the results obtained.

4.3.1 Measurement Setup

This measurement campaign is the first to measure all three statistical functions, namely the PDF, ACF, and CCF of interference from a random-access network. The measurement took place inside the Taylor Family Digital Library at the University of Calgary over a period of about 2 hours where many students use their laptops to access WiFi. The number of students studying at this location were at least 30. Two radios were used in this campaign as receivers, each with a single D-Link 2 dBi SMA antenna, and each radio was placed 0.5 m above the ground during all measurements. One radio had a fixed location, and the other radio was placed at the distances 0.5, 1, 1.5, 2, 2.5, 3, 4, 5, 6, 7, 8, 9, 10 m away from the first radio along a straight line. At each of these locations, both radios were made to record the interference for 10 minutes. The rubidium clocks were synchronized and made to provide the 10 MHz reference signal and PPS signal to each radio to keep the radios sampling at synchronized times which is essential for the CCF measurement.

Figure 4.13 shows the block diagram of a single receiver and both receivers in the measurement are identical. The rubidium clocks are left to synchronize before starting the measurement campaign to ensure that the reference clocks and PPS signals, that both receivers get, are synchronized and therefore the ADCs will be sampling at the same time. The ADC samples an in-phase and quadrature component at 25 MHz and sends them to the FPGA. The integer value representing the ADC level of the samples from the in-phase and quadrature component are i and q, respectively. The radio uses a 14-bit ADC and one of the bits are used for the sign of the signal. The Root Mean Square (RMS) voltage that this integer represents can be calculated using Equations 4.1, where V_{pp} is the ADC peak-to-peak voltage, N is the number of bits of the ADC, and R_{in} is the input ADC resistance. The power of the signal can then be calculated using Equation 4.2. The FPGA

then calculates the average interference power over a period of 2500 ADC samples, which means the FPGA outputs averaged samples at a sampling rate of 10 kHz. These samples represent the average interference power over the interval of time, $T_s = 100\mu s$ seconds. These samples are then sent to ethernet module that finally sends them to be stored in the BeagleBone Black.

$$i_{\text{rms}} = |i|\left[\frac{V_{\text{pp}}}{2^{N-1}\sqrt{2}}\right] \quad , \quad q_{\text{rms}} = |q|\left[\frac{V_{\text{pp}}}{2^{N-1}\sqrt{2}}\right] \tag{4.1}$$

$$Z = \frac{i_{\text{rms}}^2}{R_{\text{in}}} + \frac{q_{\text{rms}}^2}{R_{\text{in}}} \tag{4.2}$$

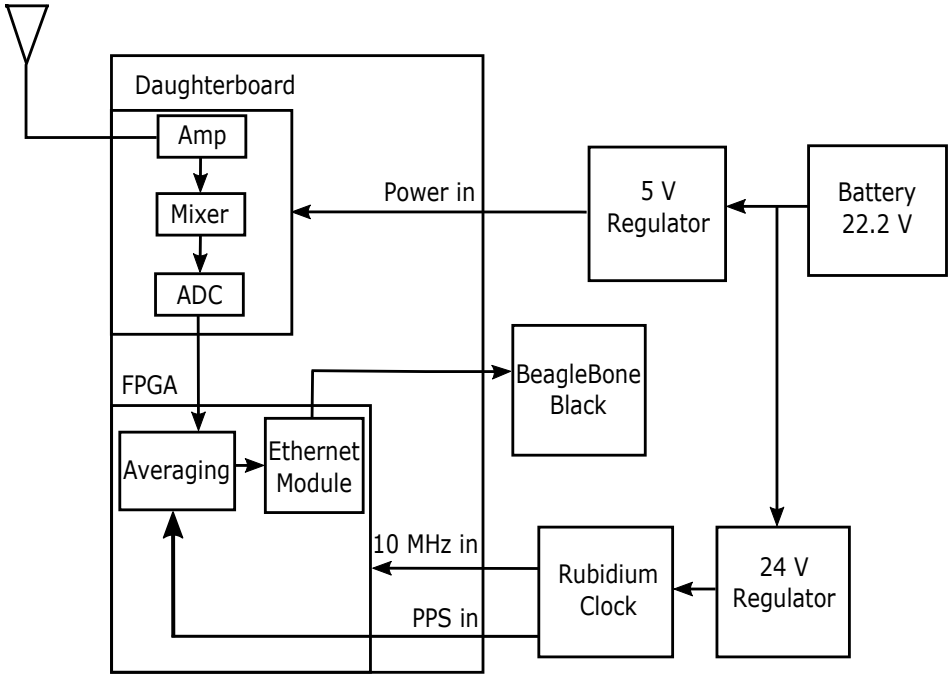

Figure 4.13: Receiver block diagram for single receiver statistical functions measurement

The radio ADCs are sampling at the same time, but it would be impossible to start the measurements at the same time on both radios and the PPS signal is used for this purpose. The radios create averaged samples at 10 kHz and the PPS creates a pulse every second, which means that every 10000 samples the PPS signal has an impulse and this specific sample is marked in both radios. If the starting times for both radio measurements were more than a second apart, the corre-

sponding PPS samples may be lost. For this reason, 4 steps are taken to ensure the synchronization of the measurements. Firstly, the start and end of a measurement is only considered from a PPS occurrence and samples before the first PPS and after the last PPS are neglected. Secondly, the first radio will always have its measurement start first and end last. Thirdly, the signal of the second radio will be correlated with the signal from the first radio multiple times, and each time removing 1 second segments from the first radio signal, for a maximum of 10 seconds, until the maximum correlation is found. This will be the starting point of both signals. Finally, the shortest length between both signals will be considered as the final length for both signals.

After the starting points and ending points of each signal are chosen, there will be 26 interference signals, 2 from each radio for each of the 13 locations. The PDF, ACF and CCF are calculated as explained in Section 3.1.3. The PDF will be obtained using interference values from all 26 interference signals. The average ACF is obtained averaging all 26 ACFs from each interference signal. The CCF is obtained by calculating the correlation coefficient between the signals of both radios at each measurement location, and then plotting these correlation coefficients against the relative distances between the radios.

4.3.2 Results

This measurement campaign aims to characterize interference in the 2.4 GHz band by obtaining the interference statistical functions, namely the PDF, ACF and CCF. The main differences in this campaign are that interference values are averaged, and the use 2 radio receivers allows the CCF to be calculated.

The average interference ACF was obtained and shown in Figure 4.14. The ACF seems to have repeated spikes occurring every 1000 sampling times, which corresponds to 100 ms. The reason for this is that access points for 802.11 send beacon packets that are sent out every 102.4 ms (on default) [64].

Figure 4.15 shows the ACF when zoomed in and the effects of the beacons are neglected. The ACF can be assumed to have a triangular shape as seen in Section 3.1.2, and the triangle width

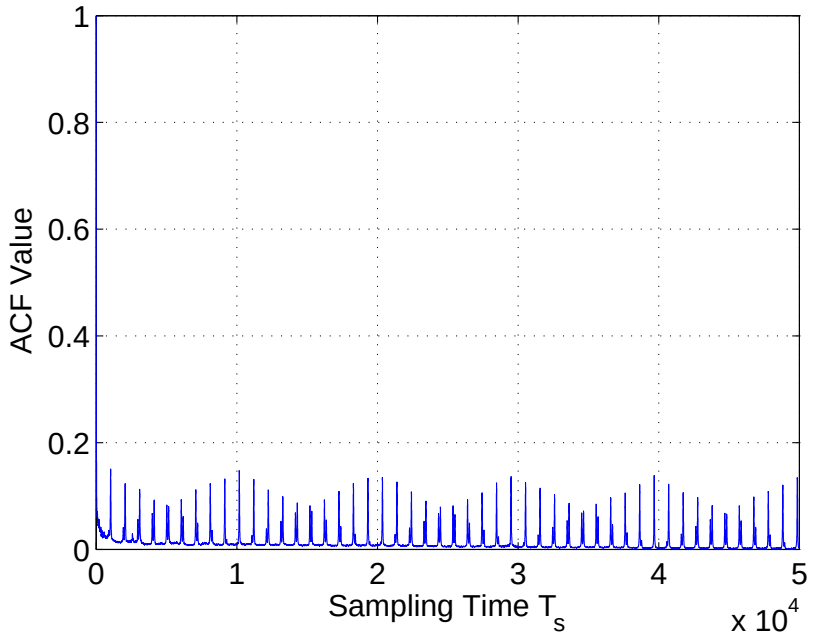

Figure 4.14: ACF with Beacon

corresponds to the average packet lengths, which was assumed by the interference model in Section 3.3.1. The ACF reaches a value less than 0.1 at about 45 samples which corresponds to average packet lengths of 4.5 ms. For the 802.11 standards, the Maximum Transmission Unit (MTU) is 2312 Bytes, and the slowest internet rates are 1 Mbps, which gives a maximum packet time of 18.5 ms seconds which is 4 times the average packet length estimated from the measurements.

Figure 4.16 shows the PDF obtained from all interference values of both radios and can also be seen to consist of multiple distributions, caused by multiple interferers. The humps that describe the different distributions, have different means representing different received powers. The differences in received power for different users could be due to their distance from the radio and due to different transmit powers. The distributions also have different probabilities of occurrence which is due to the different traffic for each user. The total PDF measured is a result of switching between the different distributions caused by each user, with their respective probabilities of utilizing the channel. More measurements of multiple network realizations are necessary to obtain a smoother

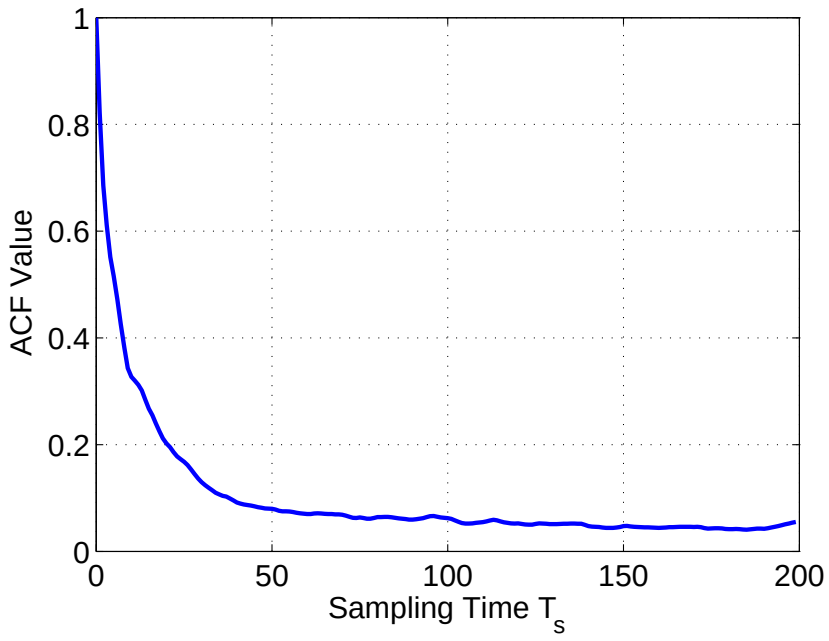

Figure 4.15: ACF without Beacon

PDF. The measurements show what is expected from this scenario and more measurements and smoother PDFs (like what would be obtained from simulations) are necessary to be able to fit the Chi-squared PDF model to these measurements. The large hump on the left is due to the noise of the receivers since the average noise power was calculated to be about -82.83 dBm.

The CCF was obtained by calculating the correlation coefficients between the interference of each radio for every measurement location. Figure 4.17 shows the CCF plotted against the distances between the radios. The correlation values remain high and quite constant for a certain distance and then quickly decay rapidly to near zero values, at about 5 m, and remain there.

The results do not seem to have smooth CCF curves that gradually decay, as was seen in simulations and predicted by the CCF model in Section 3.3.2. When calculating the CCF from simulated interference, it was observed that there was a big difference between results obtained from a single network realization, and results averaged over many network realizations. It was observed that CCFs obtained from the simulation of a single network realization varied drastically

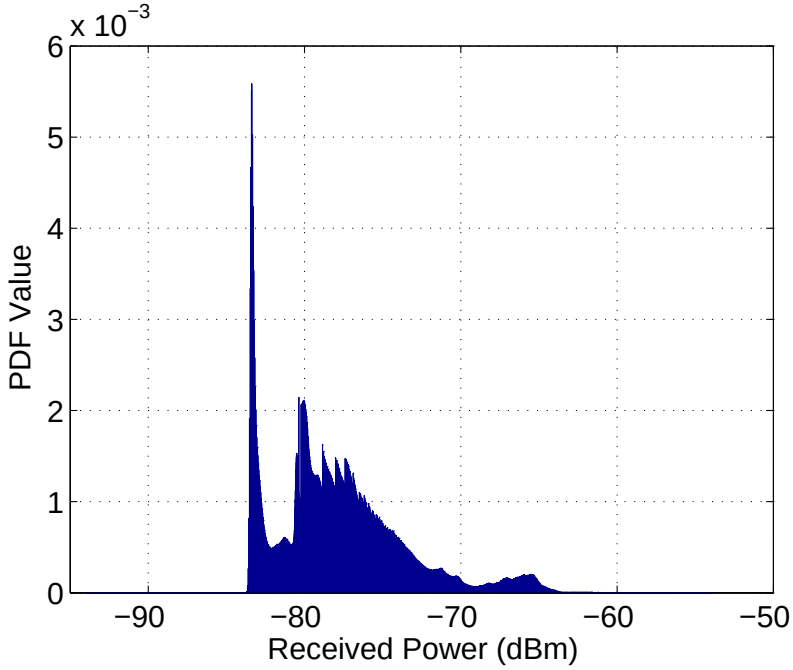

Figure 4.16: PDF for interference

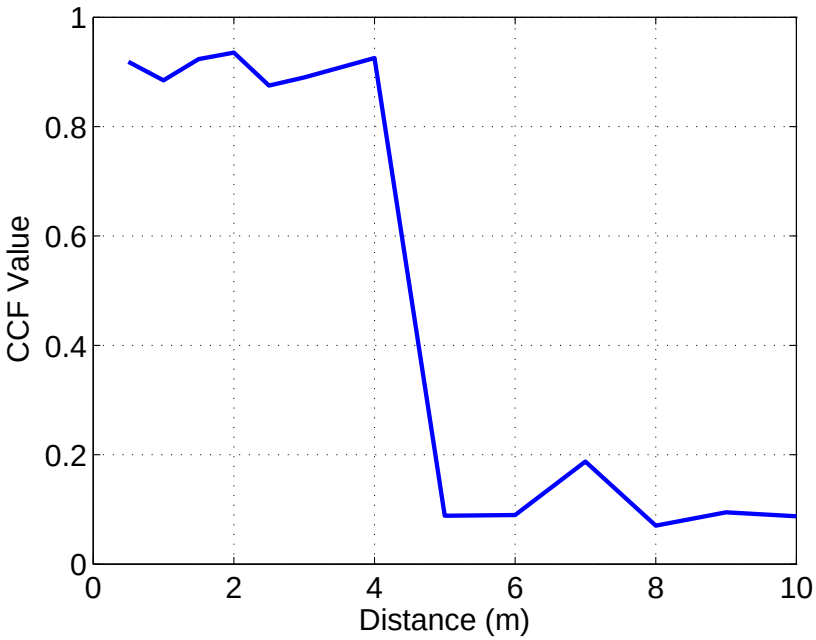

Figure 4.17: CCF for interference

between rapidly decaying CCFs, very slow decaying CCFs and in certain cases CCFs that are similar to those obtained in the measurement, that remain constant then rapidly decay to near zero values. When averaged over many network realizations, smooth CCFs can be obtained that gradually decay to zero.

This measurement campaign obtained the interference statistical functions of WiFi interference in a University library. The ACF was shown to be similar to a triangular function and values for the packet ranges were shown to be around a quarter of the MTU values. The PDF showed many users of the measured channel and a broad range in received powers. The CCF was also measured by calculating the correlation values at different distances between the two radios. This is the first measurement campaign to obtain the 3 statistical functions in a single measurement.

4.4 Conclusion

The first measurement campaign characterized the wireless propagation channel effects found at a gas refinery which measured the large-scale and small-scale channel effects. For the large-scale effects, the path loss exponent and shadowing distributions were measured. The path loss exponent was found to be 2.828 which is larger than free space path loss but lower than in urban environments. The shadowing distribution was found to not follow log-normal shadowing and was not symmetric about 0 dB. The small-scale channel effects that were measured were the coherence bandwidth, K-factor, and the antenna correlation at 0.16 m separation. The average 50% coherence bandwidth was found to be 1.36 MHz which was suitable for use of frequency diversity techniques for the Zigbee standard that uses 5 MHz channel spacing. The average K-factor was found to be -2.95 dB which means that the type of fading is Rayleigh. The antenna correlation at 16 cm antenna spacing was found to be 0.077 which is good for the use of spatial diversity techniques.

The second measurement setup was performed in a University library and aimed at extracting the statistical functions of interference in the 2.4 GHz band, namely the PDF, ACF and CCF. The PDF of the received interference power consisted of a combination of multiple distributions.

The ACF could be approximated to triangular function which corresponded to average packet lengths of 4.5 ms, which is about a quarter of the MTU. The CCF consisted of higher values when calculated using interference signals in the dBm scale instead of linear scale. The measured CCF had high values for the first few meters and then rapidly decayed which is due to measurements only considering a limited number of network realizations. More measurement realizations would produce smoother curves for the PDF and CCF.

Chapter 5

Conclusion and Future Work

This chapter will give the main conclusions reached by the work in this thesis. The contributions of this thesis were summarized in Section 1.4. The chapter will consist of 2 sections. Section 5.1 will highlight the most important conclusions in each of the chapters in the thesis. Section 5.2 will discuss future work.

5.1 Conclusions

In Chapter 2 RLNC was found to be more time and energy efficient than flooding. RLNC was found to be more resilient to interference than flooding was since it made use of repeated packets unlike flooding. An interesting observation was that the larger the node density a network has, the better the performance of RLNC while that of flooding was reduced. The simulation platform described in this chapter was the basis on which the proposed model in Chapter 3 was validated.

In Chapter 3 we described the interference as a stochastic process and defined its first and second order statistics. The process was assumed to be WSS in time and space and this assumption was shown to be reasonable which simplified the calculation of the required statistical functions. The proposed interference model simultaneously models the PDF, ACF, and CCF. A Chi-squared PDF is used since it allows for the creation of correlated signals when synthesizing interference. Derivations were provided for all the important model parameters and they were related to the network parameters of the interfering network, namely p, T_{f}, and λ. The model was found to be accurate but produces slightly better results than when using simulated interference since the model assumes a single interferer. This assumption becomes less accurate as the interference network parameter values are increased.

Chapter 4 discussed the results produced by 2 measurement campaigns. The first measurement

campaign performed, aimed at measuring the large-scale and small-scale channel effects in a gas refinery. For the large-scale effects, the path loss exponent was shown to be higher than the free space path loss but less than what is expected in urban areas. The shadowing distribution was shown to not follow the expected log-normal distribution. The small-scale channel effects that were measured were the coherence bandwidth, K-factor, and the antenna correlation at 0.16 m separation. The coherence bandwidth was small enough for frequency diversity techniques to be used with the Zigbee standard which uses 5 MHz channel spacing. The K-factor was small enough for Rayleigh fading to be assumed in this environment. The antenna correlation means that spatial diversity techniques would be viable.

The second measurement setup was performed in a University library and aimed at extracting the statistical functions of interference in the 2.4 GHz band, namely the PDF, ACF and CCF. The PDF consisted of multiple distributions that were caused by the users of the channel. The different users used the channel with different probabilities and the received interference power varied. This created the humps of the multiple distributions. More measurements from multiple network realizations would smoothen this distribution. The ACF measured showed that the triangular function approximation is a reasonable one. The ACF was used to approximate the average packet lengths as 4.5 ms, which is about a quarter of the MTU of the WiFi standard. The measured CCF had high values for the first few meters and then rapidly decayed which is due to measurements only considering a limited number of network realizations. More measurements of other network realizations would also produce a smoother CCF.

5.2 Future Work

The future work discussion will be divided into possible future points of research that could branch out of each chapter in this thesis.

The future work related to Chapter 2 is:

1. Produce a closed form optimal value for p where flooding and RLNC would ideally operate at

2. Derive closed form equations for the network coverage as functions of time and energy per node and relate them to the network parameters p, T_f, and λ

3. Improve the RLNC algorithm to further improve WSN broadcasting performance

The future work related to Chapter 3 is:

1. Produce multi-band CR simulation platform and use interference model to predict spectrum sensing performance

2. Use collaborative spectrum sensing and study trade-off of improved performance vs. increased latency and energy required for extra broadcasting

The future work related to Chapter 4 is:

1. Perform multiple measurements of the second measurement campaign to obtain smoother PDFs and CCFs that would allow more detailed comparison between measured results and the proposed interference model in Chapter 3

2. Test interference model for near field distances such as antenna separation for MIMO receivers and test CCF accuracy for at different antenna separations

3. Perform multi-band measurement campaign that captures interference characteristics over both time and frequency

Bibliography

[1] http://www.public.navy.mil/subfor/cus/Pages/sosus_origins.aspx, (Visited on 11/12/2015).

[2] C. E. Nishimura, "Monitoring whales and earthquakes by using sosus," *1994 NRL Review*, pp. 91–101, 1994.

[3] Q. Wang and I. Balasingham, *Wireless sensor networks-an introduction*. INTECH Open Access Publisher, 2010.

[4] S. Kumar and D. Shepherd, "Sensit: Sensor information technology for the warfighter," in *Proc. 4th Int. Conf. on Information Fusion*, 2001, pp. 1–7.

[5] "Ieee-sa -ieee get 802 program - 802.15: Wireless pans," https://standards.ieee.org/about/get/802/802.15.html, (Visited on 11/12/2015).

[6] J. W. Gardner and V. K. Varadan, *Microsensors, MEMS and smart devices*. John Wiley & Sons, Inc., 2001.

[7] R. Zurawski, *Industrial communication technology handbook*. CRC Press, 2014.

[8] K. Lee, "Wireless sensing and ieee 1451," in *Sensor Conf./Expo*, 2001.

[9] "Connected world - m2m basics," http://connectedworld.com/m2m-basics/, (Visited on 11/12/2015).

[10] "Neue produkte: Gsm-modul m1 - computerwoche.de," http://www.computerwoche.de/a/gsm-modul-m1,1105147, (Visited on 11/12/2015).

[11] H. Gill, "From vision to reality: cyber-physical systems," in *Presentation, HCSS National Workshop on New Research Directions for High Confidence Transportation CPS: Automotive, Aviation and Rail*, 2008.

[12] J. Wan, M. Chen, F. Xia, L. Di, and K. Zhou, "From machine-to-machine communications towards cyber-physical systems," *Computer Science and Information Systems*, vol. 10, no. 3, pp. 1105–1128, 2013.

[13] H. Ning, *Unit and ubiquitous Internet of Things*. CRC press, 2013.

[14] B. Galloway and G. P. Hancke, "Introduction to industrial control networks," *Communications Surveys & Tutorials, IEEE*, vol. 15, no. 2, pp. 860–880, 2013.

[15] R. E. Young, "Petroleum refining process control and real-time optimization," *Control Systems, IEEE*, vol. 26, no. 6, pp. 73–83, 2006.

[16] I. Johnstone, J. Nicholson, B. Shehzad, and J. Slipp, "Experiences from a wireless sensor network deployment in a petroleum environment," in *Proceedings of the 2007 international conference on Wireless communications and mobile computing*. ACM, 2007, pp. 382–387.

[17] "Isa100, wireless systems for automation- isa," https://www.isa.org/isa100/, (Visited on 11/13/2015).

[18] "Hart communication protocol and foundation - home page," http://en.hartcomm.org/, (Visited on 11/13/2015).

[19] T. Bourke, "Isa100. 11a completely obviates the need for wirelesshart," *Measurement and Testing*, vol. 1, no. 1, pp. 18–19, 2007.

[20] "Industrial networks — wirelesshart wins standards battle against isa100," http://www.controldesign.com/industrynews/2012/wirelesshart-wins-standards-battle-against-isa100/, (Visited on 11/13/2015).

[21] J. Mitola and G. Q. Maguire, "Cognitive radio: making software radios more personal," *IEEE personal communications*, vol. 6, no. 4, pp. 13–18, 1999.

[22] I. F. Akyildiz, W.-Y. Lee, M. C. Vuran, and S. Mohanty, "A survey on spectrum management in cognitive radio networks," *IEEE Communications magazine*, vol. 46, no. 4, 2008.

[23] T. M. Chiwewe, C. F. Mbuya, and G. P. Hancke, "Using cognitive radio for interference-resistant industrial wireless sensor networks: An overview," *IEEE Transactions on Industrial Informatics*, vol. 11, no. 6, pp. 1466–1481, 2015.

[24] A. Wilzeck, E. Dimitrov, and A. Tissen, "Applications of cognitive radio systems for industrial wireless automation," in *Proceedings of the 4th International Conference on Cognitive Radio and Advanced Spectrum Management*. ACM, 2011, p. 65.

[25] F. F. Digham, M.-S. Alouini, and M. K. Simon, "On the energy detection of unknown signals over fading channels," *IEEE transactions on communications*, vol. 55, no. 1, pp. 21–24, 2007.

[26] F. Penna, R. Garello, and M. A. Spirito, "Cooperative spectrum sensing based on the limiting eigenvalue ratio distribution in wishart matrices," *IEEE communications letters*, vol. 13, no. 7, 2009.

[27] S. K. Sengijpta, "Fundamentals of statistical signal processing: Estimation theory," 1995.

[28] W. A. Gardner, "Exploitation of spectral redundancy in cyclostationary signals," *IEEE Signal processing magazine*, vol. 8, no. 2, pp. 14–36, 1991.

[29] F. Chen and R. Qiu, "Centralized and distributed spectrum sensing system models performance analysis based on three users," in *Wireless Communications Networking and Mobile Computing (WiCOM), 2010 6th International Conference on*. IEEE, 2010, pp. 1–4.

[30] D. B. Johnson and D. A. Maltz, "Dynamic source routing in ad hoc wireless networks," *Mobile computing*, pp. 153–181, 1996.

[31] C. Perkins, E. Belding-Royer, and S. Das, "Ad hoc on-demand distance vector (aodv) routing," Tech. Rep., 2003.

[32] Z. J. Haas and M. R. Pearlman, "The performance of query control schemes for the zone routing protocol," *IEEE/ACM Transactions on Networking (TON)*, vol. 9, no. 4, pp. 427–438, 2001.

[33] Y.-B. Ko and N. H. Vaidya, "Location-aided routing (lar) in mobile ad hoc networks," *Wireless networks*, vol. 6, no. 4, pp. 307–321, 2000.

[34] S. Basagni, I. Chlamtac, V. R. Syrotiuk, and B. A. Woodward, "A distance routing effect algorithm for mobility (dream)," in *Proceedings of the 4th annual ACM/IEEE international conference on Mobile computing and networking*. ACM, 1998, pp. 76–84.

[35] R. Ahlswede, N. Cai, S.-Y. Li, and R. W. Yeung, "Network information flow," *IEEE Transactions on information theory*, vol. 46, no. 4, pp. 1204–1216, 2000.

[36] A. Ghasemi, "Statistical characterization of interference in cognitive radio networks," in *Personal, Indoor and Mobile Radio Communications, 2008. PIMRC 2008. IEEE 19th International Symposium on*. IEEE, 2008, pp. 1–6.

[37] M. S. Ali and N. B. Mehta, "Modeling time-varying aggregate interference in cognitive radio systems, and application to primary exclusive zone design," *IEEE Transactions on Wireless Communications*, vol. 13, no. 1, pp. 429–439, 2014.

[38] A. S. Cacciapuoti, I. F. Akyildiz, and L. Paura, "Correlation-aware user selection for cooperative spectrum sensing in cognitive radio ad hoc networks," *IEEE Journal on Selected Areas in Communications*, vol. 30, no. 2, pp. 297–306, 2012.

[39] D. Middleton, "Statistical-physical models of urban radio-noise environments-part i: Foundations," *IEEE Transactions on Electromagnetic Compatibility*, no. 2, pp. 38–56, 1972.

[40] E. S. Sousa and J. A. Silvester, "Optimum transmission ranges in a direct-sequence spread-spectrum multihop packet radio network," *IEEE journal on selected areas in communications*, vol. 8, no. 5, pp. 762–771, 1990.

[41] J. Ilow and D. Hatzinakos, "Analytic alpha-stable noise modeling in a poisson field of interferers or scatterers," *IEEE transactions on signal processing*, vol. 46, no. 6, pp. 1601–1611, 1998.

[42] M. Shao and C. L. Nikias, "Signal processing with fractional lower order moments: stable processes and their applications," *Proceedings of the IEEE*, vol. 81, no. 7, pp. 986–1010, 1993.

[43] M. Aljuaid and H. Yanikomeroglu, "Investigating the gaussian convergence of the distribution of the aggregate interference power in large wireless networks," *IEEE Transactions on Vehicular Technology*, vol. 59, no. 9, pp. 4418–4424, 2010.

[44] J. Jao, "Amplitude distribution of composite terrain radar clutter and the κ-distribution," *IEEE Transactions on Antennas and Propagation*, vol. 32, no. 10, pp. 1049–1062, 1984.

[45] E. Dall'Anese, S.-J. Kim, G. B. Giannakis, and S. Pupolin, "Power control for cognitive radio networks under channel uncertainty," *IEEE Transactions on Wireless Communications*, vol. 10, no. 10, pp. 3541–3551, 2011.

[46] X. Yang and A. P. Petropulu, "Co-channel interference modeling and analysis in a poisson field of interferers in wireless communications," *IEEE Transactions on Signal Processing*, vol. 51, no. 1, pp. 64–76, 2003.

[47] R. K. Ganti and M. Haenggi, "Spatial and temporal correlation of the interference in aloha ad hoc networks," *IEEE Communications Letters*, vol. 13, no. 9, 2009.

[48] J. Miranda, R. Abrishambaf, T. Gomes, P. Goncalves, J. Cabral, A. Tavares, and J. Monteiro, "Path loss exponent analysis in wireless sensor networks: Experimental evaluation," in *Industrial Informatics (INDIN), 2013 11th IEEE International Conference on*. IEEE, 2013, pp. 54–58.

[49] A. Miaoudakis, A. Lekkas, G. Kalivas, and S. Koubias, "Radio channel characterization in industrial environments and spread spectrum modem performance," in *Emerging Technologies and Factory Automation, 2005. ETFA 2005. 10th IEEE Conference on*, vol. 1. IEEE, 2005, pp. 7–pp.

[50] J. F. Coll, J. Chilo, and B. Slimane, "Radio-frequency electromagnetic characterization in factory infrastructures," *Electromagnetic Compatibility, IEEE Transactions on*, vol. 54, no. 3, pp. 708–711, 2012.

[51] S. Luo, N. Polu, Z. Chen, and J. Slipp, "Rf channel modeling of a wsn testbed for industrial environment," in *Radio and Wireless Symposium (RWS), 2011 IEEE*. IEEE, 2011, pp. 375–378.

[52] E. Tanghe, W. Joseph, L. Verloock, L. Martens, H. Capoen, K. V. Herwegen, and W. Vantomme, "The industrial indoor channel: large-scale and temporal fading at 900, 2400, and 5200 mhz," *Wireless Communications, IEEE Transactions on*, vol. 7, no. 7, pp. 2740–2751, 2008.

[53] S. Kozłowski, R. Szumny, K. Kurek, and J. Modelski, "Statistical modelling of a wideband propagation channel in the factory environment," in *Wireless Technology, 2008. EuWiT 2008. European Conference on*. IEEE, 2008, pp. 190–193.

[54] T. S. Rappaport, S. Y. Seidel, and K. Takamizawa, "Statistical channel impulse response models for factory and open plan building radio communicate system design," *Communications, IEEE Transactions on*, vol. 39, no. 5, pp. 794–807, 1991.

[55] P. Yegani and C. D. McGillem, "A statistical model for the factory radio channel," *Communications, IEEE Transactions on*, vol. 39, no. 10, pp. 1445–1454, 1991.

[56] J. Kunisch and J. Pamp, "Locally coherent ultra-wideband radio channel model for sensor

networks in industrial environment," in *Ultra-Wideband, The 2006 IEEE 2006 International Conference on*. IEEE, 2006, pp. 363–368.

[57] S. Savazzi, S. Guardiano, and U. Spagnolini, "Wireless channel characterization and modeling in oil and gas refinery plants," in *Industrial Technology (ICIT), 2013 IEEE International Conference on*. IEEE, 2013, pp. 1546–1551.

[58] M. Lauridsen, B. Vejlgaard, I. Z. Kovács, H. Nguyen, and P. Mogensen, "Interference measurements in the european 868 mhz ism band with focus on lora and sigfox," in *Wireless Communications and Networking Conference (WCNC), 2017 IEEE*. IEEE, 2017, pp. 1–6.

[59] K. L. Blackard, T. S. Rappaport, and C. W. Bostian, "Measurements and models of radio frequency impulsive noise for indoor wireless communications," *Selected Areas in Communications, IEEE Journal on*, vol. 11, no. 7, pp. 991–1001, 1993.

[60] F. Yang, Q. Song, and J. Zhou, "Interference effect evaluation of cognitive radio by using statistical method," in *Microwave, Antenna, Propagation and EMC Technologies for Wireless Communications, 2009 3rd IEEE International Symposium on*. IEEE, 2009, pp. 858–861.

[61] M. Gaafar and G. G. Messier, "Petroleum refinery multiantenna propagation measurements," *IEEE Antennas and Wireless Propagation Letters*, vol. 15, pp. 1365–1368, 2016.

[62] H. S. Ramos, M. G. Almiron, A. C. Frery, E. F. Nakamura, and A. A. Loureiro, "Node deployment by stochastic point processes in wireless sensor networks."

[63] A. Goldsmith, *Wireless communications*. Cambridge university press, 2005.

[64] I. S. Association, "Ieee std 802.11-2016," p. 2246, 2016.

[65] M. S. Kang and B. C. Jung, "A cognitive p-persistent csma scheme for spectrum sharing based cognitive radio networks," in *Wireless Communications and Networking Conference (WCNC), 2010 IEEE*. IEEE, 2010, pp. 1–6.

[66] H. Shah-Mansouri, M. R. Pakravan, and B. H. Khalaj, "Analytical modeling and performance analysis of flooding in csma-based wireless networks," *IEEE Transactions on Vehicular Technology*, vol. 60, no. 2, pp. 664–679, 2011.

[67] Z. J. Haas, J. Y. Halpern, and L. Li, "Gossip-based ad hoc routing," *IEEE/ACM Transactions on Networking (ToN)*, vol. 14, no. 3, pp. 479–491, 2006.

[68] V. K. Paruchuri, A. Durresi, D. S. Dash, and R. Jain, "Optimal flooding protocol for routing in ad-hoc networks," in *IEEE Wireless Communications and Networking Conference*, 2003, pp. 93–102.

[69] Y. Wu, P. A. Chou, S.-Y. Kung *et al.*, "Information exchange in wireless networks with network coding and physical-layer broadcast," MSR-TR-2004, Tech. Rep., 2005.

[70] S. Katti, S. Gollakota, and D. Katabi, "Embracing wireless interference: Analog network coding," *ACM SIGCOMM Computer Communication Review*, vol. 37, no. 4, pp. 397–408, 2007.

[71] T. Ho, M. Médard, R. Koetter, D. R. Karger, M. Effros, J. Shi, and B. Leong, "A random linear network coding approach to multicast," *IEEE Transactions on Information Theory*, vol. 52, no. 10, pp. 4413–4430, 2006.

[72] O. Trullols-Cruces, J. M. Barcelo-Ordinas, and M. Fiore, "Exact decoding probability under random linear network coding," *IEEE communications letters*, vol. 15, no. 1, pp. 67–69, 2011.

[73] "802.22-2011 - ieee standard for information technology," 2011.

[74] C. H. Kai and S. C. Liew, "Towards a more accurate carrier sensing model for csma wireless networks," in *Communications (ICC), 2010 IEEE International Conference on*. IEEE, 2010, pp. 1–6.

[75] R. K. Ganti and M. Haenggi, "Interference and outage in clustered wireless ad hoc networks," *IEEE Transactions on Information Theory*, vol. 55, no. 9, pp. 4067–4086, 2009.

[76] M. Haenggi, R. K. Ganti *et al.*, "Interference in large wireless networks," *Foundations and Trends® in Networking*, vol. 3, no. 2, pp. 127–248, 2009.

[77] V. Mordachev and S. Loyka, "On node density-outage probability tradeoff in wireless networks," *IEEE Journal on Selected Areas in Communications*, vol. 27, no. 7, 2009.

[78] M. Gudmundson, "Correlation model for shadow fading in mobile radio systems," *Electronics letters*, vol. 27, no. 23, pp. 2145–2146, 1991.

[79] I. Hunter and R. Kearney, "Generation of random sequences with jointly specified probability density and autocorrelation functions," *Biological cybernetics*, vol. 47, no. 2, pp. 141–146, 1983.

[80] N. Wiener, *Extrapolation, interpolation, and smoothing of stationary time series*. MIT press Cambridge, MA, 1949, vol. 7.

[81] J. G. Proakis, "Digital communications fourth edition, 2001," 1998.

[82] P. Komulainen, A. Tölli, and M. Juntti, "Effective csi signaling and decentralized beam coordination in tdd multi-cell mimo systems," *IEEE Transactions on Signal Processing*, vol. 61, no. 9, pp. 2204–2218, 2013.

[83] "Usrp n210 software defined radio (sdr) - ettus research," http://www.ettus.com/product/details/UN210-KIT, (Visited on 11/09/2015).

[84] "Beagleboard.org - black," http://beagleboard.org/black, (Visited on 11/10/2015).

[85] "Home :: Opencores," http://opencores.org/, (Visited on 11/11/2015).

[86] "Rubidium frequency standard - sim940," http://www.thinksrs.com/products/SIM940.htm, (Visited on 11/09/2015).

[87] http://www.documentation.emersonprocess.com/groups/public/documents/bulletins/d103222x012.pdf, (Visited on 11/09/2015).

[88] "North american certification — hazardous locations — csa group," http://www.csagroup.org/global/en/services/hazardous-locations/north-american-certification, (Visited on 11/16/2015).

[89] https://www.winncom.com/pdf/PCTEL_MHO24004NM/PCTEL_MHO24004NM.pdf, (Visited on 11/09/2015).

[90] J. G. Proakis, *Intersymbol Interference in Digital Communication Systems*. Wiley Online Library, 2001.

[91] "D-link 2dbi sma antenna for wireless pci card or router," http://wirelessroutersreviews.com/d-link-2dbi-sma-antenna-wireless-pci-card-router/, (Visited on 11/10/2015).

[92] T. K. Blankenship and T. S. Rappaport, "Characteristics of impulsive noise in the 450-mhz band in hospitals and clinics," *Antennas and Propagation, IEEE Transactions on*, vol. 46, no. 2, pp. 194–203, 1998.

[93] https://www.utdallas.edu/~torlak/courses/ee4367/lectures/lectureradio.pdf, (Visited on 11/18/2015).

[94] A. Hong, C. Schneider, G. Sommerk, M. Milojević, R. Thomä, and W. Zirwas, "Experimental evaluation of correlation properties of large scale parameters in an indoor los environment," in *Wireless Communication Systems, 2006. ISWCS'06. 3rd International Symposium on*. IEEE, 2006, pp. 55–59.

[95] "Isa100 wireless standard approved as an american national standard - isa," https://www.isa.org/, (Visited on 11/10/2015).

[96] L. J. Greenstein, D. G. Michelson, and V. Erceg, "Moment-method estimation of the ricean k-factor," *Communications Letters, IEEE*, vol. 3, no. 6, pp. 175–176, 1999.

[97] D. J. Sheskin, *Handbook of parametric and nonparametric statistical procedures*. crc Press, 2003.